3D Hydro-Morphodynamic and Fish Habitat Modelling

By

Parna Parsapour-Moghaddam

Thesis submitted to the

Faculty of Graduate and Postdoctoral Studies

In partial fulfillment of the requirements

for the Ph.D. degree in Civil Engineering

Department of Civil Engineering

Faculty of Engineering

University of Ottawa

Abstract

Meandering rivers provide fresh water and important aquatic ecosystem services, yet at the same time induce flood and erosion hazards. In the face of ongoing development pressure and changing climate, growing concern for meandering rivers has increased the demand to model accurately the flow and predict the sediment transport in a meandering river channel. Calibration and validation of these models based on comparable field-based data, as opposed to laboratory-scale experimental data, may decrease uncertainty and improve understanding of complex flow structures in natural meandering rivers. In this thesis, spatially intensive field data are utilized to develop appropriate calibration and validation methods for 3D meandering river models. Validated models are then applied to the study of morphodynamic processes and the influence of channel change on fish habitat availability in meandering rivers.

This study presents a novel methodology for use of three-dimensional (3D) velocity for improved calibration of a 3D hydro-morphodynamic model. A natural tortuously meandering river was simulated using the Delft3D hydrodynamic model. A spatially intensive acoustic Doppler current profiler (ADCP) survey was conducted throughout the study river, providing fully 3D distributed velocities for model calibration. For accurate and realistic comparison of the fully 3D predicted and measured velocities, an algorithm was developed to match the location of each ADCP bin with 3D model grid points. The results suggest that different calibration approaches can result in different calibration parameterizations whose simulated results can differ significantly. It is shown that the model which was calibrated based on the proposed 3D calibration approach had the best model performance. Depending upon the nature and objectives of the numerical modelling exercise, the results demonstrate the importance of model calibration with spatially intensive field data.

Given the importance of pressure gradients in driving secondary flow, it is worth studying how the modelled flow structures in a natural river bend can be impacted by the assumption of hydrodynamic pressure. Accordingly, the performance of hydrostatic versus non-hydrostatic pressure assumption in the Delft3D hydrodynamic modelling of a tortuously meandering river was studied. An Acoustic Doppler Velocimeter (ADV) was employed to measure the 3D flow field at a section in a sharp bend of the simulated

river at two different flow stages. The field-based ADV data were employed to validate the simulated hydrodynamic models. The results indicate the surprisingly superior performance of the hydrostatic over non-hydrostatic Delft3D modelling of the secondary flow. It was determined that the non-hydrostatic routine employed in Delft3D was not mass conservative, which diminished model accuracy.

Despite several decades of intensive study of the morphological changes in meandering rivers, less attention has been paid to confined meanders. This thesis includes a study of the meandering behavior of a semi-alluvial cohesive bed river over a 10-year period. We employed a paired sub-reach study approach, wherein one sub-reach is freely meandering and the second adjacent sub-reach is confined by a railway embankment. Channel migration and morphological changes of the channel banks along each of these sub-reaches were analyzed by comparing the historical aerial photography, light detection and ranging (LIDAR) data, bathymetric data obtained from a total station survey, and field examination.

Moreover, two different spatially intensive ADCP surveys were conducted in the study area to find the linkage between the hydrodynamics and morphological changes in the two different sub-reaches. The unconfined sub-reach displayed a typical channel migration pattern with deposition on the inner bank and erosion on the outer bank of the meander bend. On the other hand, the confined sub-reach showed greater bank instabilities than the unconfined sub-reach. In the confined sub-reach, an irregular meandering pattern occurred by the evolution of a concave-bank bench, which was caused by reverse flow eddies. The results of this study could shed light on the potential impacts of channel confinement on bank retreat and river migration in comparable case studies.

It is reasonable to expect that hydro-morphodynamic processes in rivers can affect fish habitat availability and quality, but the impact of river morphological changes on fish habitat is not well studied. Herein, we investigate the impact of morphological development of a cohesive meandering creek on the quality of fish habitat available for juvenile yellow perch (*Perca flavescens*) and white sucker (*Catostomus commersonii*). A 3D morphodynamic model was first developed to simulate the hydro-morphodynamics of the study creek over a 1-year period. Total station topographic surveys were

conducted to provide bathymetric change data for calibration of the morphodynamic module. Successful calibration efforts indicated that the developed model could be reasonably employed to predict the hydro-morphodynamics of the study creek.

Two fish sampling surveys were carried out at the beginning and the end of the study period to determine habitat utilization of each fish species in the study reach. ANOVA multiple comparison tests indicate that morphological development of the river was a significant factor for the habitat utilization of juvenile yellow perch, whereas juvenile white sucker habitat utilization was not significantly impacted by the changes in the creek morphology. It is shown that flow depth, depth-averaged velocity, and suspended sediment transport also significantly influenced presence of the juvenile yellow perch at the 5% significant level. As for the juvenile white sucker, the only significant factor was the depth-averaged velocity.

The results of the developed 3D hydro-morphodynamic model were fed into a fish habitat model. Comparison of the predicted fish habitat map of the juvenile yellow perch with the results of fish sampling surveys confirms that the habitat quality was better predicted when the impact of morphological changes was taken into account in the fish habitat modelling. The results of the proposed methodology could provide some insights into the impact of sediment transport processes on the fish community. This has important implications for effective river management.

To my parents,

to whom I owe everything I have ever achieved in my life…

To Hamidreza,

who taught me the meaning of love…

Acknowledgements

First, I would like to express my deepest thanks to my supervisor, Dr. Colin Rennie, for his invaluable, advice and continuous supports throughout my PhD studies. I am extremely grateful for his guidance, dedication, time, and patience, which helped me through many challenges and made the impossible seem possible. His immense knowledge, enthusiasm, motivation and availability made my PhD experience productive and inspiring.

I would like to thank my thesis evaluation committee: Dr. Katy Haralampides, Dr. Majid Mohammadian, Dr. Ousmane Seidou and Dr. Paul Simms for their very helpful suggestions and comments on my thesis. I would also like to thank all of my friends at the University of Ottawa, particularly, Colin Brennan, I really enjoyed our collaboration and stimulating discussions.

Last but not least, I would like to thank my parents, Vida and Hossien, and my sister, Pardis, for their unconditional love and support. Words cannot express how grateful I am for all the sacrifices you have made for me. My huge thanks to my best friend and my beloved husband who has always been by my side with patience, support, encouragement, and unwavering love. Hamidreza, without you none of these would have been possible.

Table of Contents

List of Figures

List of Tables

List of Symbols

c: mass concentration of the sediment
c_b: average sediment concentration in the near bottom computational layer
d: bed elevation
D: deposition flux
D_x , D_y, and D_z: sediment eddy diffisivities
E: erosion flux
g: gravitational acceleration
h: water depth
M: erosion parameter
q: hydrodynamic pressure
t : time
U: velocity component in the x direction
V: velocity component in the y direction
W: velocity component in the z direction
v_m: velocity component in the stream-wise direction
v_n: velocity component in the cross-stream direction
v_t: resultant velocity vector
w_s: is sediment settling velocity
k: turbulence kinetic energy
ε: dissipation of turbulence energy.
τ_{cw}: maximum bed shear stress due to waves
$\tau_{cr,e}$: critical shear stress for erosion
$\tau_{cr,d}$: critical shear stress for deposition
υ_h: horizontal eddy viscosity
υ_v : vertical eddy viscosity
ν_{mol}: kinematic viscosity
υ_v^{back}: background vertical eddy viscosity
ν_H^{back}: background horizontal eddy viscosity
ν_{SGS} : sub-grid scale (SGS) turbulence
η: water surface elevation

CHAPTER 1

Introduction

1.1 Background

Due to distinctive characteristics of meandering rivers, they have attracted river engineers' attention over the past decades. Although river meandering is a well-known subject with a long literature history, some ambiguities still exist in the source and initiation of the meandering pattern and its migration. The growing concern for meandering rivers has increased the demand to accurately model the flow and predict the sediment transport in a meandering alluvial channel. Accordingly, researchers have been trying to address present problems in river engineering by deriving methods and developing models to comprehend better these complex processes. Numerical models are powerful tools to conceptualize the natural hydro-morphodynamic processes in rivers.

Fluvial hydrodynamics and resulting morphological changes in river channels have been studied for many years (e.g. Jansen et al., 1979; Yalin and da Silva, 2001; Garcia 2008; Li and Millar, 2011). During the last few decades, numerical modelling of flow has been applied extensively as a useful tool in solving river engineering problems. Three-dimensional (3D) models may offer the opportunity to provide a more comprehensive description of the hydro-morphodynamics than 2D models. The hydro-morphodynamic processes in a meandering river bend are impacted by helical secondary flows (Thomson, 1876; Blanckaert and deVriend, 2003). Consequently, 3D models are likely more capable to reproduce 3D river hydro-morphodynamics processes compared to 1D and 2D models (Lane at el., 1999; Rodriguez et al., 2004; Kasvi et al., 2015a).

To make accurate predictions of flow characteristics and morphological changes, it is essential to evaluate properly the model performance by comparison to measurements. Given that the aim of the 3D modelling is to capture the complexities of three-dimensional flow, more extensive and expensive data are needed for calibration of such

models (van Rijn, 1989). Despite all the numerical methods that have been utilized to predict field-scale hydro-morphodynamic processes, less attention has been paid to calibrate and validate these models with 3D velocity collected in natural rivers in the field. In particular, the complexity of flow in natural meandering rivers demands that careful attention is paid to 3D model calibration for reliable prediction of the full 3D flow field. Validation of these models based on comparable field-based data may improve understanding of complex flow structures in natural meandering rivers and decrease the uncertainty associated with validation of meandering river numerical models with laboratory-scale experimental data. Nevertheless, the calibration process is disputable and still suffers from some inadequacies (Van De Wiel et al., 2011).

The dynamic interaction of hydro-morphodynamic processes and the aquatic environment defines a river's ecological characteristics (Poff and Zimmerman, 2010). Rivers provide essential habitat for aquatic organisms (Brodeur et al., 2004; Pasternack et al., 2004; Wheaton et al., 2010). To ensure improved aquatic ecosystem conditions, it is important to know how fish populations respond to ecological changes and how different fish species are linked to their habitats (Portt et al., 2006). River hydro-morphodynamics influence the quality of habitat for fish and other aquatic species (Brodeur et al., 2004; Pasternack et al., 2004; Wheaton et al., 2010). For example, suspended sediment transport can influence the water temperature and dissolved oxygen levels and consequently can lead to aquatic organism biological impacts (Kjelland et al., 2015).

It is important to study morphological changes of a river and the corresponding sediment loads to manage and preserve fish populations (Sullivan and Watzin, 2010). Numerical simulation of fish habitat is often performed to provide insight for effective river management and environmental impact assessment (Tash and Litvaitis, 2007). Several fish habitat models have been developed which can be employed to preserve an aquatic habitat or declining species (de Kerckhove et al. 2008). Nevertheless, few studies considered river morphodynamic processes in the fish habitat modelling (Kerle et al., 2002; Baptist et al., 2002; Hauer et al., 2007).

In the following sections, each of the topics introduced above will be discussed in more detail by reviewing the relevant literature.

1.1.1 **Meandering Rivers**

Due to the unique characteristics of meandering rivers, they have long attracted people's attention. In the distant past, Leonardo da Vinci, for the first time, illustrated meanders of the Santerno River in Italy (Ghinassi et al., 2016). The word "meander" was first used by the ancient Greeks who named a curving river in west central Turkey, Maiandros. The Latin meaender finally came to refer to any curving river (Güneralp et al., 2012). Meandering rivers also became politically important since their shifting locations played an important role in defining the countries' borders. Over the past few centuries, river scientists and engineers have paid careful attention to the movement, development, and decay of river meanders (e.g., Thomson, 1876; Einstein, 1926; Bridge and Jarvis, 1976; Thompson,1986; Ikeda and Parker 1989; Demuren, 1993; Blanckaert and de Vriend, 2003; Piégay et al., 2005; Lanzoni and Seminara, 2006; Krapesch et al., 2009; Blanckaert, 2011; Demers et al., 2011; Kasvi et al., 2015a,b; Choné and Biron, 2016).

Meandering rivers have been shown to have intricate hyrdo-morphological behavior. The flow in a river bend is generally more complex compared to a straight part of a reach. The flow in a river bend is a 3D phenomenon and has a component normal to the section-averaged flow direction. This transverse velocity component is typically called secondary flow, which is a result of two opposing forces acting on water flow in a bend. An outward centrifugal force leads to super-elevation of the water surface on the outer bank, and thus an inward pressure gradient (Blanckaert and De Vriend, 2004). Near the water surface, where the velocity is higher than the average cross-sectional velocity, the centrifugal force exceeds the transverse pressure gradient and thus, the flow is driven outward. On the contrary, near the bed where the velocity is small compared to the mean velocity, the dominant pressure gradient force drives the flow towards the inner bend (Robert, 2003). Over the past few decades, several attempts have been made by river researchers to measure this induced secondary circulation (Bridge and Jarvis, 1976; Bathurst et al., 1979; Thompson, 1986; Ferguson et al., 2003; Rodriguez et al., 2004). The secondary currents can impact the velocity distribution, boundary shear stress and consequently sediment transport, mixing throughout the water column, lateral bed slope, and shape of the channel topography (Blanckaert and de Vriend,

2003). Although river meandering is a well-known topic with a long literature history, some ambiguities still exist in the initiation of the meandering pattern, its migration, and the impact of confining medium on the hydro-morphodynamics of the meandering rivers.

1.1.2 **Hydro-morphodynamic modelling**

Numerical modelling of natural meandering rivers has always been a challenge. During the last few decades, numerical modelling of flow has been applied extensively as a useful tool in solving river engineering problems. Using computational methods, numerical models solve sets of non-linear differential equations describing hydro-morphodynamics of river channels. Depending on the conditions of a problem, diverse numerical modelling methods may be employed. 2D models are very common tools for hydro-morphodynamic simulation. However, since most of these models are not able to account for the vertical flow field structure and thus, secondary flow, they are not reliable in sharp meandering rivers unless semi-empirical sub-models are used to model the generated secondary flow (Blanckaert and de Vriend, 2003).

Since an induced secondary flow is a dominant phenomenon in meandering rivers (Blanckaert and de Vriend, 2003; Wilson et al, 2003), it is critical to develop a model that is capable of reproducing the flow circulations in natural meandering rivers. The complex nature of the flow in curved channels generally requires a 3D simulation (Lane et al., 1999; Rodriguez et al., 2004; Kasvi et al., 2013a). 3D hydrodynamic modelling in meandering open-channels has been established since the late 1970s (Zeng et al., 2008) and due to the advancement in computer technology, 3D models are now widely applied in flow and sediment transport modeling (e.g. Shimizu et al., 1990; Olsen and Stokseth, 1995; Sinha et al., 1998; Lane et al., 1999; Wu et al., 2000; Koçyigit et al., 2002; Zeng et al., 2005; Khosronejad et al., 2007; Ruther and Olsen 2007; Zeng et al., 2008; Van Sabben, 2010; Sinha et al., 2012; Kamel et al., 2014; Vermeulen et al., 2015).

Shimizu et al. (1990) developed a 3D hydrodynamic model to simulate a meandering channel assuming hydrostatic pressure. They simplified their full 3D model in which they assumed that the vertical distribution of the longitudinal velocity is logarithmic. Predicted results were compared with the experiments and the calculated results from a 2D

model. It was indicated that the 3D model more precisely reproduced the flow field than the 2D model. Lane et al. (1999) investigated the predictive capability of a 3D versus a 2D model. The 3D model was based on the fully RANS (Reynolds-averaged Navier–Stokes) equations, and they used a finite volume approach for the governing equations discretization. They compared the simulated results with a measured data set collected from a natural river channel confluence. They suggested that a 3D model has better predictive capability compared to a 2D model, particularly when the 2D model does not account for the effect of secondary flow.

Ferguson et al. (2003) studied the flow separation at the inner banks in meander bends. They found that the spatial variability of the flow properties was less predicted by the 3D model compared to the real field measurements. They suggested that CFD models can adequately be used in the simulation of the flow separation in bends. Rodriguez et al. (2004) compared the results of a depth-averaged model with a secondary flow correction and a 3D numerical model with the measured velocity data of a meandering reach. They used STREMR, which is a depth-averaged 2D model, and FLOW-3D, which solves the fully 3D RANS equations. Their study showed that the 2D model could simulate the main flow features; however, modelling complicated flow structures, such as recirculation zones, requires 3D models. Kasvi et al. (2013a) illustrated that despite the employment of a secondary flow correction in their 2D model using SMS TUFLOW software, the 2D model did not predict the fluvial characteristics corresponding to the creation of the scroll bar at the inner bank of a low-sinuosity meander bend. Kasvi et al. (2015a) compared 2D versus hydrostatic 3D models generated with Delft3D. They found that the 3D model was deemed superior due to its ability to predict vertical and near-bed flows.

Studies of river morphological behavior are crucial for understanding river condition and the associated quality and availability of aquatic habitat. However, morphodynamic processes have been recognized as one of the least understood natural phenomena (Wu, 2007). This makes it difficult to predict the long-term consequences of river manipulations. Consequently, several morphodynamic models have been developed over the past decades in an attempt to improve understanding of river morphodynamics. Moreover, there has always been a challenge for an appropriate choice of the

morphodynamic model depending on the condition and complexity of the study area (Papanicolaou et al., 2008). The state-of-the-art of morphodynamic modelling typically involves 2D modelling (Pinto et al., 2012). However, direction and magnitude of the bed shear stress, which has a significant influence on the sediment transport, may not be accurately estimated from a 2D model (Lesser et al., 2001). This could be the case for meandering rivers, where we have dominant secondary flow structures. On the other hand, due to the complex nature of cohesive sediments, prediction of the erosion and sedimentation of the cohesive bed river is rather a challenge (Haralampides and Rodriguez , 2006; Peixoto et al., 2017). Secondary flow occurrence would increase the sidewall shear stress in the cohesive river banks (Papanicolaou et al., 2007).

3D hydrodynamic models can be further divided to hydrostatic and non-hydrostatic models. Due to the lower computation cost, hydrostatic models are widely used in natural field-scale flows (Zhang et al., 2014). 3D hydrostatic models can generally be described as accurate models in water engineering where the vertical velocity is comparatively small (Casulli and Stelling, 1998). However, there are some cases where the vertical acceleration, and thus non-hydrostatic pressure, cannot be neglected. Such cases include topography with abrupt changes, short waves, intensive density gradient, and strong vertical circulation (Deltares, 2014). 3D non-hydrostatic hydrodynamic models have recently become computationally possible due to the advancement of technology and have been employed in curved open channels (eg., Demuren,1993; Sinha et al., 1998; Wilson et al.,2003; Khosronejad et al., 2007; Leupi and Altinakar, 2005; Rüther and Olsen, 2007; Zeng et al., 2008; Vermeulen et al., 2015).

1.1.3 **Evaluation of model performance with field measurements**

Numerical models should have the capability to model natural rivers considering their dynamics and variability. To make accurate predictions of flow characteristics and morphological changes, it is essential to calibrate the model properly. Calibration of a hydrodynamic model is commonly done by adjusting the model inputs such that model outputs match available measured data (Papanicolaou et al., 2010). Nevertheless, the calibration process is disputable and still suffers from some inadequacies (Van De Wiel et al., 2011). Accordingly, a 3D hydrodynamic model of a meandering river could still

have drawbacks in quantitative prediction of hydraulic variables if its performance has not been properly evaluated (Kasvi et al., 2015a).

Previous studies that used field measurements for evaluation of the model were shown to have problems with quantitative estimation of hydraulic variables (Dargahi, 2004; Rodriguez et al., 2004; Nicholas et al., 2012). Furthermore, expensive data are required for calibration of a 3D model to acquire reliable and realistic predictions from these models (van Rijn, 1989). Some of the traditional calibration attempts involve reproducing the flow depth; however, a calibrated model that correctly simulates the observed water elevation can not necessarily reproduce the 3D flow field (Wagner and Mueller, 2002). Accordingly, comprehensive field work should be conducted to apprehend the intricacies of a 3D flow field (Mashriqui, 2003). In particular, the complexity of flow in natural meandering rivers demands that careful attention is paid to 3D model calibration for reliable prediction of the full 3D flow field.

To calibrate the model reliably, it is important to have accurate measurements of the flow field. Traditional methods to measure flow velocity in rivers, such as propeller meters, provide sparse data (Stone and Hotchkiss, 2007). The Acoustic Doppler Velocimeter (ADV) is a broadly used hydro-acoustic instrument which facilitates numerical model calibration and validation (eg. Lohrmann et al. 1994; Sontek 1997; Afzalimehr and Rennie 2009; Rennie and Hay 2010; Sukhodolov 2012, Jamieson et al. 2013). An ADV functions based on the principle of Doppler shift to measure turbulent velocity at a point. The ADV measurement technique and use in rivers are well described in the literature (Lohrmann et al., 1994; Sontek, 1997; Lane et al., 1999; Afzalimehr and Rennie, 2009; Rennie and Hay, 2010; Sukhodolov, 2012; Jamieson et al., 2013). More recently, acoustic Doppler current profilers (ADCPs) have been extensively applied to estimate the mean flow velocity field (Abad et al., 2004; Garcia et al., 2007; Vermeulen et al., 2011). These instruments can provide spatially dense velocity fields (e.g., Rennie and Millar 2004, Rennie and Church 2010, Jamieson et al. 2011, Venditti et al. 2014). The ADCP measures vertical profiles of velocity vectors and can calculate discharge based on a traverse of the channel section. Flow velocities are calculated according to the reference frame of the ADCP. If the instrument is mounted

on a moving boat, a boat velocity correction should be applied to attain the flow velocity in earth coordinates.

Wagner and Mueller (2002) calibrated and validated a 2D model using ADCP velocity data collected at different cross-sections. Viscardi et al. (2006) conducted 3D ADCP velocity measurements to analyze the flow pattern in cross-sections spaced every $100m$ in a river bend. They compared the results based on 3D-RANS simulations using the SSIIM model with the velocity field obtained from the ADCP. Williams et al. (2013) calibrated their developed 2D model using spatial observations of depth and depth-averaged velocity obtained with an ADCP. They showed that proper calibration is critical for accurate prediction of lateral variations in depth-averaged velocity; calibration based only on water level and depth was inadequate. They subsequently employed spatially continuous ADCP data to find linkage between morphodynamic and hydrodynamic processes (Williams et al., 2015). Kasvi et al. (2015b) evaluated the model performance with measured ADCP and multi-temporal mobile laser scanning data. The authors suggested improving the calibration and validation data to determine the reasons for the mismatch between simulations and measurements.

1.1.4 **Delft3D numerical modelling**

The present study employs Delft3D to simulate hydro-morphodynamic processes in cohesive meandering rivers. Delft3D is a widely used hydro-morphodynamic open source code which is developed by Deltares and has a broad range of applications in river studies (e.g. Van Maren, 2007, Rinaldi et al., 2008; Sloff, 2010, Moerman, 2011; Spruyt et al., 2011; Williams et al., 2013; Schuurman et al., 2013; Staines and Carrivick, 2015; Kasvi et al., 2015[a,b]; Javernick et al., 2016; Williams et al., 2016; Singh et al., 2017; Su et al., 2017; Mohammed, 2017).

This code includes different components interacting individually or in combination with other modules over a mutual interface (Deltares, 2014). Delft3D is capable of modelling 2D or 3D hydro-morphodynamics over a rectilinear or a curvilinear grid. The Delft3D hydrodynamic model solves 3D Navier–Stokes equations for incompressible

flow under Boussinesq assumptions. The partial differential equations include 3D flow continuity and momentum equations:

$$\frac{\partial u}{\partial x}+\frac{\partial v}{\partial y}+\frac{\partial w}{\partial z}=0 \tag{1-1}$$

$$\frac{\partial u}{\partial t}+u\frac{\partial u}{\partial x}+v\frac{\partial u}{\partial y}+w\frac{\partial u}{\partial z}=-g\frac{\partial \eta}{\partial x}+\nu_h\left(\frac{\partial^2 u}{\partial x^2}+\frac{\partial^2 u}{\partial y^2}\right)+\frac{\partial}{\partial z}\left(\nu_v\frac{\partial u}{\partial z}\right) \tag{1-2}$$

$$\frac{\partial v}{\partial t}+u\frac{\partial v}{\partial x}+v\frac{\partial v}{\partial y}+w\frac{\partial v}{\partial z}=-g\frac{\partial \eta}{\partial y}+\nu_h\left(\frac{\partial^2 v}{\partial x^2}+\frac{\partial^2 v}{\partial y^2}\right)+\frac{\partial}{\partial z}\left(\nu_v\frac{\partial v}{\partial z}\right) \tag{1-3}$$

The vertical momentum equation is reduced to the hydrostatic pressure assumption for cases where the gravity is much higher than the vertical acceleration:

$$\frac{\partial p}{\partial z}=-\rho g \tag{1-4}$$

where h is the water depth, η is the water surface elevation, u and v are the depth averaged velocities in x and y directions, respectively, and u, v and w represent velocity components; g is the gravitational acceleration; t is the time; υ_h and υ_v are, respectively, horizontal and vertical kinematic eddy viscosity coefficients. Various options are available for turbulence closure modelling, including the two equation $k-\varepsilon$ model.

The morphodynamic module of Delft3D is capable of simulating the sediment transport of suspended load and bedload for non-cohesive sediments and suspended load for cohesive sediments. The morphological module of Delft3D has been validated by Lesser et al. (2004). Delft3D morphodynamic modelling incorporates feedback of updated bathymetry to the hydrodynamic flow calculation, thus, hydrodynamic modelling can be carried out by employing the correct bathymetry. The 3D advection-diffusion equation (mass-balance) is solved for calculation of suspended sediment transport:

$$\frac{\partial c}{\partial t}+\frac{\partial uc}{\partial x}+\frac{\partial vc}{\partial y}+\frac{\partial (w-w_s)c}{\partial z}=\frac{\partial}{\partial x}\left(D_x\frac{\partial c}{\partial x}\right)+\frac{\partial}{\partial y}\left(D_y\frac{\partial c}{\partial y}\right)+\frac{\partial}{\partial z}\left(D_z\frac{\partial c}{\partial z}\right) \tag{1-5}$$

where c is mass concentration of the sediment ($\mathrm{kg/m^3}$), D_x , D_y, and D_z are sediment eddy diffisivities ($\mathrm{m^2/s}$), and w_s is sediment settling velocity ($\mathrm{m/s}$). Eddy diffisivities and local flow velocities are calculated according to hydrodynamic model results. Various standard sediment transport formulations can be used for non-cohesive bedload sediment transport. As for the cohesive sediment transport, erosion flux or deposition flux is computed based on the Partheniades-Krone formulations (Partheniades, 1965).

The Delft3D 3D model can be further divided to hydrostatic and non-hydrostatic modules.

Despite the growing concern of the 3D morphodynamic modelling, few studies conducted Delft3D 3D morphodynamic modelling in meandering rivers. The Kleinhans group (Kleinhans et al., 2008; Schuurman et al., 2013; Schuurman and Kleinhans, 2015) have employed Delft3D to create 3D models to predict morphodynamics of meandering and braided rivers; however, their studies have focused on bifurcation dynamics with non-cohesive sediments. Kasvi et al., (2015a) studied the sensitivity and functionality of 2D and 3D hydro-morphodynamic Delft3D models. However, their results were limited to short-term (one flood event) morphodynamic processes. Moreover, their results focused on a sandy bed river bend.

1.1.5 **River morphodynamics and fish habitat**

Dynamic interaction of the hydro-morphodynamic processes and the aquatic environment define a river's ecological characteristics (Poff and Zimmerman, 2010). For an enhanced aquatic ecosystems conditions, one needs to know how the fish inhabitants react to the ecological changes and how different fish species are related to their habitats (Portt et al., 2006). River hydro-morphodynamics influence the quality of habitat for fish and other aquatic species. Suspended sediment transport can influence the water temperature and dissolved oxygen levels and consequentially can lead to the aquatic organism biological impacts (Kjelland et al., 2015). It is important to study the river's morphological changes and the corresponding sediment load to manage and preserve fish populations (Sullivan and Watzin, 2010).

One way of obtaining information about the fish populations in rivers is to conduct a fish sampling survey. Electrofishing is among the widely used methods for fish sampling surveys (e.g. Sharber and Sharber Black, 1999; Rosenberger and Dunham, 2005; Temple and Pearsons, 2007). The method uses an electromagnetic field, generated by two electrodes, to attract and stun the fish before they are caught. This method is relatively harmless to fish (Temple and Pearsons, 2007). To further predict the impact of river ecological changes on the riverine fish and consequently the ecosystem, several

fish habitat models have been developed. Such models have been employed to preserve an aquatic habitat or declining species (Tash and Litvaitis, 2007; De Kerckhove et al., 2008). Habitat modeling has been effectively employed since the 1980s (Mouton et al., 2007). Fish habitat models can quantify a river's ecological condition and can be used to investigate the impact of different restoration plans (Tash and Litvaitis, 2007; De Kerckhove et al., 2008). Over the past few decades, different metrics of habitat quality and flow complexity have been developed (see de Kerckhove et al. 2008).

One of the most widely used methods is habitat suitability index (HSI) modelling, which quantifies the quality of habitat to support particular species at different life stages (Bovee, 1986; Hardy, 1998; Fukuda, 2009; Conallin et al., 2010). The habitat suitability index varies from 0 (the most unsuitable condition) to 1 (optimal condition) for a given species in a study area. HSI is broadly used to assess the ability of a habitat to support a particular species. Typically, a suitability curve is developed for each relevant habitat parameter (e.g., depth, velocity, substrate, etc.). Mathematical combinations of curves for these various habitat parameters, such as geometric or arithmetic means, can produce an overall suitability index ranging from 0 (unsuitable) to 1 (optimal). Despite the fact that several fish habitat models have been developed over the past few decades, few studies have considered river morphological changes in the fish habitat modelling.

Kerle et al., (2002) indicated that long-term morphodynamic changes in the man-made secondary channels in the river Rhine could significantly affect the habitat availability. Similarly, Baptist et al., (2002) indicated that fish habitat quality, in the secondary channel developments of the river Rhine, was impacted by the morphological changes. They used a 2D version of Delft3D to model the hydro-morphodynamics. The outputs of the model were then fed into a fuzzy habitat model, Casimir. However, in this study, a fish sampling survey was not conducted, and therefore, the fish habitat model could not be validated. Accordingly, the correlation between the morphodynamic changes and the availability of the fish habitat was not studied.

Hauer et al., (2007) showed that instability of riffles would negatively affect the nase (*Chondrostoma nasus*) reproduction at the Austrian lowland Sulm River. Accordingly,

they suggested that morphological studies should be considered in the river restoration projects. Hauer et al., (2008) studied how juvenile nase could be impacted by the morphodynamic processes in the same river. They combined the results of 1D and 2D hydrodynamic models with the fish habitat model. Sedimentation and erosion of the study river were obtained by terrestrial surveys within three years. They also conducted an electrofishing survey to study how the juvenile nase react to the morphological changes. The results of this study confirmed the reduction in the fish habitat suitability by the channel morphological changes; however, no morphodynamic simulation was employed. Moreover, the correlation of the sedimentation and erosion with the available fish habitat was not studied.

Escobar-Arias and Pasternack (2010) evaluated in-stream ecological functionality based on the shear stress dynamics. However, calculated bed shear stress from the hydrodynamic numerical model may not be a good representative of the intricate dynamics of the sediment process and the impact of bed level changes on the hydraulics. Noack (2012) used the CASiMiR habitat model to simulate the suitability for reproduction of gravel-spawning fish. This study used a 3D morphodynamic model to account for the morphodynamic processes and considered the impact of bed level changes on the hydraulics. However, their habitat model was mainly based on the water depth, flow velocity as well as the dominant substrate, and the dynamic sedimentation and erosion processes were not correlated to the fish habitat.

1.2 Significance, objectives and novel contributions

3D modelling of meandering rivers still has challenges for accurate quantitative prediction of the flow hydro-morphodynamics. Models are sensitive to user-defined input parameters, and proper calibration of these parameters is essential. The review of the present state-of-the-art in the calibration of a 3D hydro-morphodynamic model revealed that relatively little attention has been paid to proper calibration of a 3D numerical model. Conventional calibration methods have mostly been based on adjusting the model inputs to match the measured data at discrete locations in the study reach (Papanicolaou, 2010). These methods do not account for the spatial distribution of the

3D flow field. Meanwhile, calibration attempts that use depth-averaged velocities could suffer from some inaccuracies (Kasvi et al., 2015a).

This study presents a novel methodology for use of 3D velocity data obtained with an ADCP for improved calibration of a 3D hydrodynamic model. 3D calibration with intensive velocity measurements leads to a model specifically parameterized to predict the 3D flow field. Using field observations of fully distributed 3D velocities throughout a natural river provides an opportunity for 3D model calibration that accounts for the variability and dynamics of the complex flow field in a meandering river. Moreover, it provides a detailed comparison between field measurements and simulated 3D model results throughout the model domain. The proposed calibration approach can advance model prediction of 3D flow complexity, and subsequently, enhances the potential for estimation of river processes such as channel morphodynamics and contaminant mixing.

Despite all attempts in numerical modelling of flow in rivers, less attention has been paid to validate such models for sharply curved bends using field data (Rodriguez et al., 2004; Kasvi et al., 2015a; Vermeulen et al., 2015). There are challenges in 3D hydrodynamic modelling of natural meandering rivers with complex bathymetry. Irregularity of the geometry and velocity distribution in natural rivers makes their flow structure more complex compared to laboratory experiments (Ferguson et al., 2003). The state of the art of the 3D hydrodynamic models revealed that these models have rarely been validated with the 3D velocity collected from the real field-based data of the natural rivers (Rodriguez et al., 2004). Validation of these models based on comparable field-based data may improve understanding of complex flow structures in natural meandering rivers and could help to develop a model which best replicates the dynamics of natural meandering rivers. Moreover, given the importance of pressure gradients in driving secondary circulation, it is worth investigating if hydrodynamic pressure can influence secondary circulation. Due to the higher computational cost of non-hydrostatic modelling, it is important to know whether a 3D hydrostatic model can be adequate for simulation of the flow structures in a natural river bend.

Delft3D-Flow is one of the most widely used hydro-morphodynamic models for river flow simulation (e.g. Williams et al., 2013; Javernick et al., 2016; Kasvi et al., 2015a,b).

However, it is still not clear to what extent one can rely on the results of a Delft3D hydrostatic model of a natural meandering river. To the best of our knowledge, the effect of hydrodynamic pressure assumption in Delft3D modelling of the secondary flow has still not been studied. This study aims to assess the performance of the hydrostatic versus non-hydrostatic hydrodynamic modelling of secondary flow in a tortuously meandering river using the Delft3D-Flow model. Performance of both models is assessed by comparing their results with velocity data collected in a sharp meander bend of a natural meandering river using an ADV.

There are still some uncertainties on the source and initiation of the meandering pattern and its migration. Particularly, the morphology and dynamics of confined meandering rivers are relatively poorly studied. The present study examined the migration behavior of two adjacent sub-reaches of a meandering creek to study the impact of confining medium on the river's hydro-morphodynamics. Both of these sub-reaches are meandering channels with cohesive bed and banks, but one is confined by a railway embankment. Given the prevalence of confined meandering rivers, enhancing the understanding of their behavior in the landscape is of essential and practical importance for sustainable river management.

The ecological condition of a river system, to a great extent, depends on its physical habitat (Maddock, 1999). Most morphodynamic-fish habitat studies have focused on the bed sediment grain size and distribution rather than the pattern and location of erosion and sedimentation. The long-term impacts of sediment transport on the aquatic species are still not well understood and more studies are needed to alleviate the potential effects of the sediment transport on the fish community (Kjelland et al., 2015). Accordingly, it is of practical and essential importance to identify and protect the fish which are sensitive to channel sedimentation and its associated sediment loads (Sullivan and Watzin, 2010).

The present study, for the first time, studies the correlation between a river's morphological development and the fish community. First, a 3D hydro-morphodynamic Delft3D model is developed for a natural cohesive meandering river. Total station topographic surveys were conducted to provide bathymetric change data for the morphodynamic module calibration. Spatially intensive ADCP surveys were also

conducted in the study area to yield data for the hydrodynamic module calibration. The 3D hydro-morphodynamic model was then calibrated based on the proposed 3D calibration approach and was run for a one-year period to assess how the fish habitat quality changed over this period. We performed two fish sampling surveys during the study to find correlation between the availability and utilization of physical fish habitat and the location of the erosion-sedimentation of the study creek. The results of the 3D hydro-morphodynamic model were then employed to develop a fish habitat model of juvenile yellow perch. It is proposed that the methodology and the parameters employed herein could be useful in similar case studies.

In summary, the present thesis will include the following novel contributions:

I. To propose a new methodology for use of 3D ADCP velocity data for improved calibration of a 3D hydrodynamic model.

II. To assess the performance of the hydrostatic versus non-hydrostatic hydrodynamic modelling of secondary flow in a tortuously meandering river using the Delft3D-Flow model.

III. To study the influence of meander confinement on hydro-morphodynamics of a cohesive meandering channel.

IV. To develop a long term 3D simulation of a natural cohesive meandering river and to find the impact of the river's morphological development on the fish habitat quality. This will involve development of a fish habitat model that specifically considers sediment erosion and deposition processes.

1.3 Thesis outline

The main outcomes of the present thesis are three published and one ready to submit journal papers:

I. Parsapour-Moghaddam, P., & Rennie, C. D. (2018). Calibration of a 3D hydrodynamic meandering river model using fully spatially distributed 3D ADCP velocity data. *Journal of Hydraulic Engineering*, 144(4), 04018010.

II. Parsapour-Moghaddam, P., & Rennie, C. D. (2017). Hydrostatic versus nonhydrostatic hydrodynamic modelling of secondary flow in a tortuously

meandering river: Application of Delft3D. *River Research and Applications*, 33(9), 1400-1410.

III. Parsapour-Moghaddam, P., & Rennie, C. D. (2018). Influence of meander confinement on hydro-morphodynamics of a cohesive meandering channel. *Water*, 10(4), 354.

IV. Parsapour-Moghaddam, P., Brennan, C. P., Rennie C. D., Elvidge, C. K., Cooke, S. J. (2018). Impact of channel morphodynamics on fish habitat utilization. Submitted.

The papers above form Chapters 2-5 of this thesis. The thesis is thus structured as follows. Chapter 2 is in line with the first objective of this thesis. This section proposes a novel methodology for an improved calibration of a 3D numerical model. Fully spatially distributed 3D ADCP velocity data were employed for calibration of a 3D hydrodynamic model in an attempt to alleviate the existing uncertainties of the calibration procedure. The results of different calibration approaches were compared to show the importance of choosing a proper calibration method based on the requirements of a problem. A natural tortuously meandering river was first simulated using the 3D hydrodynamic model. Total station survey was conducted to collect the bathymetric data of the study area. Spatially intensive ADCP surveying was conducted in the studied meandering channel to provide comprehensive field measurements for model calibration. To accurately and realistically compare the fully 3D predicted and measured velocities, a Matlab code was developed to match the location of each ADCP bin with 3D model grid points. The results of the proposed methodology were then analyzed.

It is shown that a properly calibrated 3D hydrodynamic model can better simulate the complex 3D flow field in a natural meandering river. The results suggest that different calibration approaches result in different calibration parameterizations whose simulated results can differ significantly from one another. This elucidates the importance of model calibration with comparable field data based on the nature and objectives of the numerical model. This process improves model prediction of 3D flow complexity, which

in turn enhances subsequent use of the model for estimation of river processes such as channel morphodynamics and contaminant mixing. The outcomes of this chapter are published in the Journal of Hydraulic Engineering (paper I).

Chapter 3 is in accordance to the second objective of the thesis. This section aims to assess the performance of the hydrostatic versus non-hydrostatic pressure assumption in 3D hydrodynamic modelling of a secondary flow using the Delft3D model. A 3D hydrodynamic model of a natural meandering river was developed. An ADV was employed to measure the 3D flow field in a sharp bend of the simulated meandering river during two different flow scenarios. The field-based ADV data were then employed to validate the simulated hydrodynamic models. To evaluate the performance of each model, different error statistics were calculated.

The results of this chapter illustrate the superior performance of the hydrostatic over nonhydrostatic 3D modelling of the secondary flow using Delft3D. Several possible reasons for the unfavorable performance of the nonhydrostatic version of Delft3D were discussed. Considering the uncertainties that may arise in both modelling and field measurements, the 3D hydrostatic Delft3D model is shown to be capable of reasonably predicting the river bend flow structures in the studied meandering creek. The results of this study are published in the River Research and Applications journal (paper II).

Chapter. 4 is in line with the third goal of this thesis. This chapter is a study of the hydro-morphodynamics of two adjacent sub-reaches of a meandering creek, located in the City of Ottawa, Canada. Both of these sub-reaches are meandering channels with cohesive bed and banks, but one is confined by a railway embankment while the other sub-reach is freely meandering. Channel migration and morphological changes of the channel banks along each of these sub-reaches are analyzed by comparing the historical aerial photography (2004, 2014), light detection and ranging (LIDAR) data (2006), bathymetric data obtained from a total station survey (2014), and field examination. Two different spatially intensive ADCP surveys were conducted in the study area to find the linkage between the hydrodynamics and morphological changes in the two different sub-reaches.

The results of this chapter reveal that the unconfined sub-reach tends to have a typical channel migration pattern with deposition on the inner bank and erosion on the

outer bank of the meander bend. In the confined sub-reach, an irregular meandering pattern occurred by the evolution of a concave-bank bench, which is caused by reverse flow eddies. The sinuosity of the confined sub-reach decreased in the 10-year study period. The results of this study demonstrate the physical mechanisms by which meander confinement can change the meandering pattern and hydro-morphological characteristics of a cohesive bed creek. The results of this study led to a publication in the Water journal (paper III).

Chapter 5 is in line with the fourth objective of the present thesis. The impact on fish habitat quality due to channel morphodynamics in a cohesive meandering creek was studied. Specifically, the impact of morphological development of a cohesive meandering creek on the quality of fish habitat available for juvenile yellow perch and white sucker was examined. A 3D morphodynamic model was first developed to simulate the hydro-morphodynamics of the study creek over a 1-year period. Two total station topographic surveys were conducted to provide bathymetric changes needed for the morphodynamic module calibration. Spatially intensive ADCP survey was conducted to come up with the data for the hydrodynamic module calibration. Two fish sampling surveys were carried out to determine the habitat utilization of each fish species in the study reach. The model predictions of morphodynamic changes (erosion and deposition) were incorporated into a fish habitat availability assessment at the end of the study period.

The results of ANOVA multiple comparison tests indicate that morphological development of the river was a significant factor ($\alpha < 0.05$) for the habitat utilization of juvenile yellow perch, whereas juvenile white sucker habitat utilization was not significantly impacted by the changes in the creek morphology. It is shown that juvenile yellow perch mostly utilized habitat where deposition occurred whereas they avoided areas of erosion. Flow depth, depth-averaged velocity and suspended sediment transport also significantly influenced presence of the juvenile yellow perch at the 5% significant level. As for the juvenile white sucker, the only significant habitat variable was the depth-averaged velocity. The results of the developed 3D hydro-morphodynamic model were then fed into the fish habitat model. Comparison of the predicted fish habitat map of the juvenile yellow perch with the results of fish sampling

surveys shows that the habitat quality is better predicted when the impact of morphological changes is taken into an account in the fish habitat modelling. The results of this study and the proposed methodology could provide some insights into the impact of sediment transport processes on the fish community. This has important implications for effective river management. The author conducted the morphodynamic and fish habitat modelling as well as the data analysis and ADCP surveying. This study is first authored by Parsapour-Moghaddam. This work has been submitted to a peer-reviewed journal (paper IV).

Finally, chapter. 6 summarizes the main conclusions of the present thesis followed by recommendations for future studies.

Other outcomes of this research not included in this thesis are:

V. Brennan, C. P., Parsapour-Moghaddam, P., Rennie, C. D., & Seidou, O. (2018). Continuous prediction of clay-bed stream erosion in response to climate model output for a small urban watershed. *Hydrological Processes*, 32(8), 1104-1119.

VI. Parsapour-moghaddam P., Rennie C.D., Slaney J. (2018). “Hydrodynamic simulation of an irregularly meandering gravel-bed river: comparison of mike 21 FM and Delft3D-Flow models”, *River Flow, Ninth International Conference on Fluvial Hydraulics*, Lyon, France.

VII. Parsapour-moghaddam P., Rennie C.D., Elvidge C., Cooke S. J (2017). “3D hydrodynamic-habitat modelling for prediction of yellow perch habitat”, *37th IAHR World Congress*, Kuala Lumpur, Malaysia.

VIII. Parsapour-Moghaddam, P., & Rennie, C.D. (2017). 3D versus 2D calibration of a 3D hydrodynamic model. *37th IAHR World Congress*, Kuala Lumpur, Malaysia.

IX. Parsapour-moghaddam P., Rennie C.D., Midwood J., Cvetkovic M., Cooke S.J. (2015). Influence of channel erosion on fish habitat utilization. *36th IAHR World Congress*, Hague, Netherlands.

X. Parsapour-Moghaddam, P., & Rennie, C. D. (2015). ADCP validation of 3D morphodynamic modelling in clay-bed meandering rivers. *36th IAHR World Congress*, Hague, Netherlands

XI. Parsapour-Moghaddam, P., & Rennie, C.D. (2014). Morphodynamic modelling of a tortuous meandering clay bed river using Delft3D: Stillwater Creek, Ottawa. *River Flow, International Conference on Fluvial Hydraulics*: 1163-117.

CHAPTER 2

Calibration of a 3D Hydrodynamic Meandering River Model Using Fully Spatially Distributed 3D ADCP Velocity Data[1]

Abstract

This study employs fully spatially distributed three-dimensional (3D) velocity data for improved calibration of a 3D hydrodynamic model. Conventional calibration methods do not account for the spatial distribution of the fully 3D flow field. This study compares the results of the proposed calibration approach with those available in the literature to show how choosing different calibration methods can change the model predictive capability. The proposed calibration approach can advance model prediction of 3D flow complexity, and subsequently, enhances the potential for estimation of river processes such as channel morphodynamics and contaminant mixing. To test the proposed methodology, a tortuously natural meandering river is simulated using the Delft3D hydrodynamic model. Spatially intensive acoustic Doppler current profiler (ADCP) velocity data collected throughout the river model domain provide fully 3D distributed velocities for model calibration. For accurate and realistic comparison of the fully 3D predicted and measured velocities, an algorithm is developed to match the location of each ADCP bin with 3D model grid points. The results of this study demonstrate that the fully 3D calibration method leads to a different calibrated model parameterization than that obtained from conventional calibration approaches. T-test analysis illustrates that, with or without implementation of the Horizontal Large Eddy Simulation (HLES) model option, the model results are sensitive to the user input background horizontal eddy viscosity, confirming the importance of an appropriate calibration of the developed 3D model. Results of different calibration approaches are validated using 3D velocity data

[1] This chapter has been published as: **Parsapour-Moghaddam, P**., & Rennie, C. D. (2018). Calibration of a 3D Hydrodynamic Meandering River Model Using Fully Spatially Distributed 3D ADCP Velocity Data. Journal of Hydraulic Engineering, 144(4), 04018010.

collected at a bend section in the river using an Acoustic Doppler Velocimeter (ADV). It is shown that the proposed 3D calibration approach results in the best model performance. The results of this study suggest that the proposed methodology can provide a better calibration potential for simulation of natural meandering rivers with complex geometry.

Keyword: 3D Hydrodynamic modelling; Delft3D; 3D calibration; ADCP; ADV; natural meandering river

2.1 Introduction

2.1.1 Numerical modelling

Fluvial hydrodynamics and resulting morphological changes in river channels have been studied for many years (e.g. Jansen et al. 1979; Yalin and da Silva 2001; Garcia 2008; Li and Millar, 2011). During the last few decades, numerical modelling of flow has been applied extensively as a useful tool in solving river engineering problems. Numerical models are powerful tools to simulate river processes. Using computational methods, numerical models solve sets of non-linear differential equations describing hydro-morphodynamics of river channels. Particularly for smaller space-time domains, 3D models are now widely applied in flow and sediment transport modeling (e.g. Shimizu et al. 1990; Olsen and Stokseth 1995; Sinha et al. 1998; Lane et al. 1999; Wu et al., 2000; Koçyigit et al. 2002; Zeng et al. 2005; Khosronejad et al. 2007; Ruther and Olsen 2007; Zeng et al., 2008; Van Sabben, 2010; Sinha et al., 2012; Kamel et al. 2014; Parsapour-Moghaddam and Rennie 2014). Depending on the conditions of a problem, diverse numerical modelling methods may be employed.

The Delft3D package is an extensively used 3D hydro-morphodynamic open source code which is developed by Deltares and can be utilized in a broad range of applications. (e.g. Hosseini and Coonrod, 2011; Trouw et al., 2012; Williams et al., 2013, Canestrelli et al., 2014; Schuurman and Kleinhans, 2015, Javernick et al., 2016; Kail et al., 2015, Kasvi et al., 2015). Several studies have applied numerical models to meandering rivers. The complex nature of the flow in curved channels generally

requires a 3D simulation (Lane et al., 1999; Rodriguez, 2004; Kasvi et al., 2013a). However, 3D hydrodynamic modelling of meandering rivers could still have drawbacks in quantitative approximations of hydraulic variables (Kasvi et al., 2015a). In the present study, Delft3D is employed to develop a 3D hydrodynamic numerical model of a natural tortuously meandering river. The results of the developed model are evaluated against fully spatially distributed 3D ADCP velocity data.

2.1.2 **Model calibration with field measurements**

Numerical models should have the capability to model natural rivers considering their dynamics and variability. To make accurate predictions of flow characteristics and morphological changes, it is essential to calibrate the model properly. Calibration of a hydrodynamic model is commonly done by adjusting the model inputs such that model outputs match available measured data (Papanicolaou et al., 2010). Nevertheless, the calibration process is disputable and still suffers from some inadequacies (Van De Wiel et al., 2011). Previous studies that used field measurements for evaluation of the model were shown to have problems with quantitative estimation of hydraulic variables (Dargahi, 2004; Rodriguez et al., 2004; Nicholas et al., 2012). Furthermore, expensive data are required for calibration of a 3D model to acquire reliable and realistic predictions from these models (van Rijn, 1989). Some of the traditional calibration attempts involve reproducing the flow depth; however, a calibrated model that correctly simulates the observed water elevation can not necessarily produce the 3D flow field (Wagner and Mueller, 2002). Accordingly, comprehensive field work should be conducted to apprehend the intricacies of a 3D flow field (Mashriqui, 2003). In particular, the complexity of flow in natural meandering rivers demands that careful attention is paid to 3D model calibration for reliable prediction of the full 3D flow field.

To calibrate the model reliably, it is important to have accurate measurements of the flow field. Traditional methods to measure flow velocity in rivers, such as propeller meters, provide sparse data (Stone and Hotchkiss, 2007). More recently, acoustic Doppler current profilers (ADCP) have been extensively applied to estimate the mean water velocity field (Abad et al., 2004; Garcia et al., 2007; Vermeulen et al., 2011;

Vermeulen et al., 2014, Vermeulen et al., 2015). These instruments can provide spatially dense velocity fields (e.g., Rennie and Millar, 2004; Rennie and Church, 2010; Jamieson et al., 2011; Venditti et al., 2014), which facilitate numerical model calibration and validation. For example, Alvarez et al. (2016) recently validated a Detached Eddy Simulation model of canyon flow using cross-sectional ADCP velocity data.

Wagner and Mueller (2002) calibrated and validated a 2D model using ADCP velocity data collected at different cross sections. Viscardi et al. (2006) conducted 3D ADCP velocity measurements to analyze the flow pattern in cross-sections spaced every 100 m in a river bend. They compared the results based on 3D-RANS (Reynolds averaged Navier Stokes) simulations using the SSIIM model with the velocity field obtained from the ADCP. Williams et al. (2013) calibrated their developed 2D model using spatial observations of depth and depth-averaged velocity obtained with an ADCP. They showed that proper calibration is critical for accurate prediction of lateral variations in depth-averaged velocity; calibration based only on water level and depth would not be adequate. They subsequently employed spatially continuous ADCP data to find linkage between morphodynamic and hydrodynamic processes (Williams et al. 2015).

Parsapour-Moghaddam and Rennie (2015) utilized depth-averaged velocity obtained from an intensive spatial ADCP survey to calibrate a 3D morphodynamic model. They concluded that the developed validated model can be utilized for improved approximation of boundary shear stress and sediment processes. Kasvi et al. (2015a) made a sensitivity analysis of 2D and 3D models in a natural meandering river. They evaluated the model performance with measured ADCP and multi-temporal mobile laser scanning data. They showed that both 2D and 3D models could agreeably simulate depth-averaged velocity; however, there was a significant difference between the predicted and measured near-bed flow. The authors suggested improving the calibration and validation data to determine the reasons of the mismatch between simulations and measurements.

The present state-of-the art in calibration of a 3D hydrodynamic model revealed that relatively little attention has been paid to proper calibration of a 3D numerical model. Conventional calibration methods mostly used available data measured at a few

sections. On the other hand, 3D modelling of meandering rivers still has challenges for accurate quantitative prediction of the flow hydrodynamics. Models are sensitive to user-defined input parameters, and proper calibration of these parameters is essential. This study proposes a novel methodology for calibration of a 3D numerical model. We compare the results of different calibration approaches to show the importance of choosing a proper calibration method based on the requirements of a problem. In the present study, we employ fully spatially distributed 3D ADCP velocity data for calibration of a 3D hydrodynamic model in an attempt to alleviate the existing uncertainties of the calibration procedure.

2.1.3 **Objectives, novelty and structure**

The objective of this study is to present a methodology for use of 3D ADCP velocity data for improved calibration of 3D hydrodynamic models. We also intend to demonstrate that a properly calibrated 3D hydrodynamic model can better simulate the complex 3D flow field in a natural meandering river. To the best of our knowledge, fully spatially distributed 3D ADCP velocity data have not previously been used for calibration of a 3D hydrodynamic model. We compare the results of the proposed calibration approach with conventional methods, available in the literature, to show how employing different calibration methods could change the model predictive capability. Model calibration with fully spatially distributed 3D distributed velocity data provides detailed comparison between field measurements and simulated 3D model results throughout the model domain. The calibration process provides the opportunity for improved estimates of spatially varying calibration parameters such as Manning roughness and background horizontal eddy viscosity, both of which may vary significantly throughout a river domain with complex geometry. This process improves model prediction of 3D flow complexity, which in turn enhances subsequent use of the model for estimation of river processes such as channel morphodynamics and contaminant mixing.

In this study, we focus on model calibration of the 3D hydrodynamics. To this end, a natural tortuously meandering river is first simulated using the 3D hydrodynamic model.

The study area is depicted in Section 2.2, followed by detailed description of the numerical model in Section 2.3.1. Spatially intensive ADCP surveying was conducted in the studied meandering channel to provide comprehensive field measurements for model calibration. The methods employed for field measurements are explained in Section 2.3.2. Finally, a Matlab code was developed for statistical comparison of the predicted and measured 3D velocity fields (Section 2.3.3), which allows for improved model calibration and validation (Section 2.4). We conclude with a discussion (Section 2.5) and conclusion (Section 2.6).

2.2 Study area

This study aims to simulate hydrodynamic characteristics of Stillwater Creek, a tortuously meandering clay-bed river in the City of Ottawa, Canada. Figure 2.1 illustrates the study site location. The length of the studied area is 190 m, with a slope of 0.0026 and an average width of 8 m. Close to the upstream of the creek (~ 434858 m, 5020570 m), there is a culvert under a farm road ford, which was an attempt to engineer off-channel habitat for the native cool water fish community. However, due to the misalignment of the culvert, it led to excessive erosion and exacerbated tortuous meandering in the downstream end of the reach. Since construction of the culvert and ford, the sinuosity of the channel has increased from about 2.2 to 2.8 (Parsapour-Moghaddam and Rennie, 2014). A numerical model of the reach was developed to facilitate management of the river to optimize habitat for the fish community.

2.3 Research methodology

In this section the 3D numerical model, the field measurements, and the proposed calibration procedure are described.

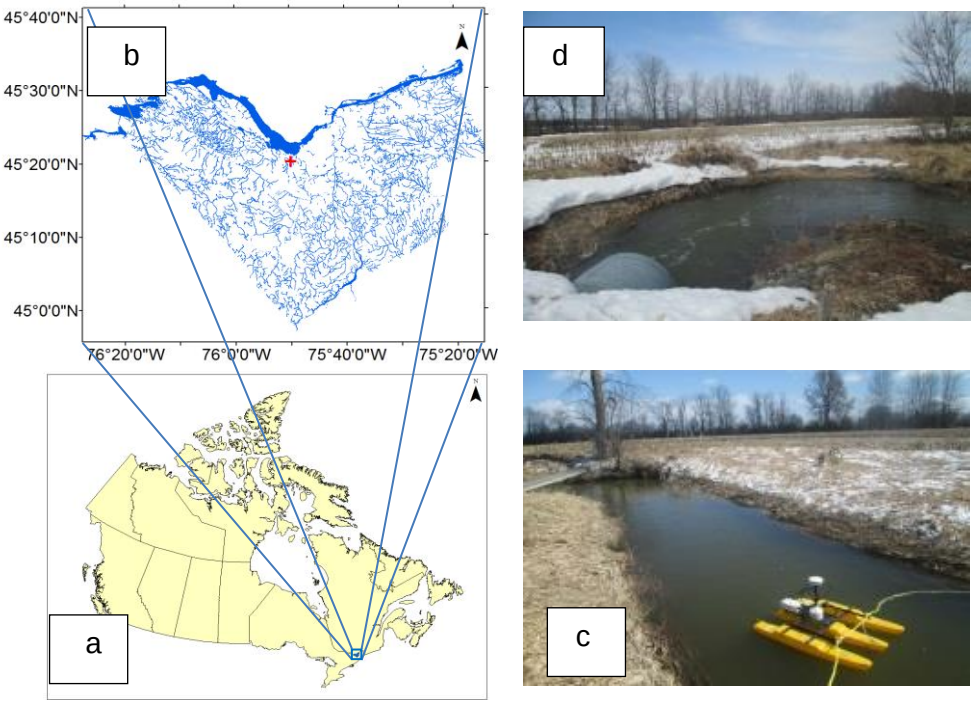

Figure 2.1. (a) Location of the study area in Canada [adopted from https://www12.statcan.gc.ca], (b) Studied reach located in the drainage network of the Ottawa area; Stillwater Creek drains northward to Ottawa River [adopted from http://data.ottawa.ca/en/dataset/rivers], (c) ADCP surveying in the area of study looking downstream toward the end of the reach, (d) The location of the culvert, flow from South (bottom) to North (top)

2.3.1 **Numerical modelling**

The Delft3D modelling package (Delft-Flow version 4.01.01) was used for 3D hydrodynamic simulation of a natural meandering river. Delft3D is an open source code developed by Deltares. This code consists of different modules that can be employed independently or in combination with other modules (Deltares, 2014). Delft-Flow simulates multi-dimensional (2D or 3D) hydro-morphodynamic processes on a rectilinear or a curvilinear grid. The standard 3D hydrostatic formulation of Delft3D was employed. It solves non-linear 3D shallow water equations based on 3D Navier-Stokes equations under Boussinesq assumptions for incompressible flow. The 3D shallow water equations include flow continuity and 3D momentum equations in the two horizontal directions. No vertical momentum equation is employed, and hydrostatic pressure is assumed. Vertical velocity is thus determined from flow continuity. The effects of non-hydrostatic pressure in sharp bends and scour locations have been

previously studied (Vermeulen et al., 2015; Li and Zheng, 2016). The authors are currently studying hydrostatic versus non-hydrostatic hydrodynamic modelling of secondary flow in strongly meandering rivers using Delft3D. Further details on numerical aspects of Delft3D can be found in Lesser et al. (2004) and Deltares (2014).

The model domain covered the study area previously described in Section 2.2 (Figure 2.2). Total Station survey was conducted to collect the topography and bathymetric data (Figure 2.3a). To account for simulation of overbank flow, areas adjacent to the river and above the existing culvert were also included in the domain. A curvilinear grid was then built with an average grid resolution of $0.5\ m$ and a time step of $0.0025\ s$ to meet the stability condition. The mesh was refined until reasonable results were obtained, and finer grids were employed in the areas with higher velocity gradient (grid resolution ~ $0.25\ m$). Figures 2.2a and 2.2b show the generated mesh over the study area and orthogonality of the grid as an indication of mesh quality. Figure 2.2c illustrates the initial flow depth in the study reach.

A sigma coordinate grid was used indicating that regardless of the local water depth, the number of active layers was constant (Deltares, 2014). To resolve the logarithmic velocity profile throughout the water column, smaller layer thickness was used near the bed; that is, from the river bed to the water surface layer thicknesses (percentages of water depth) were as follows: $2, 3, 4, 6, 8, 10, 12, 15, 20, 20\ \%$. Moreover, to simulate flow through the culvert in the reach, the culvert module of Delft3D was employed. Based on the ADCP measurements, a downstream water level of 61 m and an upstream discharge of 0.85 m^3/s were specified as the boundary conditions of the reach. The 3D k– ε turbulence closure model, based on the eddy viscosity concept of Kolmogorov and Prandtl, was employed to account for the effect of 3D turbulent motions. In Delft3D-Flow, eddy viscosity is assumed to be anisotropic; i.e., the horizontal eddy viscosity is much larger than the vertical eddy viscosity. Delft3D calculates the vertical eddy viscosity (ν_v) based on the following equation:

$$\nu_v = \nu_{mol} + \max(\nu_{3D}, \nu_v^{back}) \quad (2\text{-}1)$$

In the above equation, ν_{mol} is kinematic viscosity of water and ν_{3D} is calculated based on the 3D-turbulence closure model. The parameter ν_v^{back} is the background or

“ambient” vertical eddy viscosity, which is a user-defined value, and accounts for all types of unresolved mixing. Horizontal eddy viscosity (ν_H) is calculated based on the below equation:

$$\nu_H = \nu_v + \nu_H^{back} + \nu_{SGS} \quad (2\text{-}2)$$

Where ν_v accounts for the 3D turbulence. The parameter ν_H^{back} is a background horizontal eddy viscosity, which is a user defined input file associated with the horizontal turbulence that is not resolved by the Reynolds-averaged shallow-water equations. The parameter ν_{SGS} is referred to as the sub-grid scale (SGS) turbulence which is not resolved by the horizontal grid. Delft3D-Flow uses horizontal large eddy simulation (HLES) for simulation of the larger scale horizontal turbulence. The corresponding v_{SGS} is then calculated via a SGS-turbulence model (Deltares, 2014).

As will be shown, the value set for the background horizontal eddy viscosity can impact the results significantly both in cases where HLES was employed or when it was turned off. Consequently, calibration of the background horizontal eddy viscosity (ν_H^{back}) is the primary focus of this study. We will illustrate the importance of a proper calibration of a 3D hydrodynamic model of a meandering river using Delft3D.

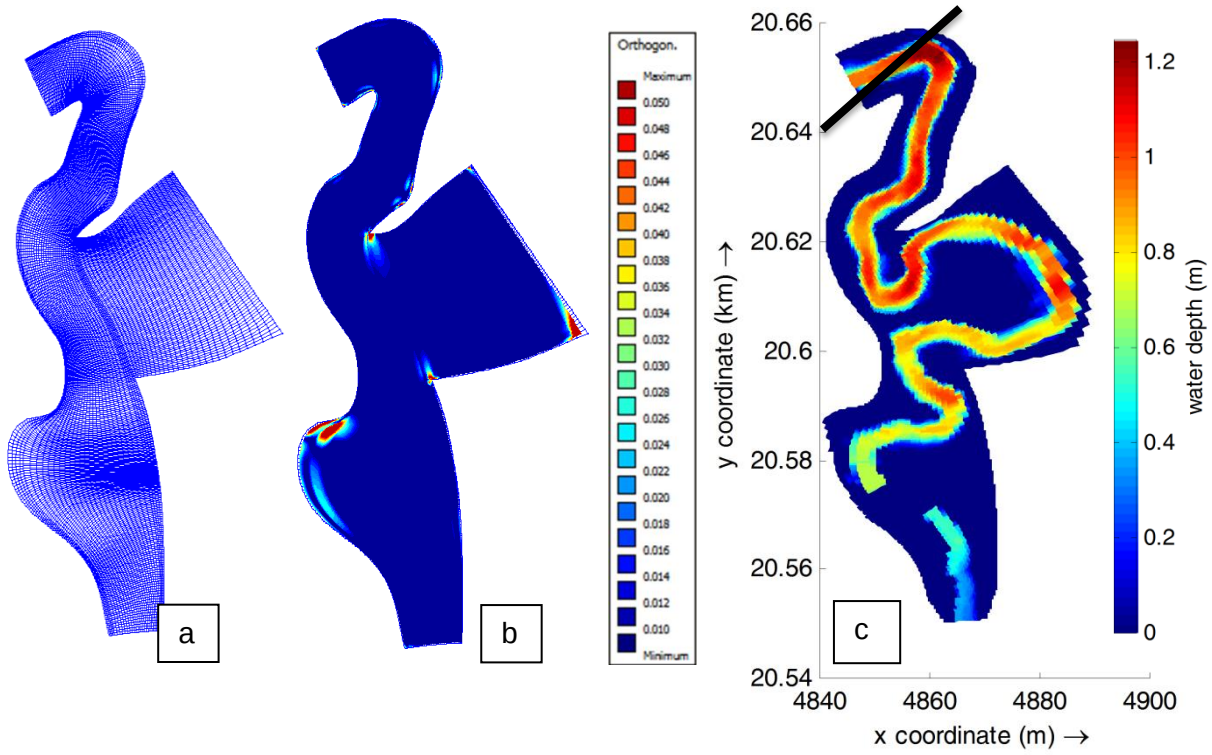

Figure 2.2. (a) Computational mesh (b) Orthogonality of the generated grids (c) Initial water depth in the study area; note that the first two digits of the UTM East (X) and North (Y) coordinates are removed from the plot. The black line shows the cross section used for the results validation (Figure 2.9).

2.3.2 **Intensive field survey**

In this study, fully spatially distributed 3D velocity data were acquired by intensive spatial ADCP survey of Stillwater Creek on 16 April 2014 (Figure 2.3b). An ADCP is a hydroacoustic instrument that measures the 3D flow velocities using the Doppler effect of backscattered sound waves within the vertical water column. Flow velocities are calculated according to the reference frame of the ADCP. If the instrument is mounted on a moving boat, a boat velocity correction should be applied to attain the flow velocity in earth coordinates (Simpson, 2001). An ADCP deployed on a moving boat can be appropriately utilized to determine the 3D flow field and bathymetric data (e.g., Rennie and Church, 2010; Jamieson et al. 2011; Muste et al., 2012; Venditti et al., 2014; Williams et al. 2015). Further detailed information on ADCP theory is available in

Simpson and Oltman (1993), Morlock (1996), Simpson (2001), Muste et al. (2004), and Rennie and Church (2010).

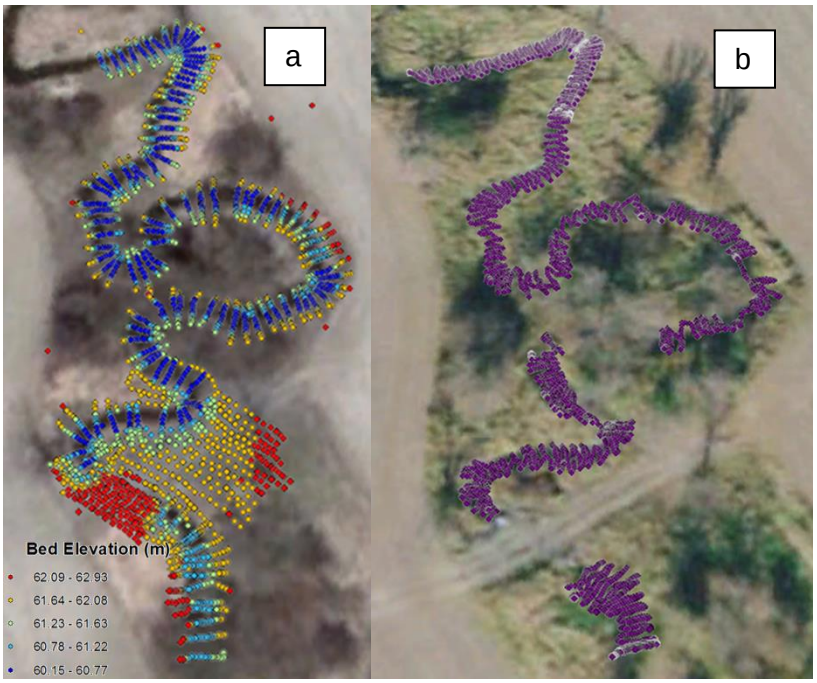

Figure 2.3. (a) Total station surveyed points (b) Track of ADCP survey on the study reach. Background image is taken from the Google Earth.

In this study, a Sontek M9 River Surveyor ADCP was mounted on an Ocean Sciences trimaran riverboat. The compass was calibrated *in situ*. The M9 River Surveyor used $1\,Hz$ sampling frequency. Average flow depth was $0.7\,m$ and ADCP average vertical resolution (bin size) was $0.026\,m$. The trimaran was manipulated with ropes by two operators standing at each side of the river, who moved the boat downstream in a zigzag pattern in closely spaced transects ($0.25\,m$ to $1\,m$ spacing). It is worth noting that due to the presence of a log jam during our survey that could not being removed, we were not able to survey a portion of the neck of the largest meander (Figure 2.3b). Furthermore, ADCP data were collected in greater density in the downstream bend because we were particularly interested in good calibration in this location. Post processing of the measured data was done using in-house Matlab codes

(Rennie and Church, 2010). The intensively surveyed 3D flow velocities were then employed for calibration of the 3D hydrodynamic model of a strongly meandering channel.

2.3.3 **Model calibration**

To study whether different calibration approaches yield diverse calibration parameters, we calibrated the developed 3D model based on three different approaches. At first, we calibrated the 3D model based on a typical calibration approach in which the available data in a few sections would be employed (e.g., Parsons et al., 2013; Vermeulen et al., 2014; Vermeulen et al., 2015). We used the fully 3D velocity flow field which were averaged out in the repeated transects in a riffle and two pool sections of the study area. We refer to this approach as the discrete section calibration approach. It should be noted that in this study, the ADCP measurements were carried out in a spatial zig-zag pattern. Thus, in order to account for the velocity data in the repeated surveyed sections, we considered sections that were close enough (~0.25 cm) to be studied as repeated transects. We used the velocity data of four ADCP transects which were interpolated to the grid employed for data analysis (e.g. Jamieson et al., 2011). Another calibration approach was carried out based on spatial distribution of the depth-averaged velocities (e.g., Williams et al., 2013). This calibration approach exploits a spatial coverage of the study area; however, it considers the depth-averaged velocities as opposed to the fully 3D velocities. Henceforth, we refer to this method as the 2D calibration.

The proposed improved calibration procedure involved comparison of collocated simulated and measured 3D velocities throughout the 3D domain. That is, the simulated 3D velocity components were compared with those obtained by ADCP both spatially and vertically throughout the water column. This approach is referred to the 3D calibration approach. A Matlab code was developed for this purpose. In this code, based on their measurement locations the ADCP single bin 3D velocities are matched to grid points of the 3D numerical model. Co-location is non-trivial, because model grid cells and ADCP velocity bins are non-coincident and vary in size throughout the

domain. The grid cells have variable yet fixed horizontal dimensions, but fluctuate in the vertical dimension based on local depth. Due to SmartPulse on-the-fly changes in measurement mode, the M9 ADCP velocity bins vary in vertical dimension, with larger bin sizes utilized for greater flow depths. Consequently, centres of model grid cells and ADCP velocity bins were matched in the present work. For each grid point in the boundary mesh, all ADCP measured velocity bin locations were searched. If the horizontal distance between the centres of the model grid point and an individual ADCP velocity bin was less than $5\ cm$, then the coordinates of the matched points were saved. In the next step, the matched points were compared vertically to collocate modelled velocity cells and individual ADCP bin points. Specifically, a measured ADCP bin was matched to a modelled cell if the vertical distance between their centres was less than 1cm. This procedure was repeated for all grid points in the boundary mesh to yield a data set of matched collocated measured and predicted 3D velocities throughout the domain.

To assess the accuracy of the model after calibration, the following model error statistics were employed:

$$MAE = \sum_i^n \frac{|x_{mod} - x_{obs}|}{n} \tag{2-3}$$

$$MAE_R = \sqrt{MAE_x^2 + MAE_y^2 + MAE_z^2} \tag{2-4}$$

$$MAE_H = \sqrt{MAE_{\bar{x}}^2 + MAE_{\bar{y}}^2} \tag{2-5}$$

where x_{obs} indicates measured velocity at bin *i* and x_{mod} represents simulated velocity at the collocated grid cell, MAE stands for mean absolute error, MAE_R is the resultant of MAE for each velocity component in the x (east), y (north), and z (vertical) directions, and MAE_H is the resultant mean absolute error based on depth-averaged velocity components in the horizontal x and y directions.

Background horizontal eddy viscosity (ν_H^{back}) and Manning roughness (n) were the model parameters varied to improved model performance. Manning roughness incorporates interactions of the flow with the boundary while horizontal eddy viscosity accounts for internal shear stresses of the fluid caused by flow turbulence

(Papanicolaou et al., 2010). First, sensitivity analysis and initial calibration on $\nu_H^{back}$and *n* were performed to determine which of these two parameters most influenced model results. To this end, the fully 3D calculated error statistic MAE_R was used to compare simulated 3D velocities with collocated 3D ADCP velocities. As will be shown below, the model proved to be more sensitive to the background horizontal eddy viscosity. The model was then calibrated in detail by optimizing ν_H^{back} to minimize the calculated MAE_R, which ensured that the predicted model results best matched the observations.

2.4 Results

Figures 2.4 and 2.5, respectively, show the $\mathrm{MAE_R}$ velocity error cumulative distribution function (CDF) for each sensitivity analysis model run, varying Manning roughness and background horizontal eddy viscosity within reasonable ranges. To study the effect of the HLES model on the simulation results, we also employed HLES while setting background horizontal eddy viscosity to zero. It should be emphasized these sensitivity analyses were done based on the 3D velocity vectors both spatially and vertically all through the study reach. Comparing Figure 2.4 and 2.5, one can infer that the velocity error distributions vary more significantly with changes in the background horizontal eddy viscosity compared to the Manning roughness. It should be noted that analysis based on a reasonable range of background horizontal eddy viscosity confirmed that the change in the Manning roughness could not significantly affect the velocity error distributions. Moreover, it can be seen that using the HLES model alone cannot necessarily guaranty reliable model predictions (Figure 2.5). This confirms the necessity of an appropriate calibration of the background horizontal eddy viscosity even in the cases where HLES is employed. Based on Figure 2.4, Manning roughness was set to be 0.015 which yielded the lowest CDF velocity error and resulted in the reasonable approximation of the channel roughness based on the flow measurements and channel geometry. Subsequently, background horizontal eddy viscosity was used for further calibration.

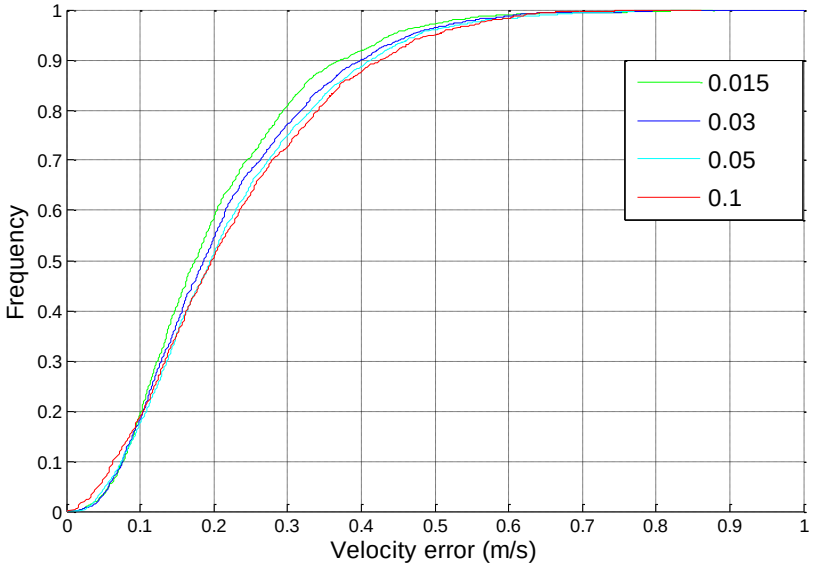

Figure 2.4. Cumulative frequency velocity error distributions for roughness sensitivity analysis. The legend shows different values of Manning roughness.

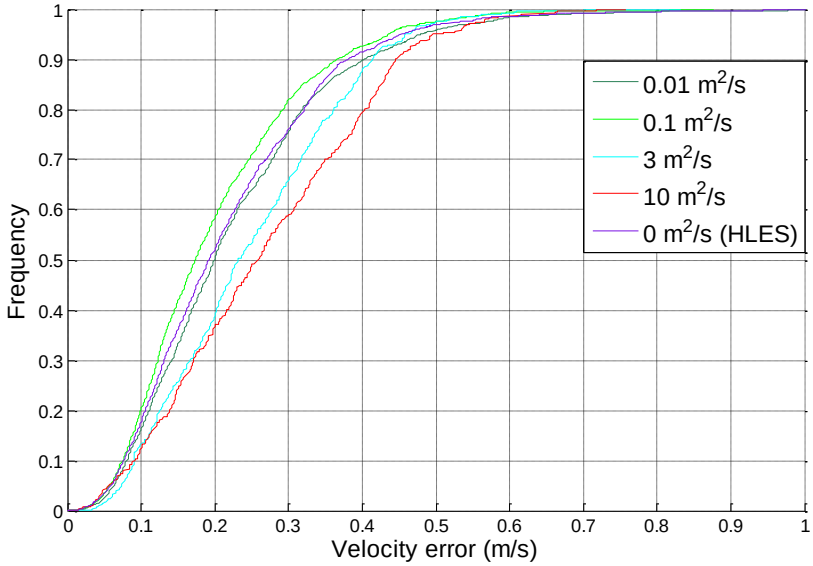

Figure 2.5. Cumulative frequency velocity error distributions for background horizontal eddy viscosity sensitivity analysis. The legend shows different values of background horizontal eddy viscosity.

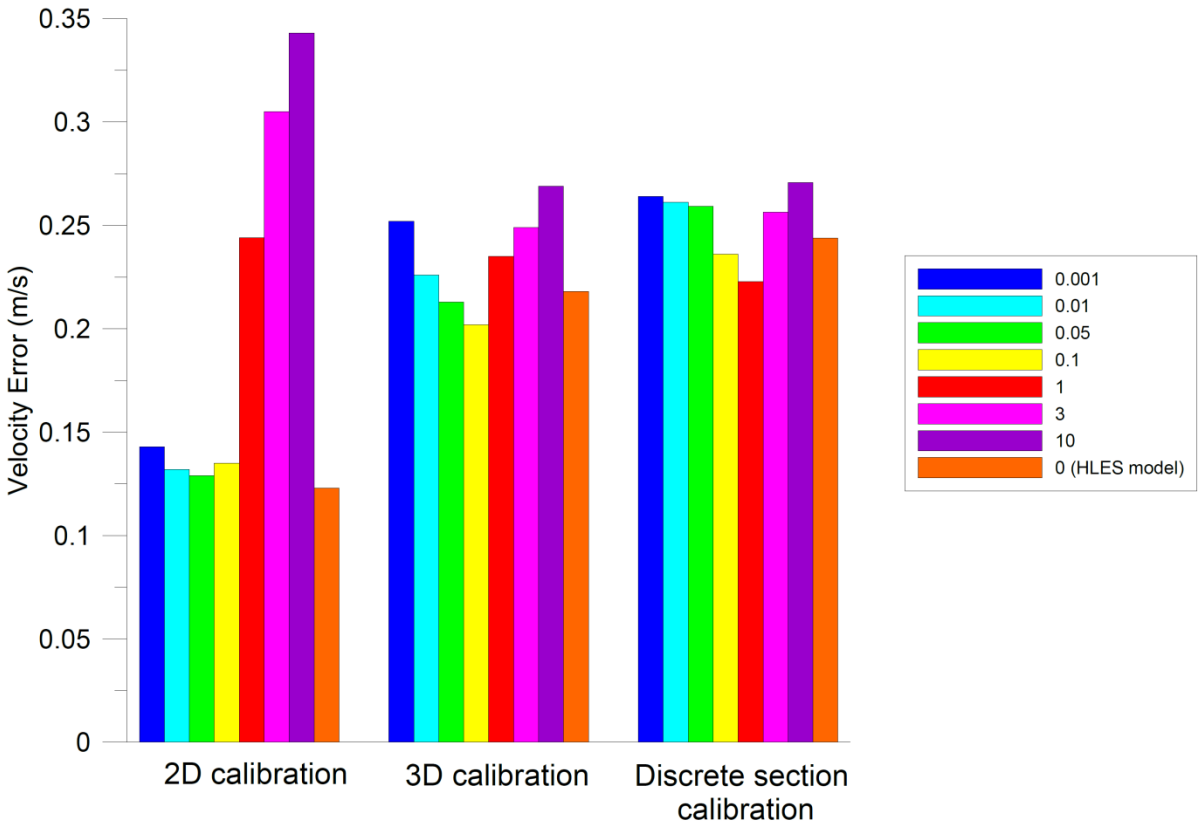

Figure 2.6. Velocity errors obtained in different calibration approaches; $\mathbf{MAE_H}$ in the 2D calibration and $\mathbf{MAE_R}$ for 3D calibration and discrete section calibration. The legend describes the background horizontal eddy viscosity (m^2/s) employed for each model run, with values provided in the same order as the bar graphs for each calibration method.

Figure 2.6 shows the results of the different calibration approaches explained in Section 3.3. As can be seen, $\nu_H^{back} = 1\, m^2/s$ was obtained using the discrete section calibration, and 2D calibration led to the HLES model in which $\nu_H^{back} = 0\, m^2/s$. In the cases that HLES model option was not employed, 2D calibration indicated that $\nu_H^{back} = 0.05\, m^2/s$ had the lowest amount of velocity error whereas 3D calibration led to $\nu_H^{back} = 0.1\, m^2/s$ either with or without the HLES model. Thus, it can be seen that different calibration approaches resulted in diverse calibration parameterizations.

Moreover, it can be inferred that the 3D calibration approach is more sensitive to small changes in the background horizontal eddy viscosity.

To study which calibration method can produce more accurate fully 3D flow modelling results, we examined models run employing the values of ν_H^{back} found as optimum using each of the calibration approaches. As explained above, optimum ν_H^{back} values were 0.1 m^2/s (3D calibration), 1 m^2/s (discrete section calibration), and either 0.05 m^2/s or 0 m^2/s with HLES (2D calibration). Each model was evaluated using modelled versus measured regression statistics. Regression analyses were done separately on horizontal velocity vector components in the fully spatially distributed 3D velocity flow fields. For each case the estimated best-fit regression equation (modelled versus measured, assuming errors in modelled results), and the inverse relation (measured versus modelled, assuming errors in measured data), are provided in Table 2.1. As can be inferred from Table 2.1, use of $\nu_H^{back} = 1\, m^2/s$, as was suggested by the typical discrete section calibration approach, results in a model that does not perform satisfactorily; i.e, both the slope and inverse slope are much farther from unity than the model runs using the other ν_H^{back} values. We carry forward both the 2D and 3D calibration approaches for further analysis.

Figures 2.7 and 2.8 illustrate the model results with $\nu_H^{back} = 0.1\, m^2/s$, $\nu_H^{back} = 0.05\, m^2/s$ and also $\nu_H^{back} = 0\, m^2/s$ (HLES model). As can be seen, lower background horizontal eddy viscosity led to higher modelled depth-averaged velocities (Figure 2.7) and bed shear stresses (Figure 2.8). It can be inferred that the choice of model calibration approach heavily influences the simulated results.

Table 2.1. Regression relation parameters of the best fit analysis for results of different calibration approaches. The standard error of each parameter is shown in the parenthesis.

	ν_H^{back} (m²/s)	Slope	Intercept	Slope (inverse)	Intercept (inverse)	r square
vx	HLES Model ($\nu_H^{back} = 0\ m^2/s$)	0.734 (0.011)	-0.015 (0.003)	0.901 (0.014)	0.016 (0.003)	0.669
	1	0.537 (0.011)	-0.023 (0.003)	1.382 (0.027)	0.018 (0.005)	0.743
	0.05	0.735 (0.011)	-0.012 (0.003)	0.939 (0.014)	0.013 (0.003)	0.691
	0.1	0.718 (0.010)	-0.014 (0.003)	0.994 (0.014)	0.013 (0.003)	0.713
vy	HLES Model ($\nu_H^{back} = 0\ m^2/s$)	0.601 (0.013)	0.108 (0.004)	0.836 (0.017)	0.000 (0.006)	0.529
	1	0.390 (0.010)	0.043 (0.003)	1.588 (0.041)	-0.009 (0.008)	0.620
	0.05	0.597 (0.012)	0.088 (0.004)	0.933 (0.018)	0.003 (0.006)	0.557
	0.1	0.562 (0.011)	0.092 (0.004)	1.012 (0.019)	-0.013 (0.006)	0.569

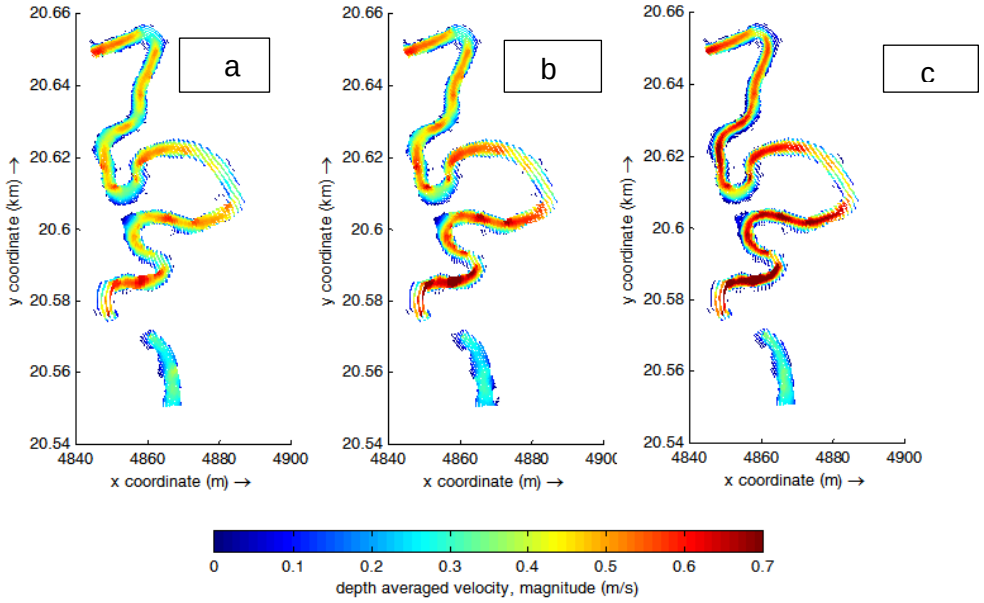

Figure 2.7. Simulated depth-averaged velocity when (a) $\nu_H^{back} = 0.1\ m^2/s$ (b) $\nu_H^{back} = 0.05\ m^2/s$ (c) $\nu_H^{back} = 0\ m^2/s$ with HLES turbulence model. Flow from bottom to top. Note that the first two digits of the X and Y coordinates are removed from the plots. The figures are shown in the same scale.

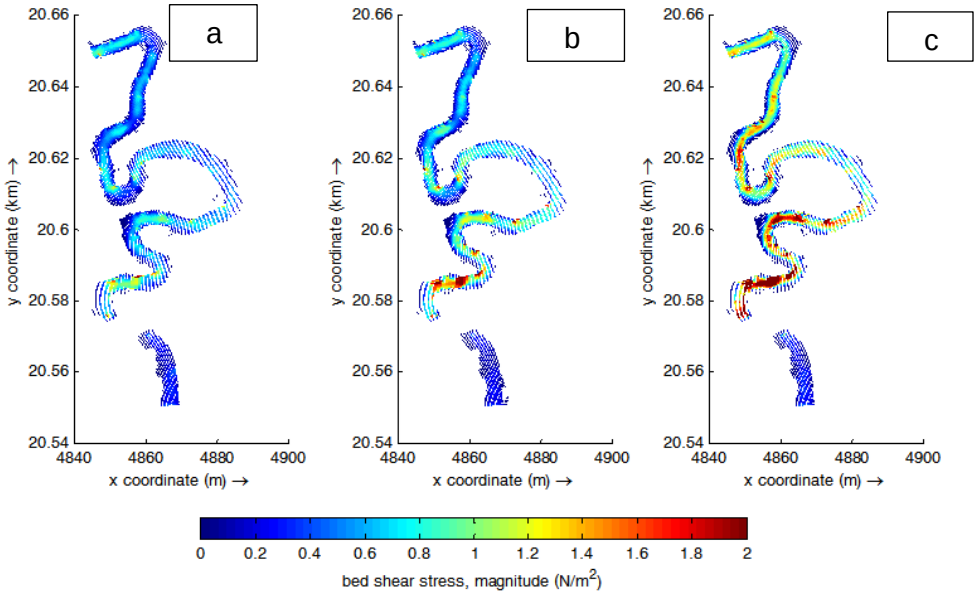

Figure 2.8. Simulated bed shear stress when (a) $\nu_H^{back} = 0.1\ m^2/s$ (b) $\nu_H^{back} = 0.05\ m^2/s$ (c) $\nu_H^{back} = 0\ m^2/s$ with HLES turbulence model. Flow from bottom to top. Note that the first two digits of the X and Y coordinates are removed from the plots. The figures are shown in the same scale.

To validate the results of the 3D model obtained with the 2D and 3D calibration approaches, we employed an Acoustic Doppler velocimetry (ADV) to measure 3D velocity at one section in the last bend of the studied reach (section location shown in Figure 2.2c). Figure 2.9 compares the measured streamwise velocity (Figure 2.9a) with the simulated values based on horizontal eddy viscosities of $0\,m^2/s$ (HLES) and $0.05\,m^2/s$ (both of which obtained from 2D calibration) and $0.1\,m^2/s$ (based on the proposed 3D calibration). As is shown, the model that was calibrated based on the proposed calibration approach (Figure 2.9b) provided the best match with the ADV measurements. Both models (Figures 2.9c and 2.9d) that were calibrated based on spatial distribution of the depth-averaged velocities (2D calibration) did not perform satisfactorily and the results did not correspond well with the measurements. It is also worth mentioning that local velocity disturbance close to the outer bank (Figure 2.9a) is due to the presence of woody debris in the studied reach which could not be simulated by the model. This velocity disruption may have caused a patch of greater error in the simulated velocity near the outer bank.

We conducted statistical t-test analysis to investigate significant differences between the simulated results obtained with $\nu_H^{back} = 0.1\,m^2/s$ and $\nu_H^{back} = 0.05\,m^2/s$, with and without implementation of the HLES model (Table 2.2). The t-test result indicates that the null hypothesis was rejected at the 5% significance level, and 0 other wise. The resulting p-values are also shown in Table 2.2. As is shown, models in which HLES was not implemented were significantly different in depth, streamwise velocity, bed shear stress, turbulent kinetic energy and even vertical eddy viscosity. In addition to these variables, the models in which HLES was employed were significantly different in the depth-averaged streamwise velocity. Figure 2.7a-b shows that even in the absence of the HLES turbulence model, the depth-averaged velocities were completely different at least in the first half of the channel. These observations provide further evidence that, regardless of the implementation of the HLES model, even small changes in the background horizontal eddy viscosity can change the model results, emphasizing the need for appropriate calibration of this sensitive parameter. Moreover, as is shown in Table 2.1, $\nu_H^{back} = 0.1\,m^2/s$ and $\nu_H^{back} = 0.05\,m^2/s$ both resulted in quite acceptable

slope regression values; however, as shown in Table 2.2 their results were significantly different.

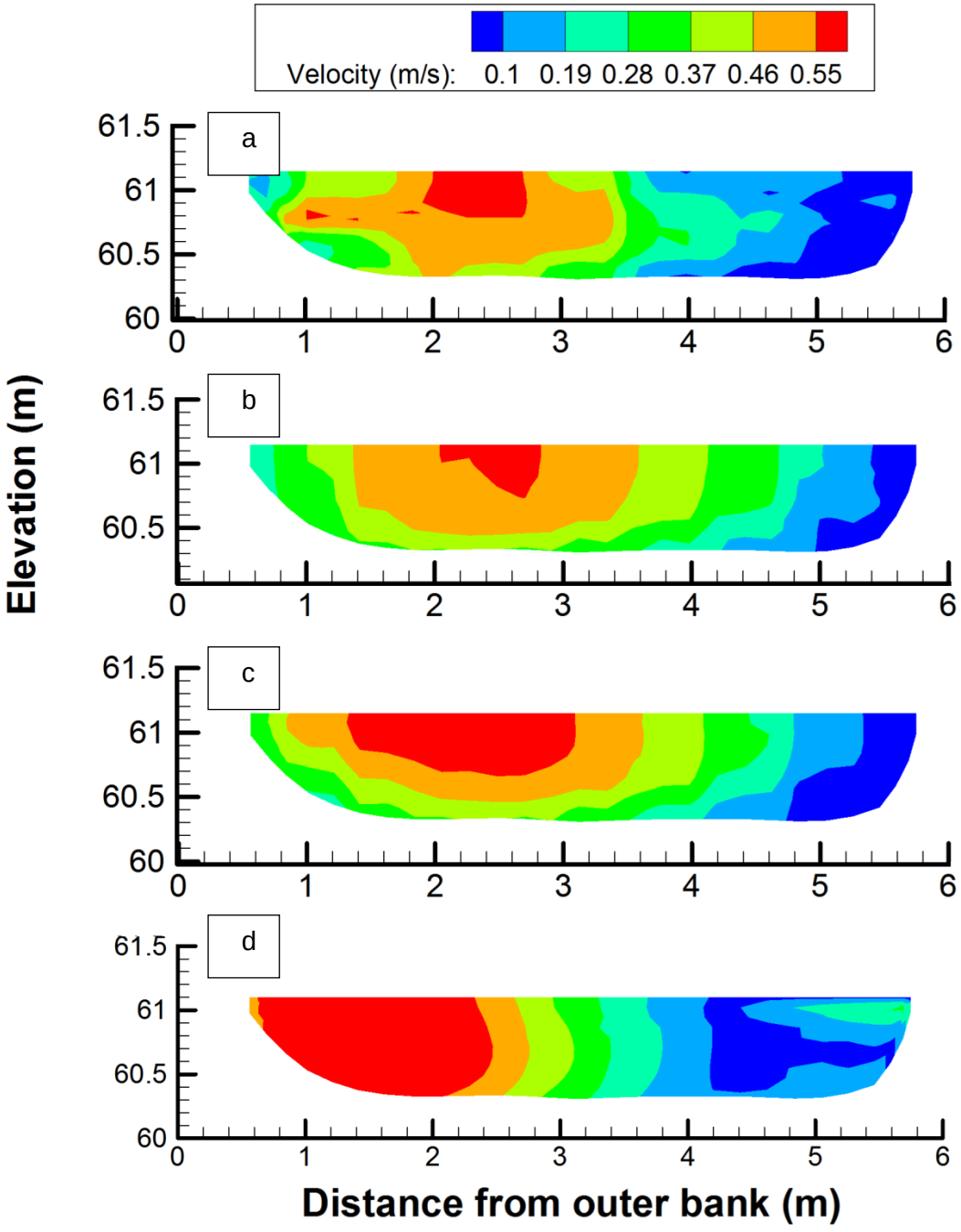

Figure 2.9. (a) Streamwise velocity obtained from ADV measurements and simulated streamwise velocity assuming: (b) ν_H^{back}=0.1 m^2/s, (c) ν_H^{back} =0.05 m^2/s, (d) $\nu_H^{back} = 0\ m^2/s$ using HLES model. Facing downstream with outer bank shown on right side. The figures are shown in the same scale.

Table 2.2. T-test analysis of the 3D hydrodynamic model using background horizontal eddy viscosity of 0.1 and 0.05 m^2/s.

	Without HLES		With HLES	
Variable	Ttest	P value	Ttest	P value
Depth	1	0.005	1	0
Depth averaged velocity-streamwise	0	0.166	1	0.033
Depth averaged velocity-crossstream	0	0.744	0	0.981
Velocity (streamwise velocity)	1	0.006	1	0.000
Velocity (cross-stream velocity)	0	0.287	0	0.917
Velocity (vertical velocity)	0	0.825	0	0.974
Bed shear stress	1	0	1	0
Turbulent energy (50% of the depth)	1	0	1	0
Vertical eddy viscosity (50% of the depth)	1	0	1	0

Figures 2.10 illustrates the cumulative frequency distributions of 3D vector error velocity magnitude in different water layers for the calibrated model ($v = 0.1\ m^2/s$). The following formulation was used to calculate the 3D vector velocity error magnitude

$$velocity\ error = \sqrt{(vx_{mod} - vx_{obs})^2 + (vy_{mod} - vy_{obs})^2 + (vz_{mod} - vz_{obs})^2} \quad (2\text{-}6)$$

where , vx, vy, vz represent the three velocity components, and mod and obs are indications of the modelled and ADCP measured velocities, respectively. As can be inferred from Figure 2.10, larger errors were observed in the near-bed layer 10. Furthermore, velocity errors were lower in the middle of the flow than near the water surface and the bed. This could be attributed to the greater influence of secondary circulation at the top and bottom that could have affected the measurements. Flow inhomogeneity between the acoustic beams and side-lobe effects could be another possible reason for this.

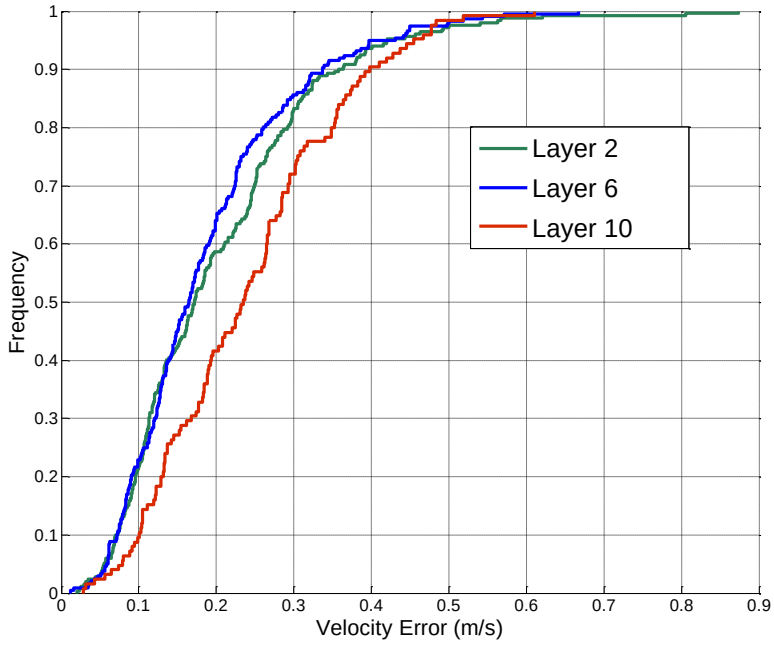

Figure 2.10. Cumulative frequency distributions of 3D vector error velocity magnitude in different water layers of the calibrated model ($\nu_H^{back} = 0.1\ m^2/s$).

To examine the significance of vertical layers, velocity component directions and background horizontal eddy viscosity on the model predictions, multiway analysis of variance (ANOVA) was performed. The resulting p-values were 0.0001, ~ 0, and 0.0496 for vertical layers, velocity component directions, and background horizontal eddy viscosity, respectively, thus all three factors were significant at 95% confidence level.

To investigate the spatial location of the velocity errors compared to the spatial ADCP survey, the locations where higher errors occurred are shown in Figure 2.11. Figure 2.11a specifies the location where the difference between simulated and measured velocity was higher than $0.15\ m/s$. Figure 2.11b illustrates the individual velocity vectors, with red and blue vectors showing measured and simulated velocity, respectively.

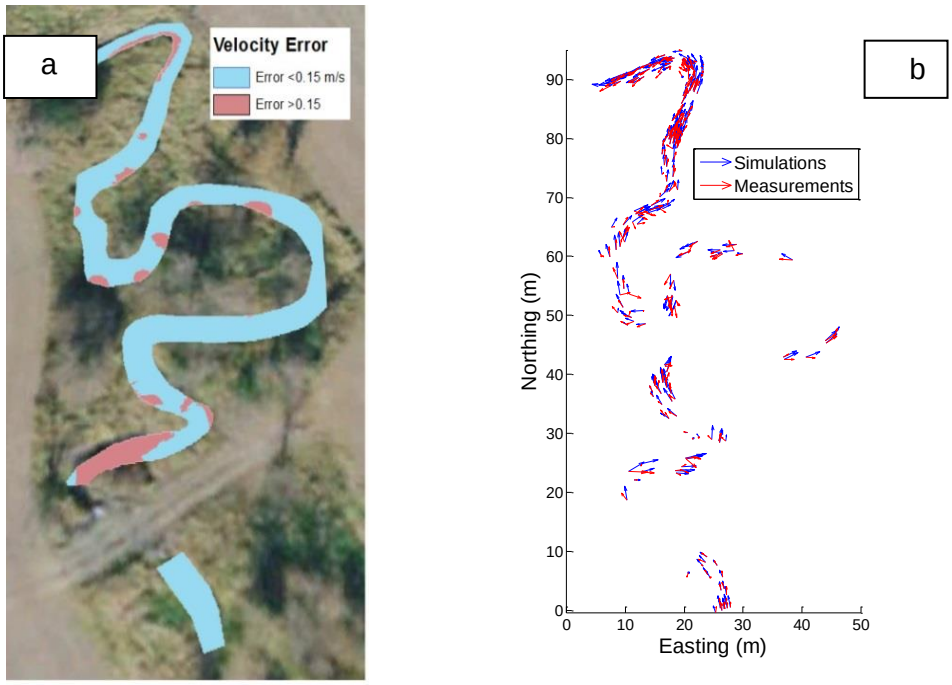

Figure 2.11. Comparison of velocity vectors from the measured 3D ADCP individual bins and the collocated calibrated model cell at all depths throughout the studied reach, interpolated to a planar horizontal surface (a) Calculated error magnitudes (b) Individual collocated simulated and measured velocity vectors. (0,0) is located at (434840.2, 5020559.7).

As is shown, maximum errors occurred mostly near the channel margins, which may have been due to ADCP compass error (Rennie and Church 2010). Large errors were observed at the downstream of the culvert, which could have been due to the local velocity disruption downstream of the culvert. Considering Figure 2.11b, one can note that most of the errors might have been due to the inaccuracies in the ADCP survey data, because in these cases, the direction of the measured velocity does not follow the flow pattern of the reach.

It is worth noting that the proposed calibration methodology provides the opportunity to calibrate the model based on spatial distribution of the background horizontal eddy viscosity. Simulation of rivers with complex geometry necessitates spatial calibration of the numerical model since calibration parameters can change significantly along the reach (Papanicolaou et al., 2010). To account for the turbulence characteristics of the flow through the study reach, the model was also calibrated using spatially distributed

background horizontal eddy viscosity which, based on our sensitivity analysis, is an important parameter for good simulation of the study reach. Several scenarios were examined in which different background horizontal eddy viscosity values were assigned to the main channel, meanders, and banks. It should be noted lower values were given to the areas of lower turbulence. Accordingly, based on 3D calibration, a set of 0.08, 0.1, and 0.12 m^2/s (first scenario) was obtained for the main channel, meanders and banks; on the other hand, based on 2D calibration, 0.01, 0.02, and 0.09 m^2/s (second scenario) were respectively obtained. It is worth noting that the results of the 2D calibration (either spatially varying or fixed background horizontal eddy viscosity) led to lower ν_H^{back}. Table 2.3 shows the estimated error in both scenarios based on 2D and 3D calibration.

Table 2.3. MAE_R analysis based on 2D and 3D calibration approach for spatially varying ν_H^{back}.

	MAE_R (m/s)	
Calibration approach	First scenario	Second scenario
3D Calibration	0.176	0.179
2D Calibration	0.135	0.124

To illustrate the impact of the resulting calibration parameter on the model results, simulated flow depth using spatially distributed ν_H^{back} based on the 2D and 3D calibration approaches was compared with the measurements (Figure 2.12). It should be noted that the first gap in the measured values corresponds to the location of the culvert and the second gap in the measurements is due to presence of the log-jam.

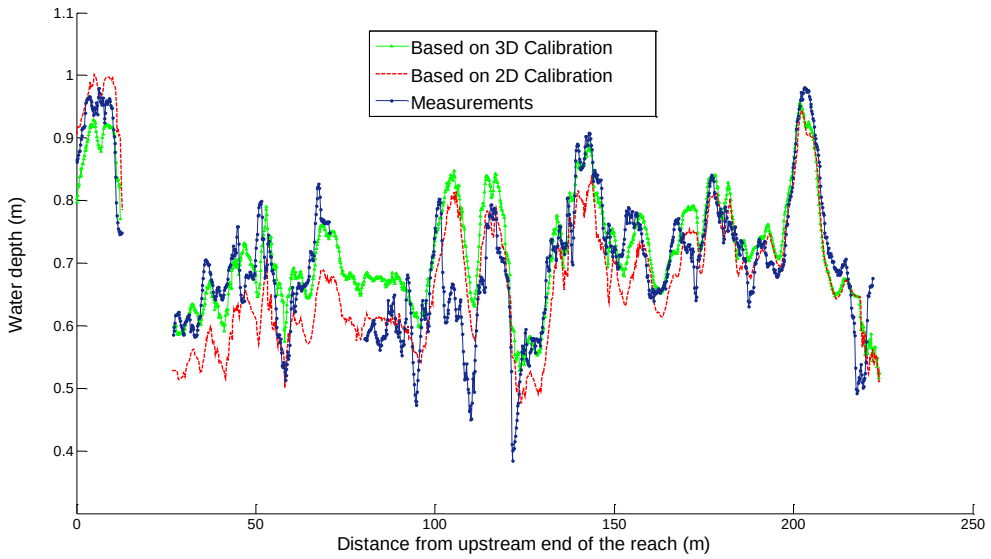

Figure 2.12. Comparison of the measured and simulated flow depth in the centre of the study reach for spatially distributed background horizontal eddy viscosity

As can be seen, simulated flow depth based on 3D calibration agrees well with the measurements while there is a discrepancy between the measured flow depth and that obtained from the 2D calibration approach. It can be inferred that the background horizontal eddy viscosity can also impact the predicted flow depth. Moreover, analysis of the depth mean absolute error resulted in 0.096m and 0.12m for the 3D and 2D calibration approaches, respectively. This confirms that the proposed 3D calibration method could better predict the flow depth throughout the reach.

2.5 Discussion

Conventional calibration methods have mostly been based on adjusting the model inputs to match the measured data at discrete locations in the study reach (Papanicolaou, 2010). These methods do not account for the spatial distribution of the 3D flow field. Meanwhile, calibration attempts that use depth-averaged velocities could suffer from some inaccuracies (Kasvi et al., 2015a). The present study employed a spatially intensive 3D velocity flow field for calibration of a 3D hydrodynamic model to alleviate existing uncertainties in the previous calibration methods. The results were

compared with the two other calibration approaches used in the literature; i.e., spatially distributed depth-averaged velocities, and 3D velocities averaged at discrete section locations in the study reach.

Comparison of the measurements with the results of the model calibrated at discrete section locations indicated that the model did not perform satisfactorily (Table 2.1). This is likely because calibration at discrete locations is dependent on how well the flow at these locations represents the flow field throughout the entire reach. However, despite averaging of ADCP data at each discrete section, the calibration data may have still included measurement errors. Further study is needed to assess the degree to which measurement error contributed to the discrepancy between the model and measurements in this calibration approach.

Using the 2D calibration approach the lowest MAE_H was achieved with $\nu_H^{back} = 0m^2/s$ (with HLES model) or $\nu_H^{back} = 0.05m^2/s$ (without HLES model), whereas using the proposed 3D calibration approach minimum MAE_R was obtained with $\nu_H^{back} = 0.1m^2/s$. This suggests the 3D hydrodynamic model required higher dissipation to match observed individual point 3D velocities than to match observed depth-averaged velocities. T-test significance analysis revealed that either with or without the HLES model, the model results were sensitive to small changes in the horizontal eddy viscosity. Validation of the results with ADV data (Figure 2.9) as well as ADCP measured flow depth along the reach (Figure 2.12) and ADCP velocities in different locations (Figure 2.13) confirmed that the model calibration based on the 3D calibration had the best model performance. These results provide a proof of accuracy and applicability of the proposed methodology.

It may be that 2D calibration will lead to a parameterization that yields lower velocity errors for depth-averaged variables, but this does not necessarily mean that it will better reproduce the 3D distribution. This could arise from the fact that 2D calibration deals with depth-averaged data which are sufficiently smoothed to produce lower errors compared to the 3D calibration method, but also because calibration of depth averaged values does not require matching of low near-bed velocities. That is, if a 3D model is

required for hydrodynamic modelling, 2D calibration may lead to a model parameterization that does not accurately simulate the fully 3D flow field.

It was shown that 2D calibration resulted in a lower ν_H^{back} (i.e. $0\,m^2/s$ when HLES was employed and $0.05\,m^2/s$ without the HLES model). This could possibly be attributed to estimation of the ADCP depth-averaged velocities, which ignored the unmeasured upper part and lowest 6% portion (due to the side lobe error). Assuming a 1/6 power law for the vertical profile of streamwise velocity, if the unmeasured upper part is greater/lower than 18% of the entire velocity profile, calculated depth-averaged velocity based on the measured portion is negatively/ slightly positively biased (Rennie, and Church, 2010). In our case, an upper unmeasured portion of 18% occurred at a depth of 0.66m which was lower than the average depth of the reach; accordingly, estimated ADCP depth-average velocities may have been positively biased. This could affect the calibration results when just depth-averaged values are used for assessment of the model performance. Alternatively, higher velocity gradients with low velocities exist near the channel bed, and thus greater model dissipation is required to match velocities in the near-bed zone. One may suppose that this can be exacerbated by the greater preponderance of matched velocity grid points with ADCP bins near the bed, due to the increased model resolution near the bed. However, the same calibrated parameterization results were found if model resolution was made uniform throughout the vertical.

A remaining outstanding and controversial issue is whether the errors between the measured and simulated values are due to ADCP measurement uncertainty (cf. Rennie and Church 2010; Moore et al. 2016) or the inability of the model to predict such values. To investigate this, vertical distributions of the horizontal velocity at different locations are shown for both ADCP measurements and the simulations (Figure 2.13). These figures demonstrate that while depth-averaged magnitudes may be comparable between measured and simulated values in a given profile, individual ADCP velocity profiles are relatively noisy. Consequently, individual bin errors may mostly be due to the ADCP measurements since such irregular vertical velocity profiles are not expected throughout the water column. Furthermore, the measured ADCP error velocities

averaged $0.02\,m/s$ with a maximum of $0.4\,m/s$, which could indicate the presence of large errors in individual bin velocities.

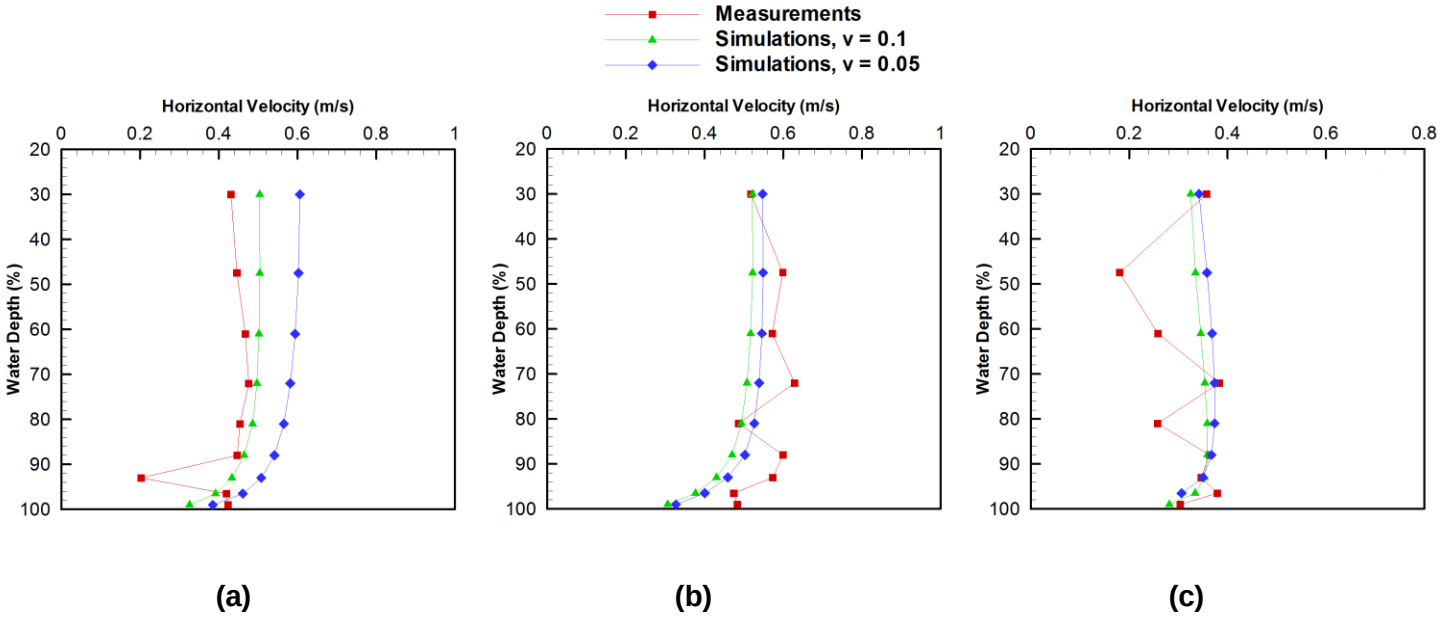

Figure 2.13. Horizontal velocity at: (a) $x = 434856.9$ $y = 5020597.1$ (b) $x = 434858.2$, $y = 5020637.7$ (c) $x = 434859.2$, $y = 5020653.5$.

Different sources can be recognized for the occurrence of these measurement errors such as compass error (particularly at turning points near channel edges), ADCP uncertainties, and GPS errors (Rennie and Church 2010). At the same time, model errors can occur due to process simplification, uncertainty of boundary conditions, and inaccuracies of the surveyed bathymetry data. Local velocity disturbances caused by wood, vegetation or log jam which cannot be captured by the model could be another cause of these errors. Thus, it is likely that discrepancies between measured and predicted values arise from both measurement and model errors. Another possible reason for discrepancies between the simulations and the measurements is how turbulence is modelled. It might be of an interest that a better agreement was obtained in the model which background horizontal eddy viscosity was calibrated compared to the model in which HLES was employed and background horizontal eddy viscosity was set to zero.

In the regression analyses we employed fully spatially distributed 3D velocity vector which can cause relatively high scatter of measurement and simulations. Regression assumes that errors occur in the dependent (ordinate) variable. Consequently, errors in the measured ADCP data can impose some uncertainty for modeled versus measured regression estimation. If errors were dominated by ADCP measurement uncertainty, then it is reasonable to suggest that the inverse slope would be a more reliable parameter for evaluation of model performance. Based on the 3D calibration approach, the inverse slope when $\nu_H^{back} = 0.1\ \mathrm{m}^2/s$ was almost one, which illustrates the capability of the model to produce comparatively accurate results. Low values of regression parameters uncertainties indicated that these analyses would be reliable. Lastly, while errors may have been dominated by ADCP uncertainty, these errors are random, and it can still be said that the fully spatially distributed 3D velocity data provided by an ADCP spatial survey provide the best available data for calibration of a fully 3D model.

2.6 Conclusion

The current state-of-the art in calibration of a 3D hydrodynamic model revealed that relatively little attention has been paid to properly calibrate a 3D numerical model. This study proposed a novel methodology for an improved calibration of a 3D hydrodynamic model. Using field observations of fully distributed 3D velocities throughout a natural river provides opportunity for 3D model calibration that accounts for the variability and dynamics of the complex flow field in meandering rivers. Conventional calibration methods, if they have employed velocity data at all, have been mostly based on the data in one or few sections of the study area; however, these methods do not account for the spatial distribution of the 3D flow field. 3D calibration with fully spatially distributed 3D velocity measurements leads to a model specifically parameterized to predict the 3D flow field. Furthermore, it allows for spatially distributed calibration parameters to better represent physical and turbulent characteristics of the flow. This could be particularly beneficial in natural meandering rivers where 3D flow features are required or in cases where, due to the complex geometry, spatial varying values should be used for model calibration.

This study compared the results of the proposed calibration approach with the typical calibration methods to show how choosing different calibration methods could change the model predictive capability. In the proposed methodology, a 3D hydrodynamic model was first developed to simulate the flow characteristics in a tortuously natural meandering river. Spatially intensive ADCP surveying was conducted in the natural meandering creek to attain fully 3D distributed velocities. These observations were then employed for 3D calibration of the developed model. To accurately and realistically compare the fully 3D predicted and measured velocities, a Matlab code was developed to match the location of each ADCP bin with 3D model grid points.

The results suggested that different calibration approaches resulted in a different calibration parameter whose simulated results could significantly differ from one another. Results of different calibration approaches were validated using an ADV. It was shown that the model which was calibrated based on the proposed 3D calibration approach had the best model performance. We studied the performance of a 3D RAN model using Delft3D with and without inclusion of a HLES model. The results confirmed that either with or without the HLES model, the calibration of background horizontal eddy viscosity plays an important role in the model performance.

The vertical distribution of the velocity error was also examined. Assessment of the cumulative distribution functions of the velocity error in each vertical water layer indicated that errors were greatest near the bed and at the water surface and least in the intermediate layers. This was likely due to greater influence of secondary circulation at the top and bottom of the water column that might have introduced some errors during the ADCP measurements. Another possible reason for this could be flow inhomogeneity between the acoustic beams and side-lobe effects. Spatial comparison of the measured and simulated fully 3D distributed flow velocity revealed that the maximum error mostly occurred near the edges of the reach and downstream of the culvert.

The results of the present study elucidated the importance of model calibration with comparable field data based on the nature and objectives of the numerical model. These results suggest that fully 3D calibration is desired to develop a model that best

reproduces the fully 3D velocity distribution. Considering the fact that computational cost of the proposed calibration approach could be fairly similar to any other calibration methods, it could provide a better calibration potential for simulation of natural meandering rivers. Further study is needed to investigate how many transects need to be surveyed to get the same results as the proposed calibration approach, if spatial distribution of the fully 3D velocities were not available.

CHAPTER 3

Hydrostatic Versus Non-Hydrostatic Hydrodynamic Modelling of Secondary Flow in a Tortuously Meandering River: Application of Delft3D[2]

Abstract

Given the importance of pressure gradients in driving secondary flow, it is worth studying how the modelled flow structures in a natural river bend can be impacted by the assumption of hydrodynamic pressure. The performance of hydrostatic versus non-hydrostatic pressure assumption in the three-dimensional (3D) hydrodynamic modelling of a tortuously meandering river is studied. Both hydrostatic and non-hydrostatic numerical models were developed using Delft3D-Flow to predict the 3D flow field in a reach of Stillwater Creek, in Ottawa, Canada. An Acoustic Doppler Velocimeter (ADV) was employed to measure the 3D flow field at a section in a sharp bend of the simulated river at two different flow stages. The results of the Delft3D hydrostatic model agreed well with the ADV measurements: the hydrostatic model predicted reasonably accurately both the streamwise velocity distribution across the section and the magnitude and location of the primary secondary flow cell. The results of the Delft3D non-hydrostatic approximation showed that the model was not conservative and could not accurately generate either the secondary flow or the streamwise velocity distribution. This study illustrated the superior performance of the hydrostatic over non-hydrostatic 3D modelling of the secondary flow using Delft3D. Several possible reasons for unfavorable performance of the non-hydrostatic version of Delft3D are discussed, including the pressure correction technique employed in Delft3D. Considering the uncertainties that may arise in both modelling and field measurements, the 3D hydrostatic Delft3D model was capable of reasonably predicting the river bend flow structures in the studied meandering creek.

[2] This chapter has been published as: **Parsapour-Moghaddam, P**., & Rennie, C. D. (2017). Hydrostatic versus nonhydrostatic hydrodynamic modelling of secondary flow in a tortuously meandering river: Application of Delft3D. River Research and Applications, 33(9), 1400-1410.

Keyword: 3D hydrodynamic modelling, Hydrostatic vs Non-hydrostatic modelling, Secondary flow, Natural meandering river, Delft3D, Field-based data

3.1 Introduction:

Over the past decades, river engineers have paid careful attention to the movement, development, and decay of river meanders (e.g. Piégay et al., 2005; Krapesch et al., 2009; Demers et al., 2011; Choné and Biron, 2016). Flow in a river bend has a component normal to the section-averaged flow direction. This transverse velocity component is typically called secondary flow which is driven towards the inner bend near the riverbed and directed to the outer bend near the water surface. Over the past few decades, several attempts have been made by river researchers to measure this induced secondary circulation (Bridge and Jarvis,1976; Bathurst et al., 1979; Thompson, 1986; Ferguson et al., 2003; Rodriguez et al., 2004). The secondary currents can impact the velocity distribution, boundary shear stress and consequently sediment transport, mixing throughout the water column, lateral bed slope and shape of the channel topography (Blanckaert and de Vriend, 2003). Since an induced secondary flow is a dominant phenomenon in meandering rivers (Blanckaert and de Vriend, 2003; Wilson et al, 2003), it is critical to develop a model that is capable of reproducing the flow circulations in natural meandering rivers.

Numerical modelling of natural meandering rivers has always been a challenge. 3D hydrodynamic modelling in meandering open-channels has been established since the late 1970s (Zeng et al., 2008). Lane et al. (1999) suggested that a 3D model, based on fully RANS (Reynolds-averaged Navier–Stokes) equations, has better predictive capability compared to a 2D model, particularly when the 2D model does not account for the effect of secondary flow. Kasvi et al. (2013a) illustrated that despite employment of a secondary flow correction in their 2D model using SMS TUFLOW software, the 2D model did not predict the fluvial characteristics corresponding to the creation of the scroll bar at the inner bank of a low-sinuosity meander bend. Kasvi et al. (2015a) compared 2D versus hydrostatic 3D models generated with Delft3D and found that both models produced similar depth-averaged flow fields. However, the 3D model was deemed superior due to its ability to predict vertical and near-bed flows.

3D hydrostatic models can be described as accurate models in water engineering where the vertical velocity is comparatively small (Casulli and Stelling, 1998). Due to the lower computation cost, hydrostatic models are widely used in natural field-scale flows (Zhang et al., 2014). However, there are some cases where the vertical acceleration, and thus non-hydrostatic pressure, cannot be neglected. Such cases include topography with abrupt changes, short waves, intensive density gradient, and strong vertical circulation (Deltares, 2014). 3D non-hydrostatic hydrodynamic models have recently become computationally possible due to the advancement of technology and have been employed in curved open channels (eg., Demuren,1993; Sinha et al., 1998; Wilson et al.,2003; Khosronejad et al., 2007; Leupi and Altinakar, 2005; Rüther and Olsen, 2007; Zeng et al., 2008; Vermeulen et al., 2015).

Despite all attempts in numerical modelling of flow in rivers, less attention has been paid to validate such models for sharply curved bends using field data (Rodriguez et al., 2004; Kasvi et al., 2015a; Vermeulen et al., 2015). Irregularity of the geometry and velocity distribution in natural rivers makes their flow structure more complex compared to laboratory experiments (Ferguson et al., 2003). There are challenges in 3D hydrodynamic modelling of natural meandering rivers with complex bathymetry, which may not be addressed properly if the model is validated with laboratory-scale experimental data. Validation of these models based on comparable field-based data may improve understanding of complex flow structures in natural meandering rivers. On the other hand, it is important to choose a numerical model which can best predict the dynamics of natural rivers (Rousseau et al., 2016). Moreover, given the importance of pressure gradients in driving secondary circulation, it is worth investigating if hydrodynamic pressure can influence secondary circulation. Due to the higher computational cost of the non-hydrostatic modelling, it is important to know whether a 3D hydrostatic model can be adequate for simulation of the flow structures in a natural river bend.

Delft3D-Flow is one of the most widely used hydrodynamic models for river flow simulation (e.g. Williams et al., 2013; Javernick et al., 2016; Kasvi et al., 2015a,b). However, it is still not clear to what extent one can rely on the results of a Delft3D hydrostatic model of a natural meandering river. To the best of our knowledge, the

effect of hydrodynamic pressure assumption in Delft3D modelling of the secondary flow has still not been studied. This study aims to assess the performance of the hydrostatic versus non-hydrostatic hydrodynamic modelling of secondary flow in a tortuously meandering river using the Delft3D-Flow model. Performance of both models is assessed by comparing their results with the velocity data collected in the sharp meander bend of a natural meandering river using an ADV. This chapter is organized as follows: Section 3.2 describes the study area and the methods employed for the field measurements. Detailed description of the numerical modelling and the governing equations are given in Section 3.3 followed by the explanation of the model setup in Section 3.3.1. The results are analyzed in Section 3.4, and discussed in Section 3.5. Overall conclusions of the study are given in Section 3.6.

3.2 Study area and field measurements

The study site was a 190 m long reach of Stillwater Creek, a tortuously meandering river located in the City of Ottawa, Canada, which flows north into the Ottawa River (Figure 3.1). Channel and flow characteristics during the high-flow are shown in Table 3.1. Following its original path, this reach meanders through agricultural lands. Analysis of historical air photos confirmed that the sinuosity of the creek has increased from nearly 2.2 (1965) to 2.8 (2013) and has the ability to create meander cut-offs (Parsapour-Moghaddam and Rennie, 2014). Bathymetric data were collected by Total Station survey in which points were collected with an average spacing of 1.5 m and 0.5 m in streamwise and cross-stream directions, respectively.

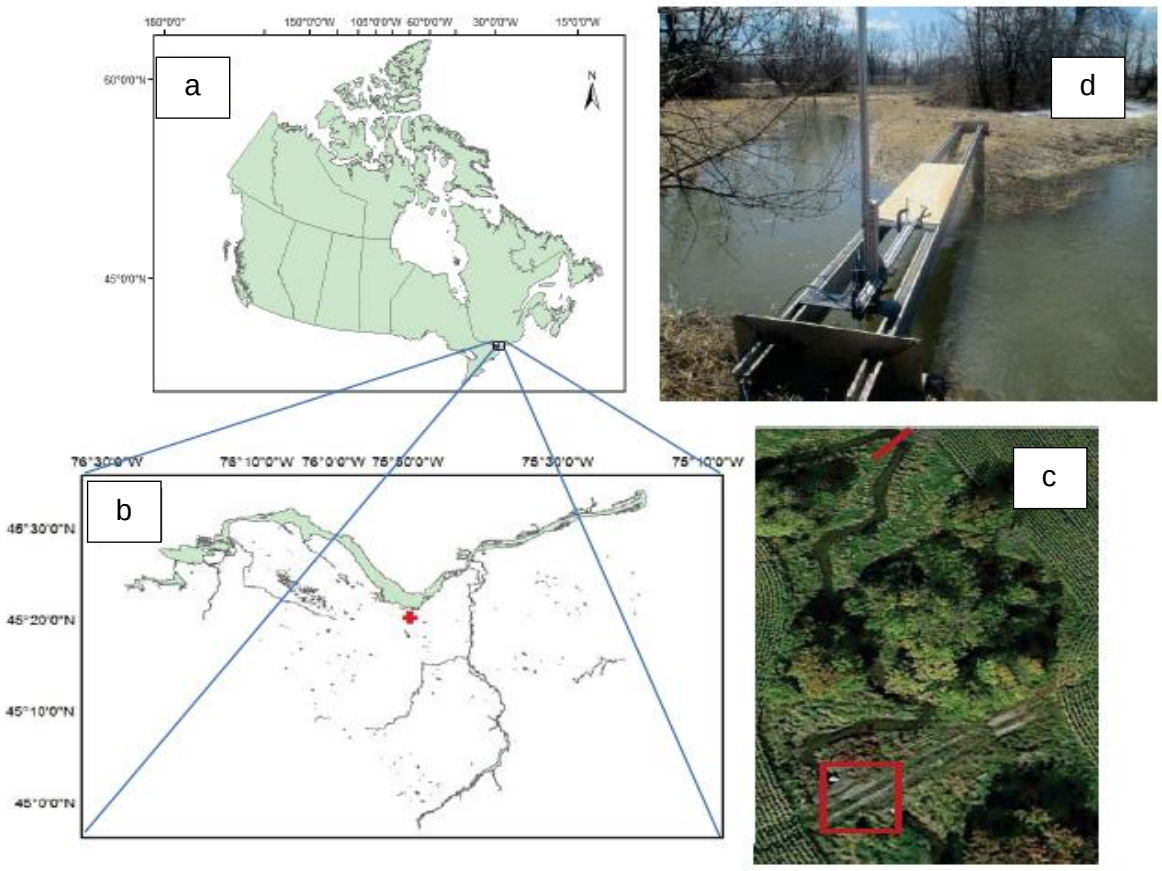

Figure 3.1. (a) Location of the study area within Canada (adopted from https://www12.statcan.c.ca), (b) study reach location in the Ottawa area (adopted from http://data.ottawa.ca/en/dataset/water), and (c) overview of the studied creek (flow from south [bottom] to north [top]), acoustic Doppler velocimeter measurement section (red line) and culvert location (red square) are shown. (d) Acoustic Doppler velocimeter measurement at a bend apex in the study area. Flow from left to right.

Table 3.1. Flow and channel characteristics during the high-flow scenario.

Channel type	Meandering
Sinuosity	2.80
Slope	0.0026
Average depth	0.7 m
Average width	8 m
Average flow velocity	0.61 m/s
Froude number	0.25
Reynolds number	424719

As is visible in Figure 3.1c, close to the upstream end of the studied reach, there is a farm road that consists of a gravel crossing and a culvert which was a previous attempt to engineer off-channel habitat. However, culvert alignment is skewed with respect to the river course, which has led to excessive erosion and strong meandering in the downstream reach (Parsapour-Moghaddam and Rennie, 2015). An acoustic Doppler current profiler (ADCP) was employed to measure the flow discharge and the water level, which were used for the upstream and downstream boundary conditions, respectively. We also conducted spatially intensive ADCP surveying throughout the entire reach to collect fully distributed 3D velocities which were used for calibration of the developed models. It should be noted that the bank full discharge was estimated to be $1.5\ m^3/s$.

To measure the 3D velocity, an ADV was employed (Figure 3.1d) at the final bend apex of the Stillwater Creek reach on April 12, 2014 (high flow) and June 14, 2014 (low flow). The ADV was deployed from a temporary bridge on an adjustable mount. Due to the difficulties we had in moving the ADV bridge during different flow regimes, we fixed the bridge in the sharpest bend of the creek; thus, the results could provide a good indication of the strongest secondary circulation (worst case scenario). Velocity data at a total of 67 points were collected during high flow, and 53 points during low flow, distributed in eight profiles across the section. At each sampling point, 90 s time series were collected at a sampling frequency of 100Hz. The ADV measurement technique and use in rivers is well described in the literature (Lohrmann et al., 1994; Sontek, 1997; Afzalimehr and Rennie, 2009; Rennie and Hay, 2010; Sukhodolov, 2012; Jamieson et al., 2013). This study employs the high-quality field-based ADV data to validate the developed 3D hydrodynamic models. Comparison is made between the results of a hydrostatic and non-hydrostatic Delft3D model to study the prediction ability of each of these models.

3.3 Numerical Modelling

The hydrostatic pressure assumption has been broadly employed in shallow water studies. Due to the smaller non-hydrostatic pressure component compared to the hydrostatic pressure component, it is often assumed that the pressure in shallow water

is hydrostatic. Thus, it would be a valid assumption to neglect the effect of non-hydrostatic pressure in shallow water modelling.

The 3D RANS equations are based on the conservation of the mass and momentum of the incompressible fluid. Using the hydrostatic pressure assumption, 3D shallow water equations can be derived based on the RANS equations. Integration of the continuity equation over the depth, considering the kinematic boundary conditions at the bed level and the water surface, yields the depth-averaged continuity equation in the Cartesian coordinates system:

$$\frac{\partial \eta}{\partial t} + \frac{\partial (hU)}{\partial x} + \frac{\partial (hV)}{\partial y} = 0 \tag{3-1}$$

where $h = \eta - d$ is the water depth, η is the water surface elevation, d is the bed elevation, U and V are the horizontal depth averaged velocities in x and y directions, respectively.

The u and v momentum equations read:

$$\frac{\partial u}{\partial t} + u\frac{\partial u}{\partial x} + v\frac{\partial u}{\partial y} + w\frac{\partial u}{\partial z} = -g\frac{\partial \eta}{\partial x} + \nu_h\left(\frac{\partial^2 u}{\partial x^2} + \frac{\partial^2 u}{\partial y^2}\right) + \frac{\partial}{\partial z}\left(\nu_v \frac{\partial u}{\partial z}\right) \tag{3-2}$$

$$\frac{\partial v}{\partial t} + u\frac{\partial v}{\partial x} + v\frac{\partial v}{\partial y} + w\frac{\partial v}{\partial z} = -g\frac{\partial \eta}{\partial y} + \nu_h\left(\frac{\partial^2 v}{\partial x^2} + \frac{\partial^2 v}{\partial y^2}\right) + \frac{\partial}{\partial z}\left(\nu_v \frac{\partial v}{\partial z}\right) \tag{3-3}$$

where u, v and w are the velocity components in x, y, and z directions, respectively; g is the gravitational acceleration; t is the time; υ_h and υ_v are the kinematic eddy viscosity coefficients in the horizontal and vertical directions, respectively. The vertical momentum equation is reduced to the hydrostatic pressure assumption:

$$\frac{\partial p}{\partial z} = -\rho g \tag{3-4}$$

The continuity equation is employed to find the vertical velocity required in the momentum equations:

$$\frac{\partial u}{\partial x} + \frac{\partial v}{\partial y} + \frac{\partial w}{\partial z} = 0 \tag{3-5}$$

Consequently, the continuity (3.5) and momentum (3.2- 3.3) equations along with the depth integrated continuity equation (3.1) form the governing equations for a 3D hydrostatic model with four variables, u, v, w and η. It should be noted that a turbulence closure model is required to estimate the eddy viscosity term.

In non-hydrostatic 3D modelling, the pressure term can be decomposed into hydrostatic and hydrodynamic pressure:

$$p = \rho g h + q \tag{3-6}$$

where q is the hydrodynamic pressure. Consequently, the momentum equations yield:

$$\frac{\partial u}{\partial t} + u\frac{\partial u}{\partial x} + v\frac{\partial u}{\partial y} + w\frac{\partial u}{\partial z} = -g\frac{\partial \eta}{\partial x} - \frac{1}{\rho}\frac{\partial q}{\partial x} + \nu_h\left(\frac{\partial^2 u}{\partial x^2} + \frac{\partial^2 u}{\partial y^2}\right) + \frac{\partial}{\partial z}\left(\nu_v\frac{\partial u}{\partial z}\right) \tag{3-7}$$

$$\frac{\partial v}{\partial t} + u\frac{\partial v}{\partial x} + v\frac{\partial v}{\partial y} + w\frac{\partial v}{\partial z} = -g\frac{\partial \eta}{\partial y} - \frac{1}{\rho}\frac{\partial q}{\partial y} + \nu_h\left(\frac{\partial^2 v}{\partial x^2} + \frac{\partial^2 v}{\partial y^2}\right) + \frac{\partial}{\partial z}\left(\nu_v\frac{\partial v}{\partial z}\right) \tag{3-8}$$

$$\frac{\partial w}{\partial t} + u\frac{\partial w}{\partial x} + v\frac{\partial w}{\partial y} + w\frac{\partial w}{\partial z} = -\frac{1}{\rho}\frac{\partial q}{\partial z} + \nu_h\left(\frac{\partial^2 w}{\partial x^2} + \frac{\partial^2 w}{\partial y^2}\right) + \frac{\partial}{\partial z}\left(\nu_v\frac{\partial w}{\partial z}\right) \tag{3-9}$$

To estimate the water surface, the continuity equation should be integrated over the total depth as shown in equation (3.1). As can be seen, as opposed to the hydrostatic pressure model, in the non-hydrostatic pressure assumption, the third momentum equation will appear and thus w can be calculated from the vertical momentum equation (3.9). Moreover, the gradient of the non-hydrostatic pressure will be taken into account in the horizontal momentum equations (3.7- 3.8). An appropriate technique should be employed to calculate the hydrodynamic pressure term q see, e.g. Casulli (1999), Busnelli (2001), Ullmann (2008), Van der Plas (2009).

In this study, Delft3D-Flow is used to simulate hydrodynamic processes in the natural meandering river. Delft3D is a modelling package which comprises several modules interacting with each other over a mutual interface (Lesser et al., 2004). This code is an open source code which is capable of simulating two or three dimensional hydrodynamic processes. Delft3D-Flow solves 3D Navier-Stokes equations under Boussinesq assumptions for incompressible flow. Turbulence closure models are used to close the RANS equations. Delft3D has four types of turbulence models for a 3D simulation (Deltares, 2014): constant eddy viscosity and diffusivity in which user defined input background values are selected; algebraic model in which the coefficient of the mixing length and turbulent energy are calculated based on the algebraic equations; $k-L$ model in which mixing length and turbulent kinetic energy are estimated by a transport equation; and finally, $k-\varepsilon$ turbulence model (used in this study) in which the coefficients for both turbulent kinetic energy and dissipation are estimated by transport equations (Mohammadi and Pironneau, 1993).

The partial differential equations are formulated based on orthogonal curvilinear coordinates. Delft3D-Flow supports two different grid systems in the vertical direction: σ model and Z-model. In the σ grid system, layers are bounded by two σ planes following the free surface and the bottom topography. A model in σ coordinates can provide a smooth topography demonstration since it is boundary fitted. However, in some cases where stratified flow occurs over a steep topography, σ grid may not have enough resolution. In the σ coordinate system, it is assumed that the vertical accelerations are much smaller than the gravitational acceleration, and thus, can be neglected. For cases in which this assumption is not valid, Delft3D-Flow can be extended with a non-hydrostatic pressure model that applies a Z grid system.

As opposed to the σ model, the Z-model is a staircase boundary with approximately parallel horizontal coordinate lines with density interfaces in the area of steep bottom topography. The σ and Z- models in Delft3D-Flow use nearly the same numerical methods in the 3D shallow-water models (Deltares, 2014). Using a proper set of initial and boundary conditions, the 3D shallow-water equations are solved based on a finite difference method using staggered grid (Arakawa C-grid). An Alternating Direction Implicit (ADI) technique is used to solve the water level equations (Stelling, 1984). In the current version of Delft3D-Flow (version 4.01.01), the non-hydrostatic option is available in the Z- model.

The non-hydrostatic mode of Delft3D was first introduced by Bijvelds (2001) and since then is available in Delft3D-Flow. In the non-hydrostatic modelling, a pressure correction technique is used to calculate the hydrodynamic pressure (Casulli,1999; Busnelli, 2001). The pressure correction technique is used along with an ADI method that is a bit different from the σ model in Delft3D (Bijvelds, 2001). The pressure correction is solved through the conjugate gradient method (CG) in which the convergence rate is dependent on the spectral properties of the coefficient matrix (Deltares, 2014).

The present study investigates the performance of hydrostatic versus non-hydrostatic hydrodynamic modelling of secondary flow in a tortuously meandering river using Delft3D. To evaluate the performance of both 3D hydrostatic and non-hydrostatic

Delft3D models, different error statistics were calculated based on the following equations:

$$MAE = \sum_{i=1}^{n} \frac{|v_{mod_i} - v_{obs_i}|}{n} \quad (3\text{-}10)$$

$$RMSE = \sqrt{\sum_{i=1}^{n} \frac{(v_{mod_i} - v_{obs_i})^2}{n}} \quad (3\text{-}11)$$

$$STD = \sqrt{\frac{\sum_{i=1}^{n} (|v_{mod_i} - v_{obs_i}| - \mu)^2}{n-1}} \quad (3\text{-}12)$$

where v_{obs_i} and v_{mod_i} indicate measured velocity and simulated velocity for i^{th} co-located point. MAE, $RMSE$ and STD stand for mean absolute error, root mean square error and standard deviation of the error, respectively. The parameter μ is the mean of all velocity error values and n is total number of co-located points. The above error statistics were calculated for each velocity component, i.e., v_m (streamwise), v_n (cross-stream), and v_z (vertical). The next section elaborates how the 3D numerical models were developed.

3.3.1 **Model setup**

Delft3D-Flow was employed for both the hydrostatic and non-hydrostatic 3D numerical simulations. An orthogonal curvilinear grid was firstly developed covering the study creek, which included area adjacent to the river to account for an overbank flow simulation. As for the vertical grid resolution, in both hydrostatic and non-hydrostatic models, 20 layers were defined to ensure that there is an adequately fine mesh to resolve the vertical water profile. To investigate the sensitivity of the model to the mesh, various grids were generated and tested. The most suitable one with a better mesh quality (smoothness, resolution, and orthogonality) was then selected with an average grid resolution of 50 cm and a time step of 0.0025s to meet the stability condition. The horizontal (and vertical) grid resolution was sufficiently fine to simulate non-hydrostatic pressure. Finer grid was employed in regions of high velocity gradient (grid resolution ~ $25\ cm$). The total station survey data were then interpolated through the generated cells. Sigma coordinates were used for the 3D hydrostatic modelling, whereas in non-hydrostatic modelling Z-model was used. Both models were run with the two different flow scenarios to simulate the site condition during ADV measurements.

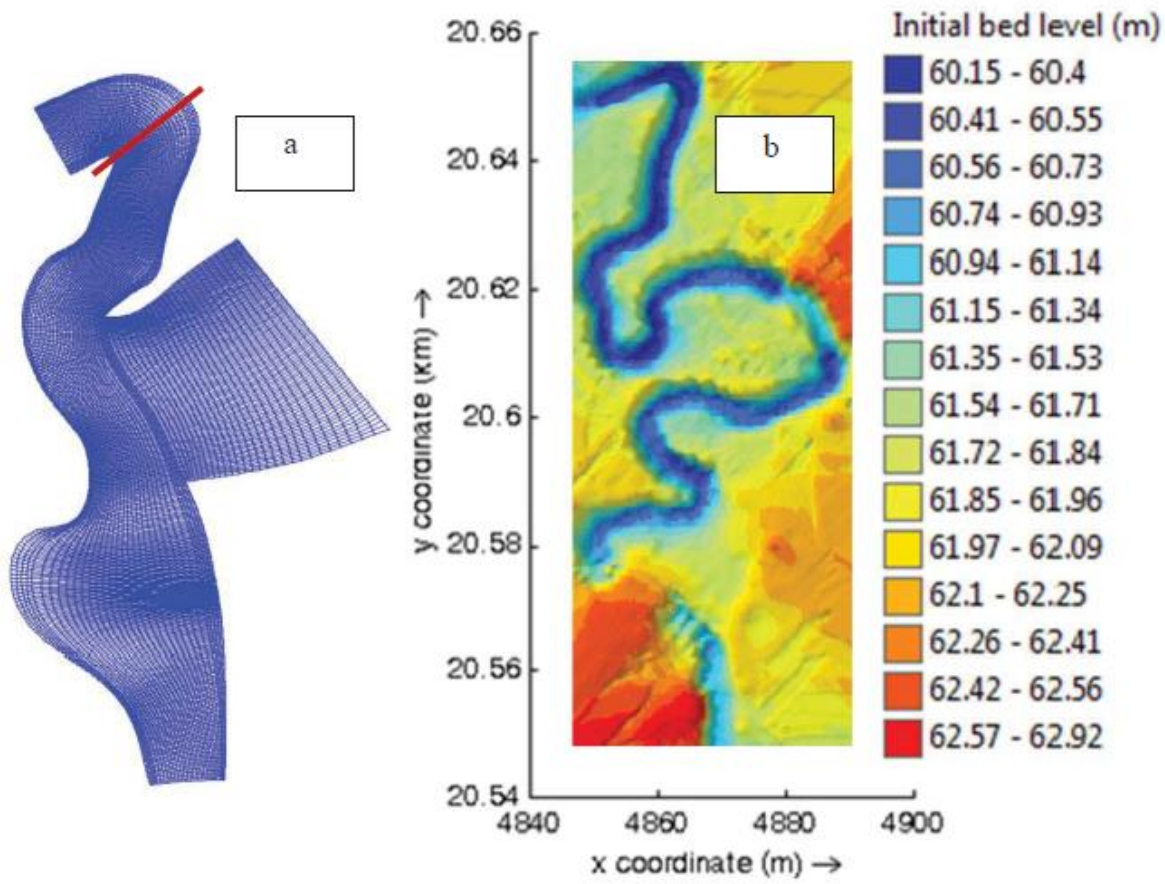

Figure 3.2. (a) The location of the measured cross-section on top of the developed grid (b) Bathymetry of the study reach. The first two digits of the X and Y coordinates are removed from the plot. Downstream water level was measured by ADCP at the end of the model reach. The culvert is located at the gap in water depth [approximately (4860 m, 20.57 km) to (4850 m, 20.575 km)].

The ADCP measured discharges and water level were 1 m^3/s and 61m for high flow, and 0.2 m^3/s and 60.7m during the low flow, respectively. We calibrated the models based on a fully 3D calibration approach in which the fully spatially distributed 3D ADCP velocity data were compared with the co-located simulated velocities. A Matlab code was developed in which ADCP single bin 3D velocities were matched to grid points of the developed 3D models. This helps to ensure that the 3D nature of the flow field is taken into account in the model calibration. The model was calibrated using the non-hydrostatic model. The same model parameters were then applied using the hydrostatic model. This was done to ensure that the non-hydrostatic model was optimized.

Consequently, Manning roughness and background horizontal eddy viscosity were, respectively, set to be 0.015 and 0.01 m^2/s. To model the existing culvert in the creek, the culvert module of Delft3D was used. The culvert location (shown in Figures 3.1c and 3.2b) and elevation were obtained based on the topography survey. The roughness of the 11 m long corrugated steel culvert was assumed to be 0.024.

3.4 Results analysis

To explore the prediction ability of 3D hydrostatic modelling versus non-hydrostatic modelling of a natural meandering river, the simulation results of each model were compared with those obtained from ADV measurements. 3D velocity flow fields were recorded at a sharp final bend apex of the study reach (Figure 3.2a) within different flow regimes.

Figure 3.3 shows the measured and modelled secondary flow during high flow discharge. As is shown, the location and magnitude of the main secondary flow cell is well predicted by the 3D hydrostatic model, and simulated streamwise velocities agree well with the measurements. As can be seen in both the measurements and the hydrostatic model, the secondary velocity vectors reached to almost 0.2 m/s which is quite high compared to the streamwise velocity. This can be due to the sharp curvature of the bend (Blanckaert, 2011). In the non-hydrostatic model, the location and centre point of the secondary flow is different from that of the measurements. Moreover, the predicted streamwise velocities do not agree with the measured values. In the non-hydrostatic model the maximum streamwise velocity reaches to 0.8 m/s whereas in both the hydrostatic model and the ADV measurements the maximum streamwise velocity is 0.55 m/s.

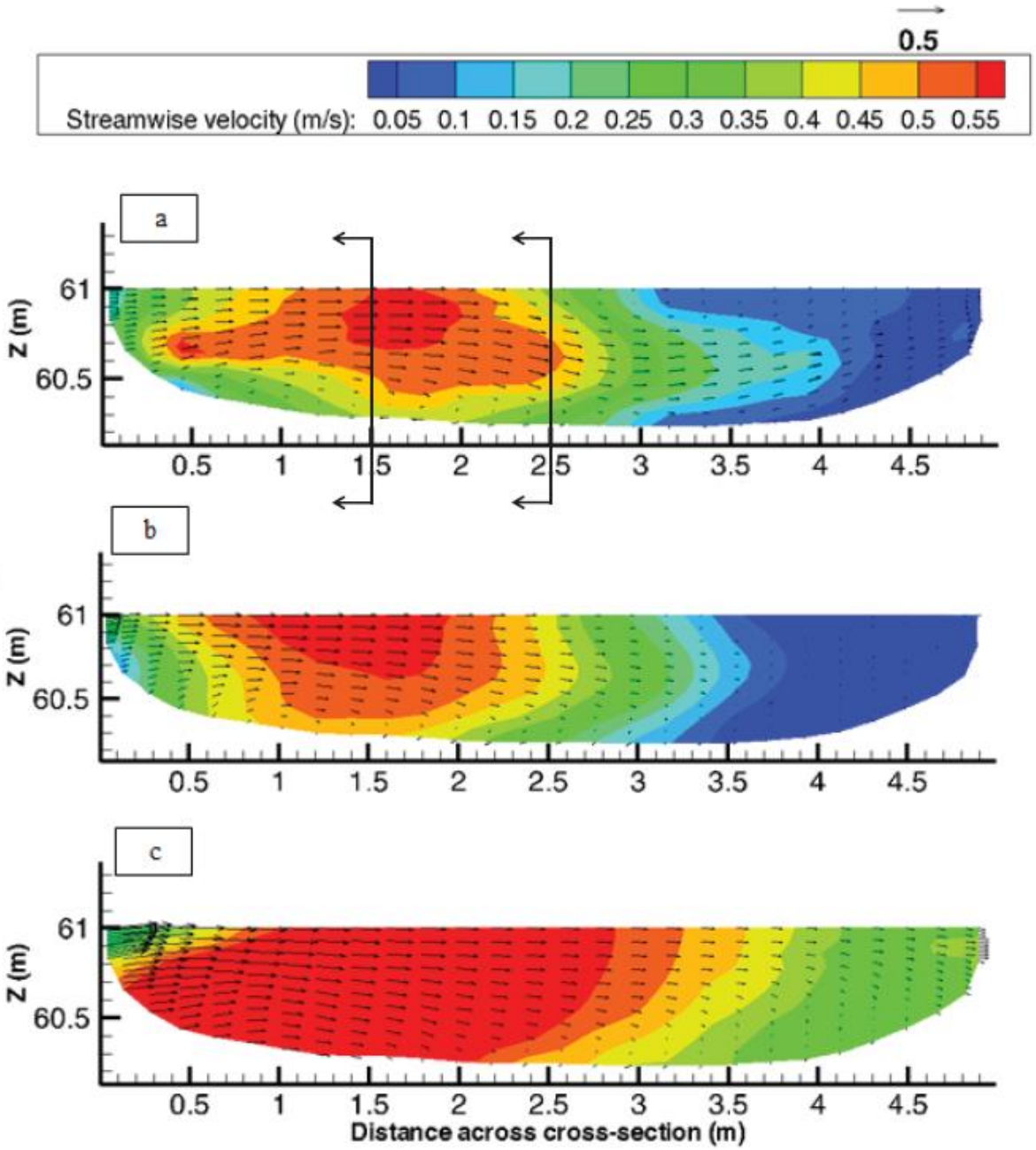

Figure 3.3. Secondary circulation (vectors) overlaid on the stream-wise velocity (contours) during high flow discharge (Q=1 m3/s) in the last sharp bend cross section, facing downstream with outer bank shown on right side: (a) ADV measurements (b) 3D hydrostatic modelling (c) 3D non-hydrostatic modelling (shown with the same scale as (a) and (b)). Arrows show the profile locations in Figure 3.5.

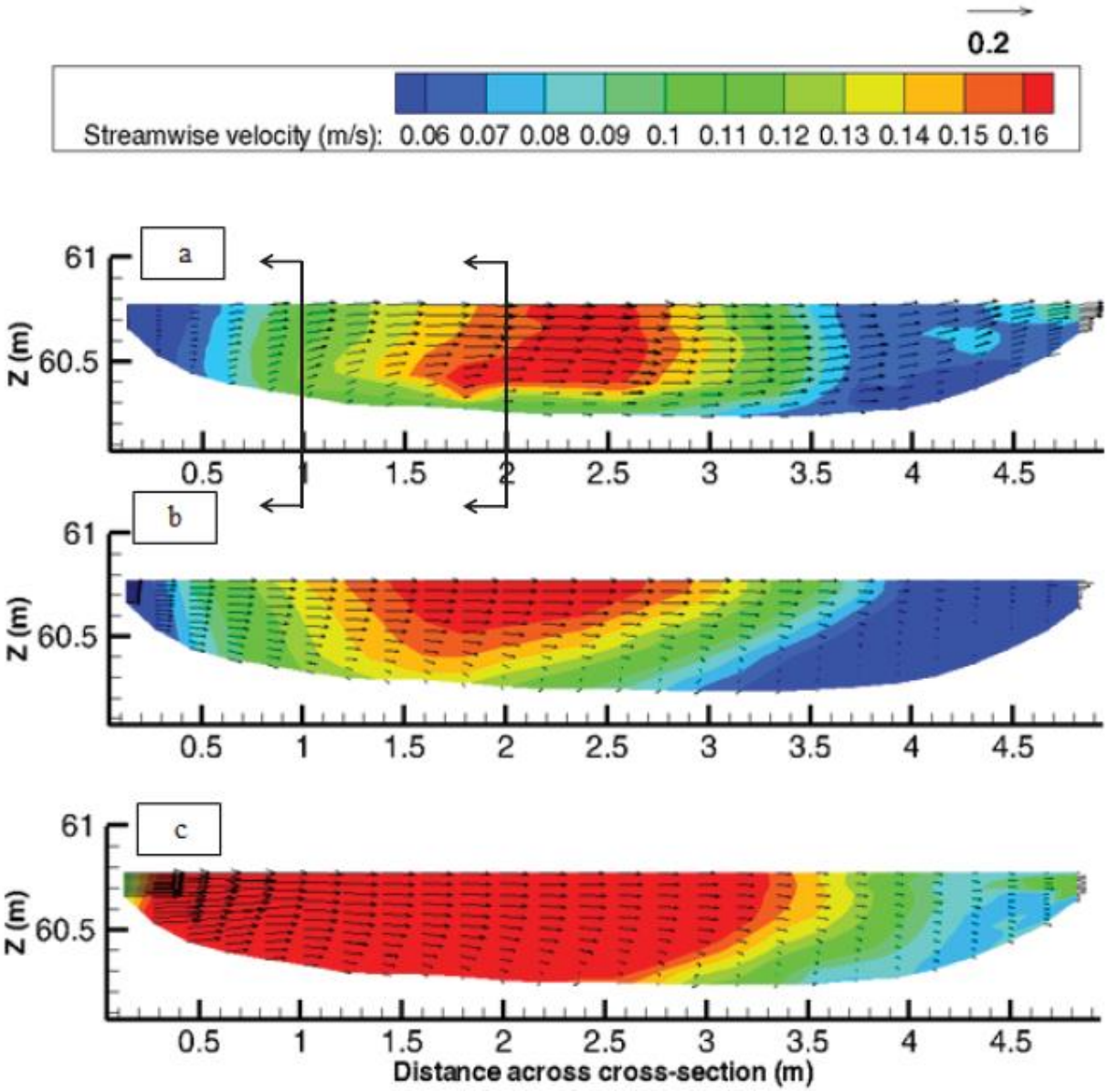

Figure 3.4. (a) Secondary circulation (vector form) overlaid on the streamwise velocity (contour form) during low flow discharge (Q=0.2 m3/s) in the last sharp bend cross section, facing downstream with outer bank shown on right side: (a) ADV measurements (b) 3D hydrostatic modelling (c) 3D non-hydrostatic modelling (shown with the same scale as (a) and (b)). Arrows show the profile locations in Figure 3.6.

Similarly, Figure 3.4 shows measured and simulated secondary flow during low flow discharge. As can be seen, the streamwise velocity and the secondary flow are better

simulated in the hydrostatic model than the non-hydrostatic model. The maximum streamwise velocity reaches to 0.27 m/s in the non-hydrostatic model whereas it is equal to 0.16 m/s in both the ADV measurements and the hydrostatic model. It should be noted that the full flow recirculation was not observed at the low flow, which is likely due to the skew of the section at low flow. The ADV bridge was set to be perpendicular to the flow during high flow; however, it may have been slightly skewed off the flow pattern during low-flow. Thus, transverse velocity may have included the influence of streamwise velocity. Table 3.2 and 3.3 show the calculated error statistics in the three dimensions (v_m, v_n and v_z) and also their resultant vector (v_t) for both hydrostatic and non-hydrostatic Delft3D models in high flow and low flow, respectively. These calculated error statistics were previously explained in equations 3.10 to 3.12. As is shown in these tables, all calculated error statistics are lower in the hydrostatic than non-hydrostatic Delft3D model during both high flow and low flow. Errors for all three velocity components and their resultant vectors in both high flow and low flow scenarios were significantly greater (α = 0.05) for the non-hydrostatic model versus the hydrostatic model.

Table 3.2. Calculated error statistics (m/s) for 3D hydrostatic and non-hydrostatic Delft3D models during the high flow scenario.

	Hydrostatic				Non-Hydrostatic			
Error Statistics	v_m	v_n	v_z	v_t	v_m	v_n	v_z	v_t
MAE	0.068	0.048	0.012	0.084	0.241	0.085	0.022	0.257
$RMSE$	0.081	0.059	0.014	0.101	0.256	0.111	0.026	0.281
STD	0.044	0.034	0.008	0.056	0.087	0.071	0.014	0.114

Table 3.3. Calculated error statistics (m/s) for 3D hydrostatic and non-hydrostatic Delft3D models during the low flow scenario.

	Hydrostatic				Non-Hydrostatic			
Error Statistics	v_m	v_n	v_z	v_t	v_m	v_n	v_z	v_t
MAE	0.022	0.038	0.008	0.045	0.085	0.047	0.009	0.098
$RMSE$	0.028	0.043	0.009	0.052	0.096	0.056	0.01	0.112
STD	0.016	0.02	0.005	0.026	0.046	0.031	0.005	0.056

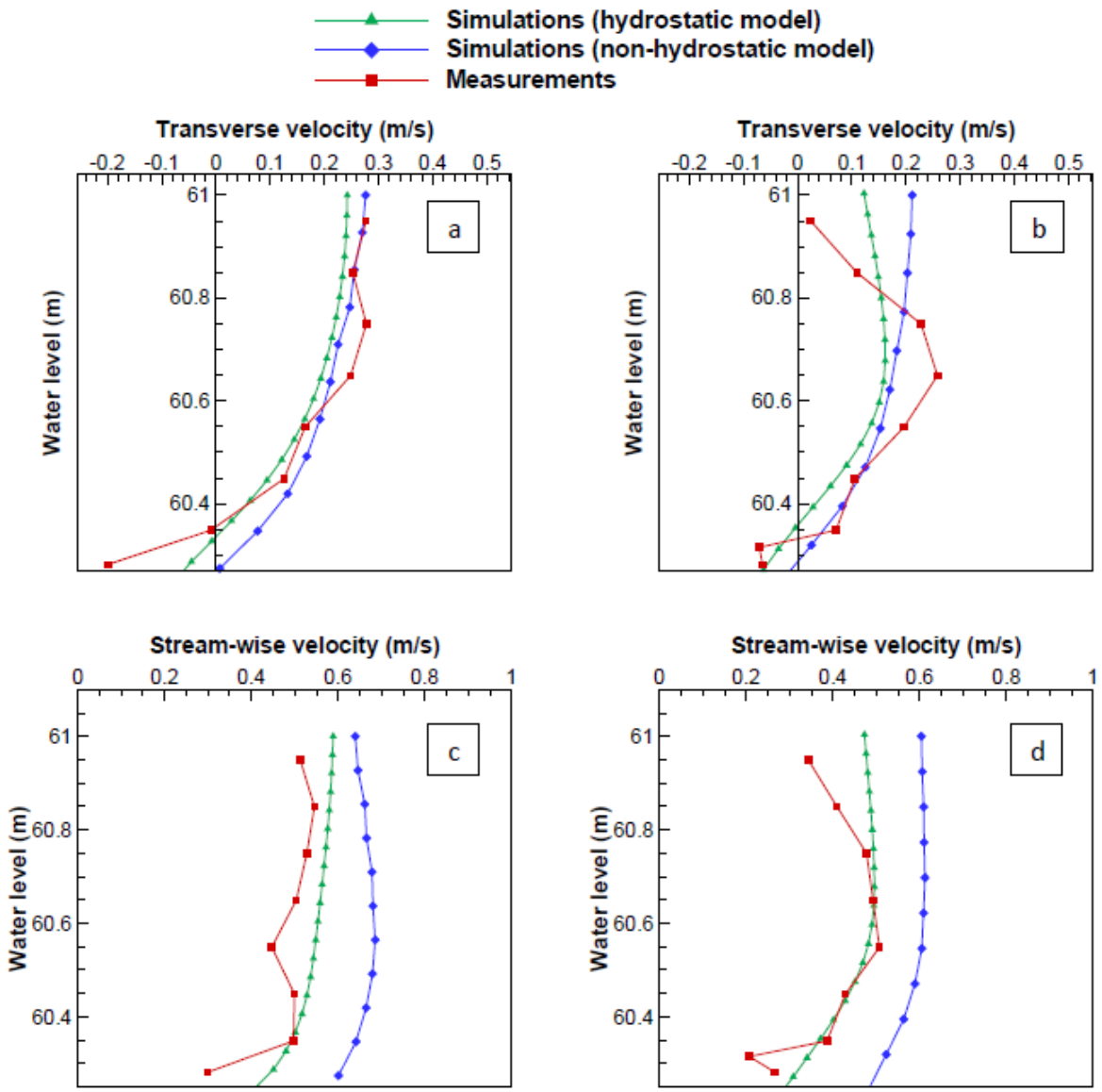

Figure 3.5. Transverse velocity profile: (a) y=1.5m (b) y=2.5m section, streamwise velocity profile at: (c) y=1.5m (d) y=2.5m, where y is the distance from the left bank along the cross section at the high flow. Refer to Figure 3.3 for location across of these profiles within the section.

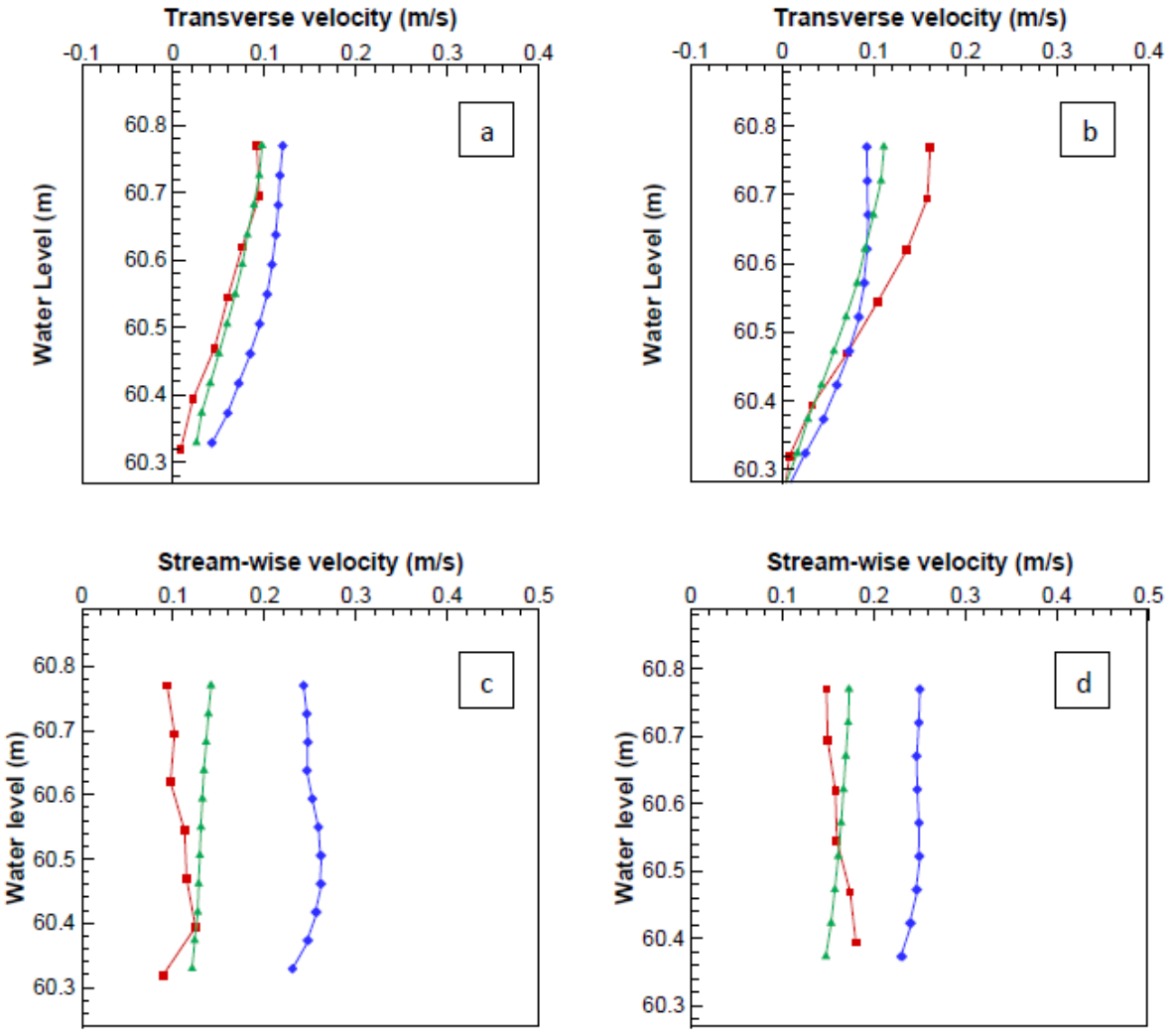

Figure 3.6. Transverse velocity profile: (a) y=1m (b) y=2m, streamwise velocity profile at: (c) y=1m (d) y=2m, where y is the distance from the left bank along the cross section at the low flow (See Figure 3.5 for the legend). Refer to Figure 3.4 for location across of these profiles within the section.

Figures 3.5 and 3.6 show transverse and streamwise velocity profiles for ADV measurements, the hydrostatic and the non-hydrostatic models during high flow and low flow scenarios, respectively. As can be seen, the hydrostatic model better predicts the measured streamwise and transverse velocities than the non-hydrostatic model. Streamwise velocity magnitudes, and negative transverse velocities near the bed, are better predicted by the hydrostatic model.

An important question that should be addressed is why the non-hydrostatic mode of Delft3D could not provide accurate results. To further study this, we first investigated why the streamwise velocity was over-predicted in the non-hydrostatic model. To this end, the instantaneous discharge in the test section based on the non-hydrostatic model was compared with that from both sigma and Z-layer coordinate versions of the hydrostatic model (Figure 3.7).

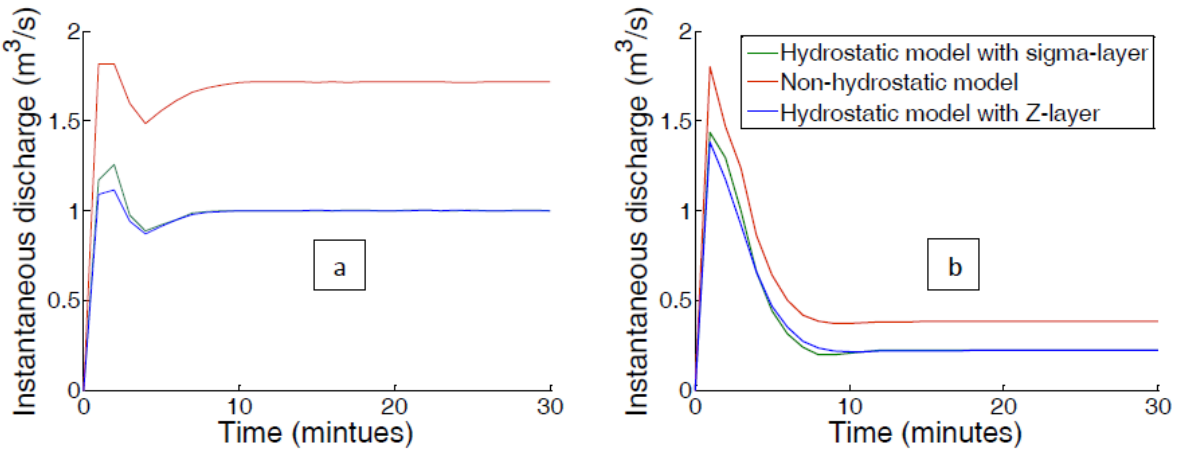

Figure 3.7. Instantaneous discharge in the bend section of the study reach (a) High-flow [Q=1m3/s] (b) Low-flow [Q=0.2m3/s]

As is shown in Figure 3.7, all models converged. However, the discharge in the high flow non-hydrostatic model (Figure 3.7a) converged to 1.7 m^3/s as opposed to 1 m^3/s, as specified for the steady upstream boundary condition. On the other hand, both versions of the hydrostatic model converged to 1 m^3/s as expected. The same phenomenon was observed in the low-flow case (Figure 3.7b), where the non-hydrostatic model discharge converged to 0.4 m^3/s, which was almost two-times of the expected input discharge of 0.2 m^3/s. It appears that the non-hydrostatic mode of Delft3D is non-conservative. To ensure that this result was not dependent on the model grid, several grids with various grid resolutions and qualities were developed and tested. The results of this analysis confirmed that regardless of the resolution and quality of the grid, the mass was not conserved in the non-hydrostatic area of the model. Moreover, based on Figure 3.7, it can be seen that this problem did not originate from use of the Z

grid coordinate system because the mass was conserved in the hydrostatic version using Z-model coordinates. Although not shown herein, we have observed similar difficulties with the mass conservation for a non-hydrostatic Delft3D model of another case study meandering river (Watts Creek, Ottawa) which was of similar scale as Stillwater Creek.

3.5 Discussion

It has been a controversial issue whether a hydrostatic model is capable of producing secondary flow in meandering channels since the vertical velocity is calculated from the continuity equation, and thus, the vertical momentum is transferred by mass. Delft3D-Flow is one of the most widely used hydrodynamic models. However, there are still large uncertainties in the degrees to which a Delft3D hydrostatic model can be reliable for simulation of a meandering river. The results of this study showed the superior performance of the hydrostatic over non-hydrostatic Delft3D model of a tortuously meandering river. There are several possible explanations of this finding.

According to Blanckaert and de Vriend (2003, 2010) the interaction mechanism between the secondary flow and the vertical distribution of the streamwise velocity plays a vital role in flow structures of a sharply curved bend. Figures 3.3, 3.4, 3.5c-d, 3.6c-d confirmed that the hydrostatic model was capable of producing a more accurate vertical distribution of streamwise velocity compared to that from the non-hydrostatic model. Consequently, better prediction of the streamwise velocity distribution of the hydrostatic model may have contributed to the superior prediction of secondary circulation in this model.

Moreover, the dominant mechanism in the main secondary flow is advective momentum transport which causes redistribution of the streamwise velocity (Blanckaert and Graf, 2004). Apparently, since momentum transportation by the secondary flow is taken into consideration in the 3D hydrostatic formulation, the hydrostatic assumption could be a reliable approximation in the hydrodynamic modelling of the tortuously meandering study reach. Furthermore, based on the results of non-hydrostatic modelling, the non-hydrostatic pressure reached to the maximum of 45 Pa which is much smaller than the existing hydrostatic pressure of 10 kPa. In other words, it

appears that dynamic pressure is less important than secondary advection in shaping the flow distribution of the study natural meandering reach.

It should also be noted that although it could be true that the outer bank cell was not simulated correctly by the Delft3D model as also reported by Van Sabben (2010), this study focused on the primary secondary flow (centre-region cell), which is stronger and more significant (Blanckaert and De Vriend, 2004).

Several reasons could possibly explain why the non-hydrostatic version of Delft3D did not perform satisfactorily. One source of error could arise from the splitting of the pressure to hydrostatic and hydrodynamic components which introduces some errors. Gaarthuis (1995) stated that the pressure-correction method was less effective when the aspect ratio of the vertical and horizontal length scale decreases. As previously mentioned, various grids of different quality and aspect ratio were tested. Nevertheless, the Delft3D non-hydrostatic model consistently proved to be non-conservative and the instantaneous discharge was changing longitudinally in the non-hydrostatic area. Ullmann (2008) stated that the results of Delft3D-Flow non-hydrostatic modelling were not quantitatively acceptable. Ullmann suggested that this could be either due to model features adopted for shallow-water situation, programming errors, or discretization of the pressure. Another source of error could be discretization error due to boundary irregularities. Van der Plas (2009) stated that the non-hydrostatic Delft3D-Flow model is a non-conservative finite-difference code. Van der Plas illustrated the importance of employing a conservative discretization technique for the momentum equations. His study showed that momentum conservative finite-volume method could be more suitable for non-hydrostatic flow, and could better discretize the kinematic boundary conditions compared to the non-hydrostatic mode of the Delft3D-Flow. Importantly, it should be noted that in the non-hydrostatic code of Delft3D-Flow, the computed pressure correction field is based on the provisional free-surface elevations. The free-surface elevation is then corrected based on a hydrostatic pressure assumption for the upper most grid cell. The assumption of hydrostatic pressure at the water surface is valid; however, neglecting the gradient of the hydrodynamic pressure in the top layer could introduce some errors in the calculation of the discharge and velocities.

3.6 Conclusion

The secondary circulation plays an important role in sharp meandering rivers. Given the importance of pressure gradients in driving secondary flow, it is worth studying if a hydrodynamic pressure assumption in 3D hydrodynamic modelling can impact the flow structures in a river bend. This study investigated the performance of the hydrostatic versus non-hydrostatic pressure assumption in 3D hydrodynamic modelling of a secondary flow using Delft3D which is a widely used hydrodynamic numerical model. An ADV was employed to measure the 3D flow field in a sharp bend of the simulated meandering river within two different flow scenarios. The field based ADV data were then employed to validate the simulated hydrodynamic models.

To evaluate the performance of each model, different error statistics were calculated. In the hydrostatic model, the MAE was 8.4% and 4.5% in high flow and low flow, respectively, which were lower than those obtained in the non-hydrostatic model; i.e, 25.7% and 9.8%. Non-hydrostatic model errors were significantly greater ($\alpha = 0.05$) in both high flow and low flow scenarios compared to those based on the hydrostatic model. The results of the 3D hydrostatic model were in good agreement with the ADV measurements. The hydrostatic model was able to reproduce reasonably accurate predictions of streamwise and transverse velocity in terms of both magnitude and location of the primary secondary flow. The results of the Delft3D model using non-hydrostatic approximation showed that the model was not mass conservative and could generate neither the secondary flow nor the streamwise velocity accurately. In sum, this study illustrated the superior performance of the hydrostatic over non-hydrostatic Delft3D modelling of the secondary flow in the studied natural meandering creek. Considering the uncertainties that may arise in both field measurements and modelling, the 3D hydrostatic Delft3D model was capable of producing the flow structures of the natural river bend with reasonable accuracy. Several reasons could be responsible for the discrepancies between the non-hydrostatic results and the measurements, including the errors that might have arisen due to the pressure correction techniques, programming errors, and non-conservancy of the non-hydrostatic module. Further study is required to determine the exact reasons for unfavorable performance of the non-hydrostatic Delft3D model and how it could be improved.

CHAPTER 4

Influence of Meander Confinement on Hydro-Morphodynamics of a Cohesive Meandering Channel[3]

Abstract

Despite several decades of intensive study of the morphological changes in meandering rivers, less attention has been paid to confined meanders. The present study examines the hydro-morphodynamics of two adjacent sub-reaches of a meandering creek, located in the City of Ottawa, Canada. Both of these sub-reaches are meandering channels with cohesive bed and banks, but one is confined by a railway embankment. Field reconnaissance revealed distinct differences in the morphological characteristics of the sub-reaches. To further study this, channel migration and morphological changes of the channel banks along each of these sub-reaches were analyzed by comparing the historical aerial photography (2004, 2014), light detection and ranging (LIDAR) data (2006), bathymetric data obtained from a total station survey (2014), and field examination. Moreover, two different spatially intensive acoustic Doppler current profiler (ADCP) surveys were conducted in the study area to find the linkage between the hydrodynamics and morphological changes in the two different sub-reaches. The unconfined sub-reach is shown to have a typical channel migration pattern with deposition on the inner bank and erosion on the outer bank of the meander bend. The confined sub-reach, on the other hand, experienced greater bank instabilities than the unconfined sub-reach. In the confined sub-reach, an irregular meandering pattern occurred by the evolution of a concave-bank bench which was caused by reverse flow eddies. The sinuosity of the confined sub-reach has decreased from 1.55 to 1.49 in the 10-year study period. The results of the present study demonstrate the physical mechanisms by which meander confinement can change the meandering pattern and morphological characteristics of a cohesive clay bed creek.

[3] This chapter has been published as: **Parsapour-Moghaddam, P**., & Rennie, C. D. (2018). Influence of Meander Confinement on Hydro-Morphodynamics of a Cohesive Meandering Channel. Water, 10(4), 354.

Keywords: Meandering rivers, Meander confinement, Cohesive bed rivers, Hydro-morphodynmics, Spatial ADCP survey.

4.1 Introduction

4.1.1 Meandering Rivers

The word “meander” was first used by the ancient Greeks who called the Büyük Menderes River, a curving river in west central Turkey, Maiandros. The Latin meaender eventually came to refer to any curving river (Güneralp et al., 2012). Meandering rivers have long attracted people’s attention due to their distinctive characteristics. In the distant past, Leonardo da Vinci illustrated meanders of the Santerno River in Italy. Later, meandering rivers became politically important because their shifting locations were used to separate nations (Ghinassi et al., 2016). Accordingly, many river scientists and engineers have studied meandering rivers over the past few centuries (e.g., Thomson, 1876; Einstein, 1926; Bridge and Jarvis, 1976; Thompson,1986; Ikeda and Parker 1989; Demuren, 1993; Blanckaert and de Vriend, 2003; Lanzoni and Seminara, 2006; Blanckaert, 2011; Kasvi et al., 2013a,b; Kasvi et al., 2015a,b; Parsapour-Moghaddam and Rennie, 2017a; Parsapour-Moghaddam and Rennie, 2018a,b). Despite the fact that river meandering is an erudite topic with a long literature history, there are still some uncertainties on the source and initiation of the meandering pattern and its migration. It is known that river meandering is associated with the bank erosion mechanism and can be influenced by the spatial progression of bars (Schuurman et al., 2016).

Daniel (1971) identified three main types of meander movement: translation, rotation and expansion. When the bend apex laterally migrates away from the channel-belt axis, the typical mode of meander-bend expansion occurs. However, if the bend apex migrates parallel to the channel-belt axis in the downstream direction, meander translation takes place, which results in downstream migration of point bars. Sometimes, these transformations include rotation, leading to development of an asymmetric meander. Meander displacement can also be a mixture of all the aforementioned processes (see Ghinassi et al., 2016 and references therein). By

definition, meander expansion involves increasing bend curvature. As opposed to meander expansion, in meander translation, downstream migration occurs at persistent sinuosity (Nicoll, 2008; Ghinassi et al., 2016).

River banks, as transitional boundaries between the 'wet-dry' areas, can play a key role in various aspects of meandering river morphodynamics. Bank erosion is a primary source of sediment delivery to the river (De Rose and Basher, 2011), and can negatively affect the quality of water and fluvial habitat over time (e.g., Simon and Klimetz, 2008; Sutarto et al., 2014). Bank erosion processes influence a wide range of social, environmental and economic factors (Nardi et al., 2013). Bank erosion leads to bank retreat and planform changes, which can influence river mobility, morphological evolution, water quality, riparian lands and aquatic habitat (Rinaldi et al., 2008). Nardi et al. (2013) identified several negative impacts of bank erosion such as land and infrastructure damage, water turbidity, as well as the dynamics of pollutants, nutrients and sediments. They also mentioned that bank erosion can have positive impacts on the morphodynamics of a river in terms of improving the river ecological condition and contributing to river self-restoration by supplying sediment. For example, bank erosion and meander progression can eventually lead to formation of an oxbow lake, which can provide excellent aquatic habitat (Choné and Biron, 2016). Consequently, bank erosion predictions are of essential importance in sustainable river management (Rinaldi et al., 2004).

4.1.2 **Bank retreat mechanism**

The physical process of bank erosion mainly includes fluvial erosion as well as the mass failure of unstable banks (Darby et al., 2007; Sutarto et al., 2014). Fluvial erosion is the removal of bank particles or aggregates due to the excess boundary shear stress of the flowing water, while mass failure of the bank is defined as the movement and detachment of bank aggregates under gravity forces (Rinaldi and Darby, 2007). The mass failure can be triggered by fluvial erosion due to undercutting of the bank profile (Darby et al., 2007; Rinaldi and Darby, 2007; Leyland et al., 2015). Numerous field observations have shown that fluvial erosion can lead to bank toe undercutting and subsequent development of cantilevers that can result in mass failure (Lawler 1995;

Pizzuto, 2009; Sutarto et al., 2014). The effect of fluvial erosion rate is thus of essential importance in mass-failure and bank retreat (Rinaldi and Darby, 2007). Rinaldi and Darby (2007) made a comprehensive review of the main bank erosion processes. They argued that the interaction between the fluvial erosion and mass failure mechanisms should be considered in bank retreat modelling.

Despite numerous well-documented previous studies devoted to the bank retreat mechanism, the erosion of cohesive river substrates is not completely understood (Simon and Collison, 2001; Pizzuto, 2009; Salem and Rennie, 2017). Unlike non-cohesive river bed sediments for which resistance to entrainment is merely mechanical, cohesive material interactions depend on the electro-chemical bonds amongst the particles (Simon and Collison, 2001). A general predictive theory for entrainment of cohesive river boundary sediments is yet to be developed, thus prediction of bank erosion in a cohesive river remains challenging (Pizzuto, 2009). Collapse and removal of cohesive river banks is also a function of both physical and electro-chemical forces (Simon and Collison, 2001). Both fluvial erosion and mass failure of a river bank also depend on the water content and pore water pressure in the bank, which are influenced by its hydrological and vegetation characteristics (Simon and Collison, 2001). Several studies have recognized the significance of pore water pressure in the erosion and removal of cohesive bed river particles or assemblages (e.g., Casagli et al., 1997; Simon and Curini,1998, Rinaldi and Casagli, 1999; Simon et al., 2000). Simon and Collison (2001) indicated that upward seepage force can surpass the existing erosion resistance and river confining stress and thereby enhance entrainment of cohesive bed sediments.

Bank instability and erosion are intrinsic characteristics of meandering rivers (Hooke, 2003). Lanzoni and Seminara (2006) illustrated how the morphodynamics of meandering rivers can be impacted by meander instability. Bank erosion and subsequent meander migration are important natural processes for both unconfined and partially confined rivers (Choné and Biron, 2016).

4.1.3 **Confined Meanders**

Although meander morphodynamics has been widely studied, less attention has been paid to confined meandering. The morphological development of a confined meander is impeded by a natural or manmade restriction. A confined meander cannot freely develop, which results in a distinctive meander pattern that differs from those presented by freely meandering rivers. Nicoll (2008) noted that the dynamics of meander migration may be affected in confined meandering rivers, and Ghinassi et al. (2016) observed that meander confinement can lead to the downstream migration of fluvial point bars.

Lewin and Brindle (1977) showed that free meandering could be hindered by bedrock or anthropogenic structures, and this can result in a square-wave shape meandering configuration. They defined three degrees of confinement: first-degree confinement takes place in wide valleys whereby the stream impinges irregularly against the confining valley wall. Lane (1957) called this type of meander a “restrained” meander. In second-degree confinement the outer side of each meander bend impinges upon the confining wall, and in third-degree confinement the meandering stream does not have space to progress.

Most river meanders do not undergo purely downstream translation. Nicoll (2008) observed downstream translation without substantial distortion only in confined meanders with limited amplitude and low curvature. Lewis and Brindle (1977) noted that downstream translation without meander deformation is prevalent in second-degree confined rivers. Nicoll and Hickin (2010) studied the planform geometry and migration pattern of several second-degree confined meandering rivers on the Canadian prairies. They related the channel-migration rate of the studied rivers to basic geomorphic and hydrologic variables. The authors indicated that the planform relations were generally consistent with those manifested by freely meandering rivers, with small yet significant differences due to the distinctive meander behavior of confined meanders.

Previous studies have shown that meander confinement can lead to development of a concave-bank bench (Page and Nanson,1982; Nanson and Page,1983, Burge and Smith, 1999; Makaske and Weerts, 2005; Smith et al., 2009). A concave-bank bench is a crescent-shaped accretion on the upstream portion of the outer bank (concave side)

of a meander bend. These deposits are generally observed in meandering rivers that migrate down valley (Daniel, 1971); however, it may also occur in unconfined meander belts (e.g., Lewin,1978; Nanson and Page,1983; Smith et al., 2009). Page and Nanson (1982) demonstrated that when the channel flow has the power to erode the channel banks, regular meandering is developed with a point bar and overbank deposition. However, in cases where the stream power hardly surpasses the shear strength of the bank material, then irregular meanders may be generated with long straight reaches and sharp bends. They showed that concave-bank benches are commonly developed when sharp meander bends migrate downstream.

The effect of manmade features on meandering river morphodynamics has been studied, particularly for river stabilization works (e.g., Jamieson et al., 2013). Nevertheless, less studied has been the morphodynamics of meandering rivers confined by structures such as railway and road embankments (Lewin and Brindle, 1977). Furthermore, the migration behavior of confined bends has been studied, most previous research has focused on second degree confinement where the river impinges against the confining edge in every meander wavelength (Nicoll and Hickin, 2010).

4.1.4 **Objectives and Structure**

As outlined above, there are still some uncertainties on the source and initiation of the meandering pattern and its migration, particularly for cohesive bed rivers. Moreover, the morphology and dynamics of confined meandering rivers are relatively poorly studied. Due to natural or manmade restrictions, confined meanders cannot freely develop, and this makes them have a meander pattern distinct from those presented by freely meandering rivers. Previous studies of confined meandering rivers have been mostly limited to second degree confinement. Moreover, to the best of our knowledge, the hydrodynamics of a confined meandering channel have not previously been studied in terms of measuring the spatial distribution of the velocity flow field. Given the prevalence of confined meandering rivers, enhancing the grasp of their behavior in the landscape is of essential and practical importance for sustainable river management.

In this study, we evaluate the meander migration dynamics in a first-degree confined meandering cohesive bed river, in which the river makes irregular contact against a

confining railway embankment. We employ a paired sub-reach study approach, wherein one sub-reach is freely meandering and the second adjacent sub-reach is first degree confined by the railway embankment. Morphodynamics of each sub-reach are measured by repeat surveying over a multi-year period. Specifically, channel migration and morphological changes of the channel banks along each of these sub-reaches are analyzed by comparing historical aerial photography, light detection and ranging (LIDAR) data and bathymetric data obtained from a total station survey.

Furthermore, channel hydrodynamics are measured in both sub-reaches by spatially intensive ADCP surveying, which, to the best of our knowledge, has not previously been conducted in a confined meander. This allows for a direct comparison of the hydrodynamic characteristics of unconfined and confined sub-reaches. Furthermore, the measured velocity fields are used to find linkages between the channel hydrodynamics and morphological changes. We are thereby able to explore how local meander confinement leads to different hydro-morphodynamic characteristics and corresponding meander morphology. The methodology employed in this study is comprehensively explained in the next section (section 4.2). Results are shown in section 4.3, followed by the discussion (section 4.4) and conclusion (section 4.5).

4.2 Methodology

4.2.1 Study Site

Watts Creek flows into the Ottawa River at Shirley's Bay in the Kanata region of the City of Ottawa, Canada (Figure 4.1). Two upstream branches (Watts Creek and Kizell Drain) join at a confluence situated [at 45.340172° latitude, -75.880610° longitude (UTM 431006 m E, 5021119 m N)]. Watts Creek has been recognized as providing important coolwater fish habitat (Dillon, 1999). Rates of channel degradation are still not clear. In this study, we mainly focus on two adjacent sub-reaches. The two sub-reaches are M3 and M4 (Figure 4.1c). Both of these sub-reaches are meandering channels with cohesive bed and banks. M4 is partially confined by the City of Ottawa rail line, and thereby is undergoing enhanced erosion. Watts Creek is a semi-alluvial channel offering a diverse habitat, with a mixture of runs, pools, and riffles. While fine clay and silt

substrate is prevalent in Watts Creek, some coarse gravel is also available. Watts Creek has a bed that consists of a high (>30%) percentage of clay, i.e., soil particles that are smaller than two to four micrometers (Salem et al., 2014). Clay particle properties cannot be as straightforwardly predicted because cohesion is dictated by electrostatic forces, which depend on the chemical composition of the clay particles. In addition, the natural consolidation state and hydraulic conductivity, organic matter, and a few other properties influence particle cohesion.

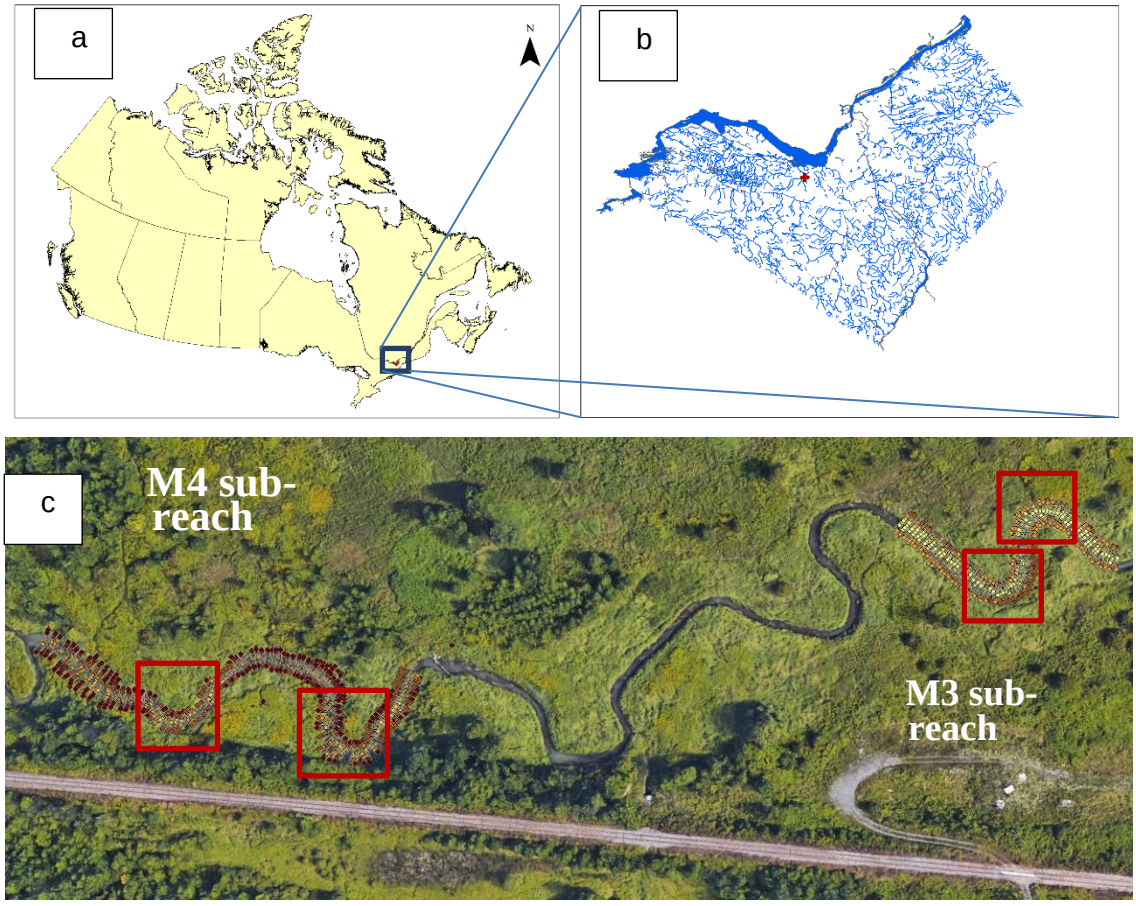

Figure 4.1. (a) Location of the study area within Canada [adopted from https://www12.statcan.gc.ca], (b) Study reach location in the Ottawa Study reach location in the Ottawa area (adopted from http://data.ottawa.ca/en/dataset/water), (c) Surveyed sections in Watts Creek sampling reaches M4 (to left) and M3 (to right) including total station surveyed points, flow from west (left) to east (right) [adopted from Google earth]. Squares show the meander locations and their referred number within each sub-reach shown in Figures 4.10 and 4.11.

The results of the bed sediment core samples collected from the entire reach indicated that all median grain sizes were in the silt or clay range which characterized them as fine grained, cohesive soils. The results of a piston-flume critical bed shear stress test suggest that the cohesive clay bed sediments in Watts Creek watershed are not heavily consolidated (Rennie, 2014).

4.2.2 **Site Reconnaissance**

Channel condition was assessed by visual observation during different flow regimes. The observations are categorized by location within each sampling sub-reach specified in Figure 4.1c. As is shown, M4 sub-reach of Watts Creek is confined by the City of Ottawa rail line. M3 and M4 are otherwise similar; they are meandering channels with cohesive bed and banks. They convey the same discharge (based on the ADCP measurements), and they have similar bed substrate and riparian vegetation. Figures 4.2-4.5 show the field conditions immediately after a spring freshet flood. Locations of erosion and channel incision were identified by exposed tree roots and steep, undercut or collapsing river banks. Observations for each sampling reach are provided below.

4.2.2.1 M4 Sampling Reach

This part of Watts Creek meanders adjacent to the City of Ottawa rail line. Overbank sediment deposits throughout this reach indicated that the previous spring freshet had overtopped the banks in the Main Creek. Figure 4.2a shows the development of a concave-bank bench on the upstream limb of the outer bend at the last sharp meander. There were indications of instabilities on the downstream portion of the outer bank of both bends in M4 (Figure 4.2b). Inner bank instability was also observed at the upstream bend in M4. As shown in Figure 4.3a, an erosion pathway cut through the inner bank point bar during the freshet flow; vertical stakes in the channel suggest failure of a previous attempt to stabilize the inner bank (Figure 4.3b). Figure 4.4a illustrates the evolution of the longitudinal-shaped bar as well as the secondary channel adjacent to the outer bank of the last meander bend. These features suggest that M4 has a very active, unstable channel, presumably due to the meander confinement by the rail line.

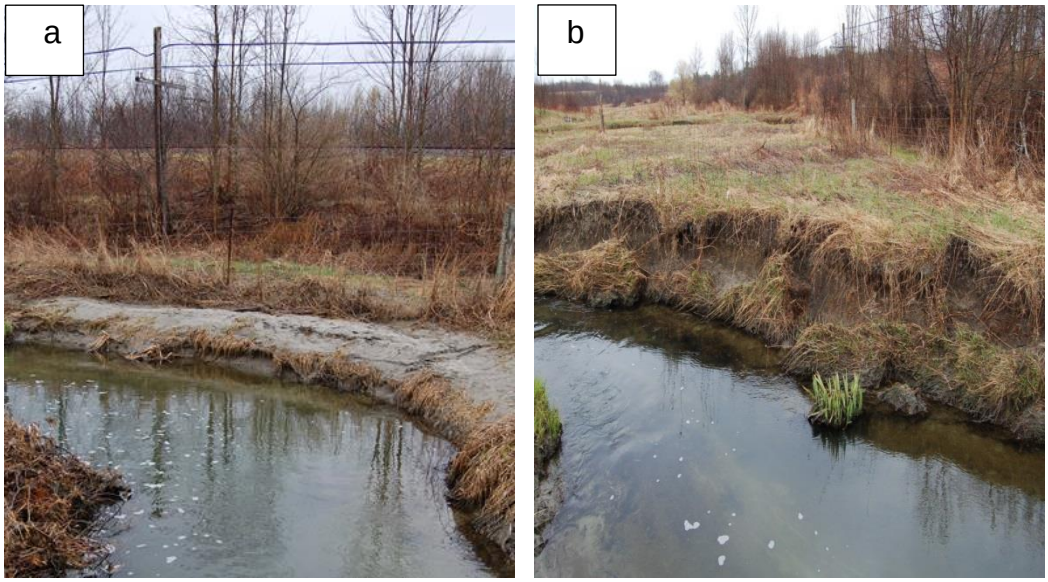

Figure 4.2. M4 sampling reach, meander bend restrained by City of Ottawa rail, facing downstream. Note the City of Ottawa rail line immediately adjacent to the south of the river: (a) Concave-bank bench formation on the upstream of the bend apex (b) The failure of outer bank, downstream of the bend apex. Pictures were taken by the authors April 30, 2014.

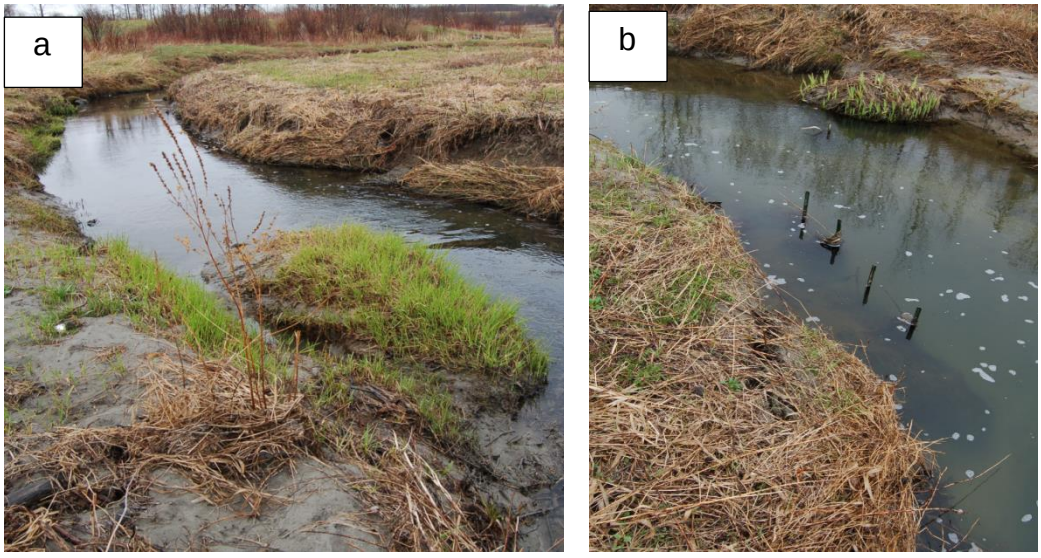

Figure 4.3. M4 sampling reach, meander bend restrained by City of Ottawa rail, facing downstream: (a) Inner bank was overtopped during the previous high freshet flow, to an erosion pathway through the inner bank. (b) Vertical metal stakes used for bank stabilization. Pictures were taken by the authors April 30, 2014.

Figure 4.4. M4 sampling reach: (a) meander bend restrained by City of Ottawa rail, facing upstream. Formation of the longitudinal bar and the secondary channel on the upstream of the outer bend apex. (b) ADCP spatial survey in the study reach. City of Ottawa rail line can be seen immediately adjacent to the south of the river. Pictures were taken by the authors April 14, 2015.

4.2.2.2 M3 Sampling Reach

Sampling reach M3 encompasses two unconfined meander bends. The channel is reasonably stable in M3, displaying only modest bank slumping on the outer bank downstream of a bend apex. This unconfined section of the creek represents a regular meandering pattern with moderate erosion on the outer bank and deposition on the inner bend (Figure 4.5b).

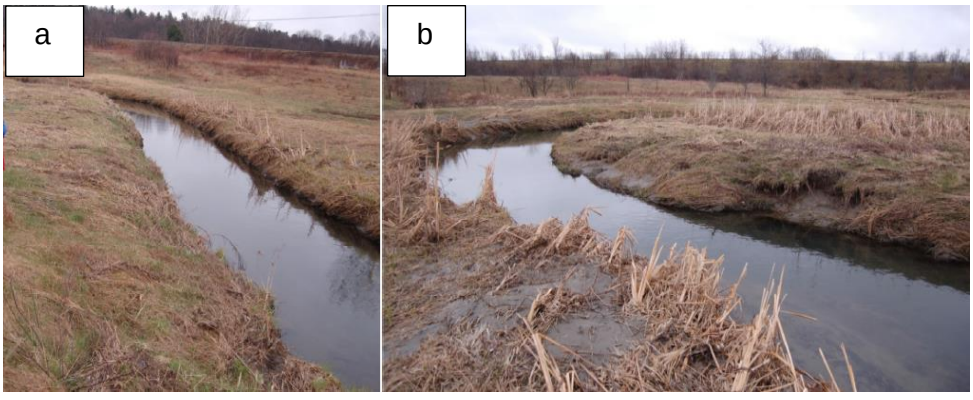

Figure 4.5. M3 facing downstream: (a) In the middle of M3, between the two major bends. (b) Last meander bend manifests regular meandering pattern with erosion on the outer band and deposition in the inner bank. Pictures were taken by the authors in April 2014.

4.2.3 **Data Collection and Analysis**

Morphological studies of the two sub-reaches were done based on the results of: (a) bathymetric survey of each section (b) available LIDAR data (c) historical aerial photographs. Topographic and bathymetric study was conducted during summer 2014 employing a total station survey to accurately distinguish the bank and bed topography. Over 4065 bathymetric points were collected in both study sub-reaches with an average spacing of 1.2 m and 0.3 m in streamwise and cross-stream directions, respectively (Figure 4.1c). The collected points were then interpolated by TIN interpolation method in ArcGIS10.2 to obtain the DEM (Digital Elevation Model) of 2014. Slope and hillshade maps were then obtained from the DEM.

The expense of river hydro-morphological field studies has increased utilization of aerial survey techniques (Biron et al., 2013). Relatively recent development of LIDAR technology allows for accurate measurements of bank locations and elevations (De Rose & Basher, 2011). The City of Ottawa has collected LIDAR data for various parts of the city during different years. This study employs available LIDAR data of the study creek from 2006 obtained from the National Capital Commission (NCC). We converted the LIDAR data to DEMs using ArcGIS. Historical aerial photographs were acquired using Google Earth. The photos were registered using georeferencing tools available in ArcGIS. Stationary ground control points for rectification were obtained using corners of the buildings, road intersections, rail trail, solitary trees and large rocks nearby the study site. Figure 4.6 shows the aerial images of the study reach from 2004 and 2014. It should be noted that both aerial photos show the site condition in the summer (June) which represents the low flow regime (discharge ~0.15 m^3/s based on 2014 ADCP measurements) in the study creek.

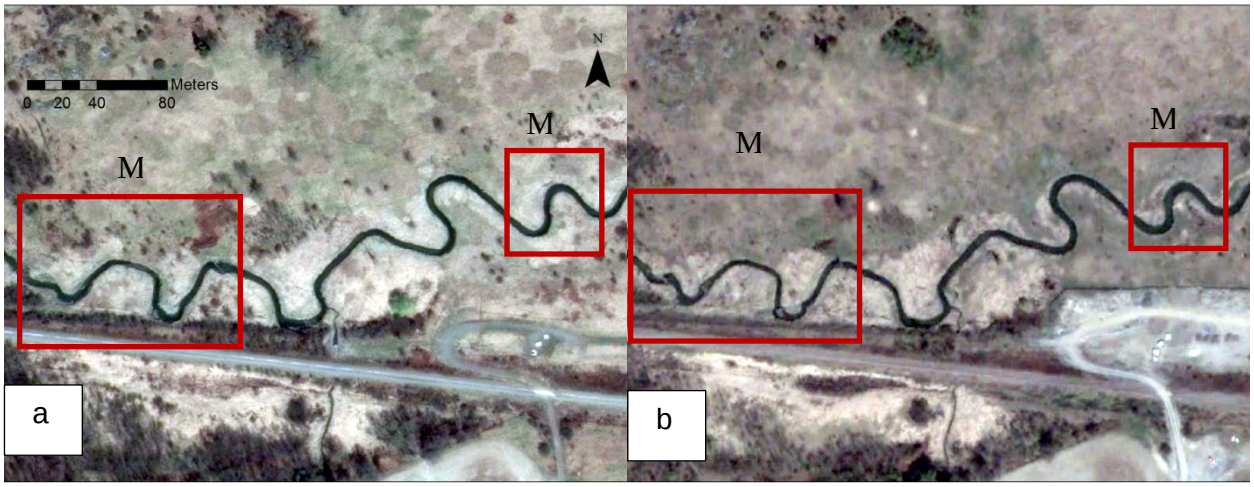

Figure 4.6. Aerial photo of the study reach adopted from Google Earth: (a) 2014 (b) 2004. Location of the each sampling reach is shown with the square.

Comparison was then made between the aerial photographs (2004 and 2014), DEMs obtained from the LIDAR data (2006) and total station surveys (2014). The river DEM maps from 2004, 2006 and 2014 were overlapped in ArcGIS and polygons were created to define the active channel boundary and the bank retreat. To distinguish the location of the base and top of the river banks during different times, slope classification maps were overlapped with the hillshade maps for both LIDAR and surveyed DEMs. This allowed for assessment of the meander behavior and bank retreat of each sub-reach. Having DEMs of the study creek at different periods also allows for measurements of elevation changes. Accordingly, the DEM from 2006 was subtracted from that of 2014 through the raster calculator tool in ArcGIS to produce a DEM difference raster to explore the amount of erosion and deposition (see Williams et al., 2015).

In order to evaluate the effect of the velocity field on the channel morphology, spatially intensive ADCP surveys were conducted in both study reaches during August (low flow) and October (high flow) 2014. A Sontek M9 River Surveyor ADCP was deployed on an Ocean Sciences trimaran riverboat (Figure 4.4b). Standing on opposite banks of the creek, we operated the trimaran boat with ropes and moved the boat downstream in narrowly spaced transects in a zigzag array. The measured depth-averaged velocity data was then post processed using in-house Matlab codes (Rennie and Church, 2010). Parsapour-Moghaddam and Rennie (2015, 2017b and 2018)

provide further details on conducting a spatially intensive ADCP survey in a clay-bed meandering river.

4.3 Results

We compared the position of the active channel mapped from 2004 aerial photography with that of 2014. This is shown for both M4 and M3 sampling reaches in Figure 4.7 and Figure 4.8, respectively. The boundaries were obtained through digitizing the channel margin based on the aerial images in ArcGIS. A sufficiently large number of vertices was employed to avoid digitization errors. Figure 4.9 shows the cumulative erosion and sedimentation that occurred in the channel margins between 2006 (based on the LIDAR data) and 2014 (based on the total station survey). This is obtained by subtracting the 2006 DEM of the study area from the corresponding 2014 DEM.

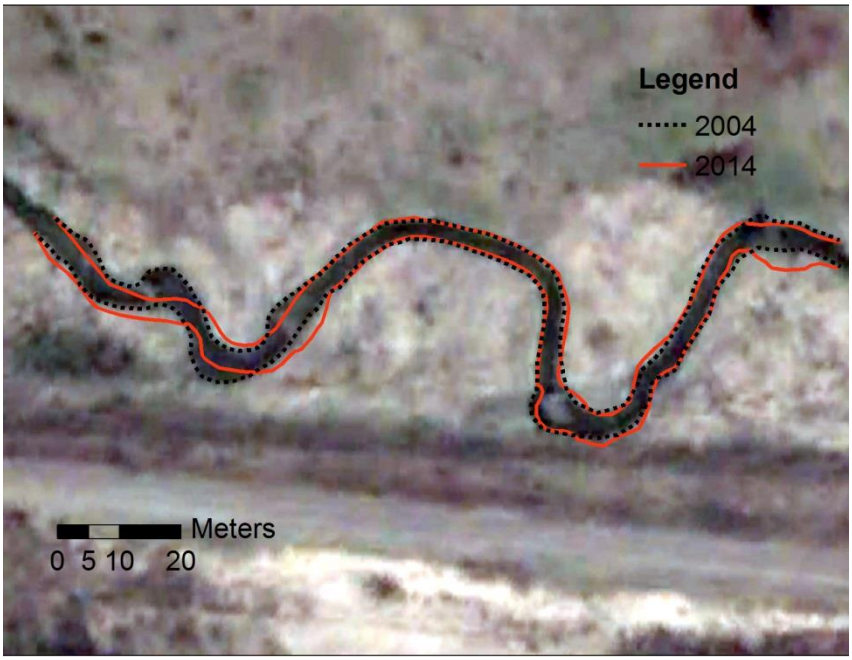

Figure 4.7. Channel margin migration along the M4 sampling reach. Flow from left (west) to right (east). Background image adopted from Google Earth image (2004).

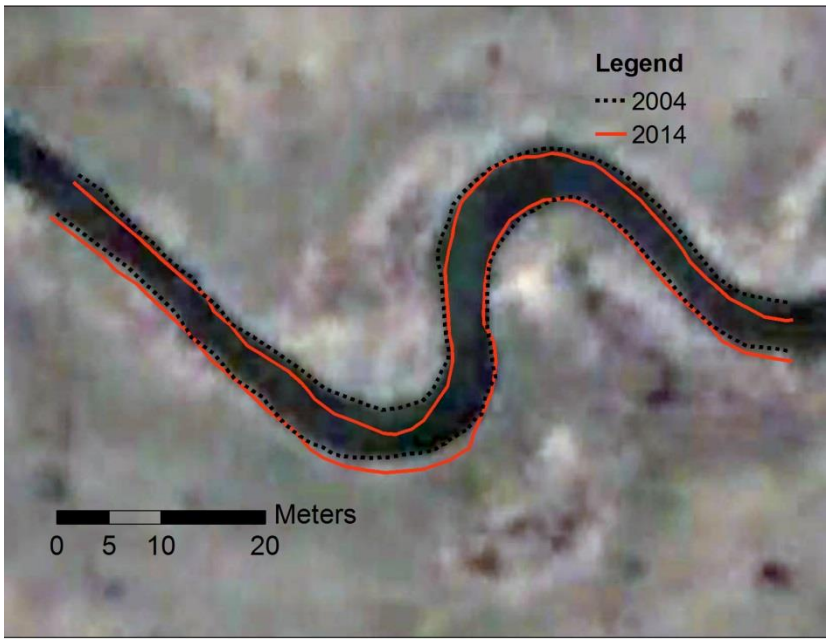

Figure 4.8. Channel margin migration along the M3 sampling reach. Flow from left (west) to right (east). Background image adopted form Google Earth image (2004)

.

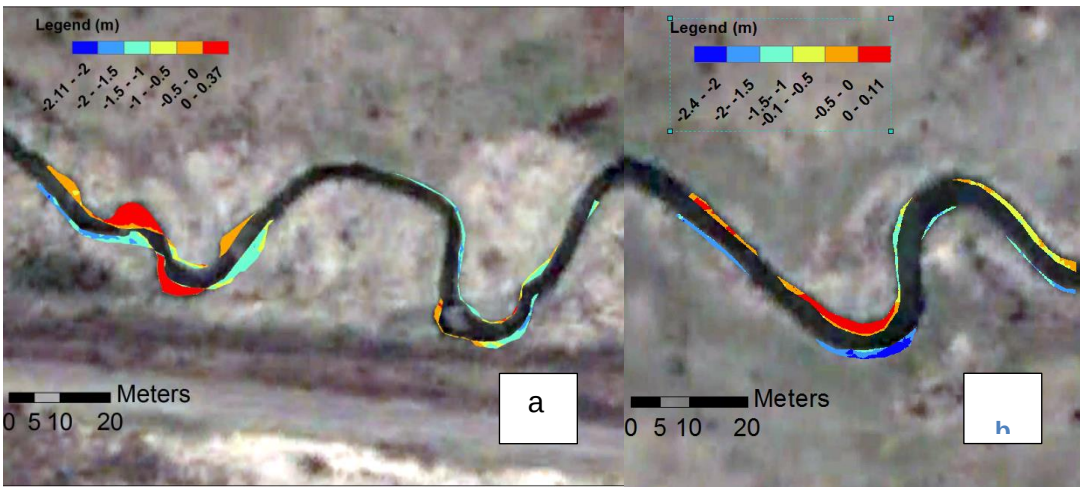

Figure 4.9. Erosion (negative) and deposition (positive) (m) from 2006 to 2014 in: (a) M4 and (b) M3 sampling reaches. Background image adopted form google earth image (2004).

Table 4.1. Channel geometry of each sub-reaches of the study creek within different years.

Sampling reach	Date	Length of the channel Path (m)	Sinuosity
M4	2004	187.88	1.55
	2014	175.27	1.49
M3	2004	106.26	1.44
	2014	107.1	1.46

Figure 4.8 shows that M3 sampling reach has experienced a typical meandering pattern in which erosion and deposition occur at the outer and inner bank, respectively. This can be seen in Figure 4.9b where negative and positive values show erosion (outer bend) and deposition (inner bend), respectively. This confirms our field observations (Figure 4.5). Table 4.1 illustrates that the sinuosity of this sub-reach has been more-or-less consistent, with only a slight increase from 2004 to 2014.

On the contrary, M4 sampling reach (Figure 4.7) has shown irregular meandering behavior. From Table 4.1, it can be inferred that the sinuosity of the channel has decreased from 1.55 to 1.49 in the 10-year period. As shown in both Figures 4.7 and 4.9a, a concave-bank bench can be observed in the upstream limb of the outer bank of the first meander bend. Furthermore, a longitudinal bar is developing in the second meander bend, which may be a precursor to concave bank bench. These results are consistent with the results of our field reconnaissance (Figures 4.2a and 4.4a). On the other hand, Figures 4.7 and 4.9a indicate the occurrence of bank erosion on the downstream of the outer bend apex at the confined meander bends. This was also observed during the field site examination (Figure 4.2b). Apparently, the sharp meander bends of M4 sampling reach migrated downstream whereas the straight portion seemed to be more stable.

To study the hydro-morphodynamics of the irregular meandering development observed in the confined sampling reach in the study creek (Figure 4.2a), ADCP depth-averaged velocities were employed. Figures 4.10 and 4.11 show the interpolated measured depth-averaged velocities during both low flow and high flow in the meander bends of the M3 and M4 sub-reaches, respectively. As shown in Figure 4.11, reverse flow

occurred in the confined meander bends while the unconfined meanders had a regular flow pattern in the streamwise direction (Figure 4.10). The reversing flow was associated with the irregular bend geometry and the flow obstruction imposed on the bend flow by the concave-bank bench.

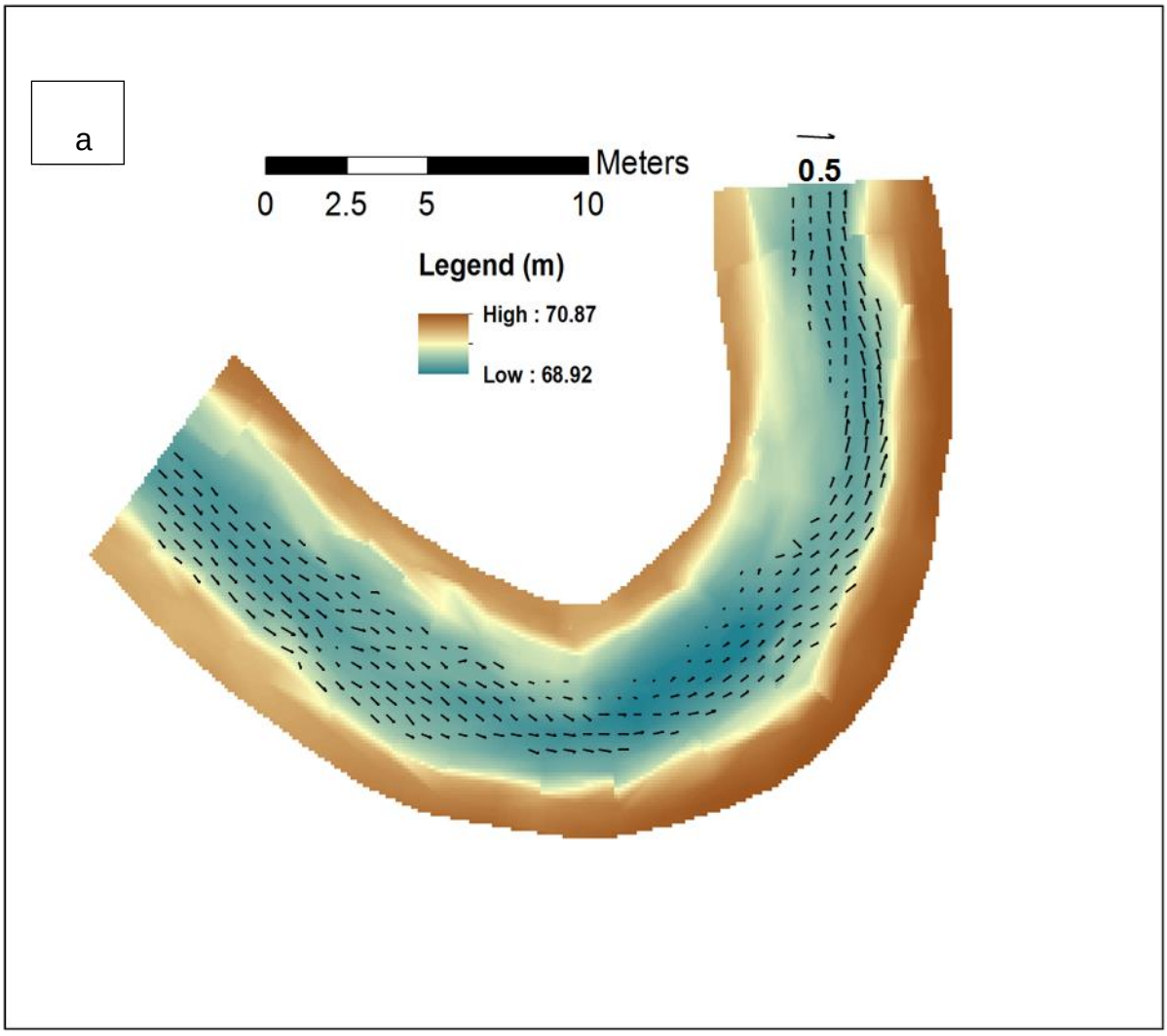

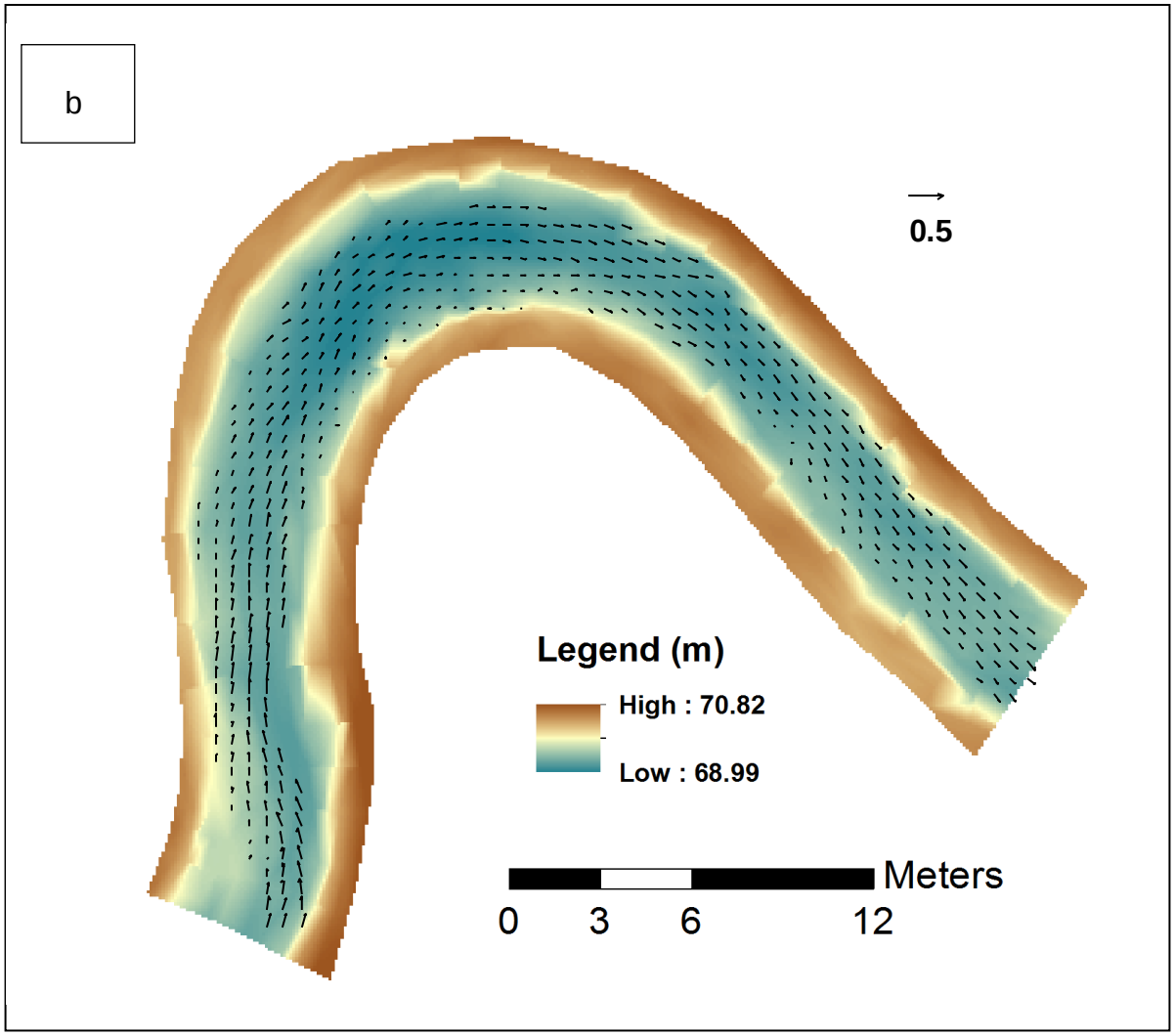
b
0.5
Legend (m)
High : 70.82
Low : 68.99
Meters
0
3
6
12

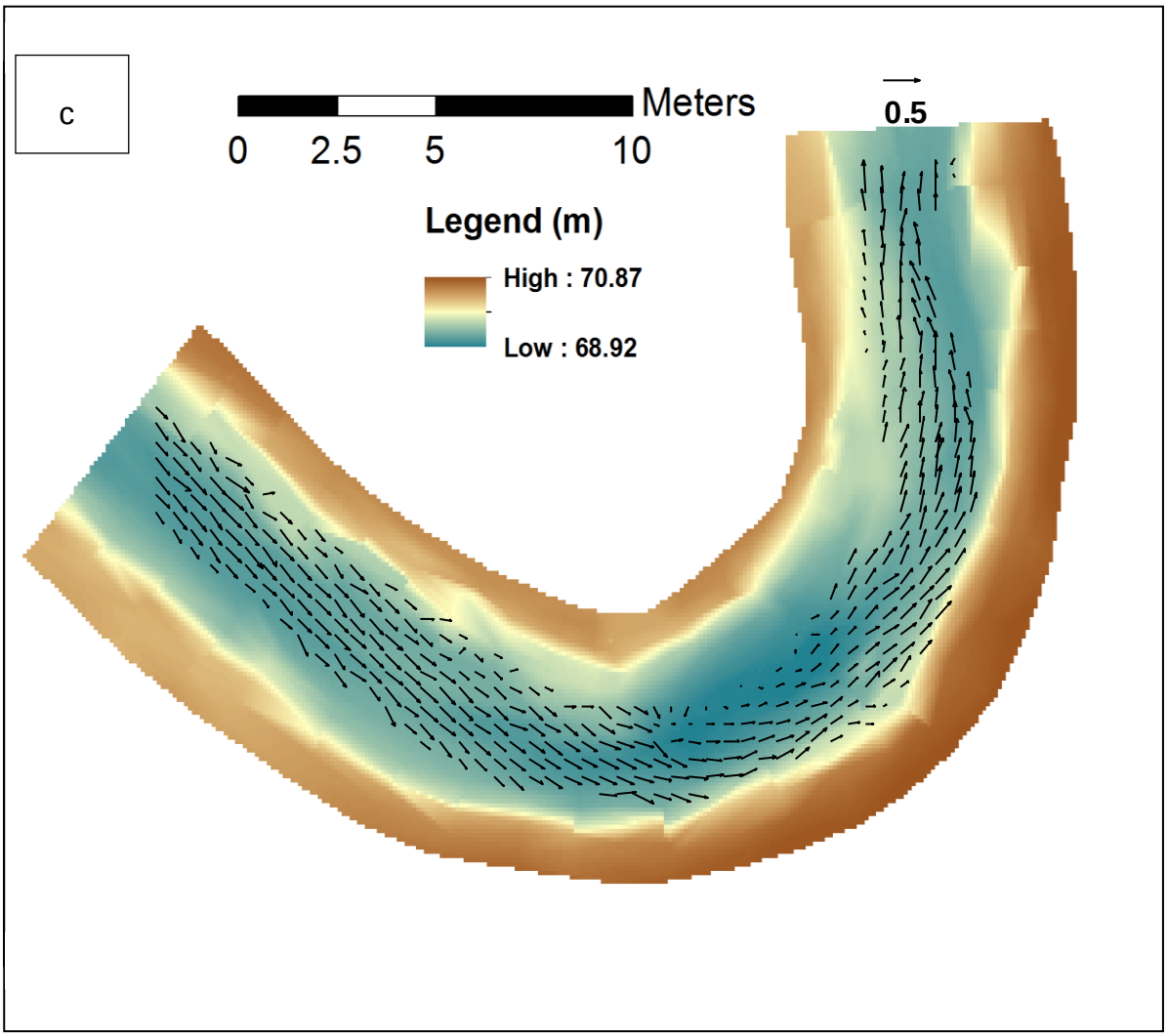
c
Meters
0
2.5
5
10
0.5
Legend (m)
High : 70.87
Low : 68.92

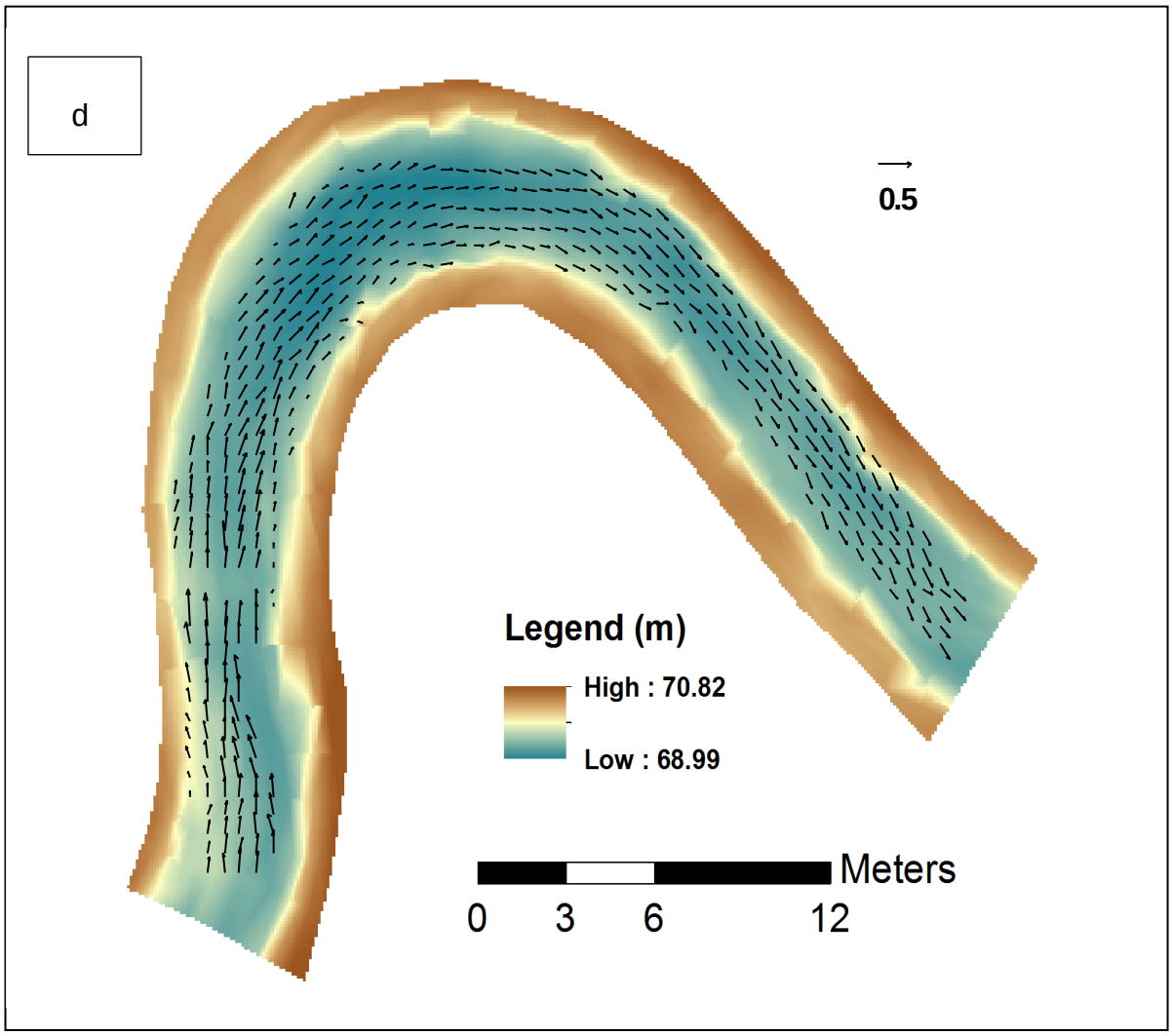

Figure 4.10. Measured depth-averaged ADCP velocities in the meander bends of the M3 sub-reach at: (a) first bend during August, 2014 (low flow), (b) second bend during August, 2014 (low flow) (c) fist bend during October, 2014 (high flow) (d) second bend during October, 2014 (high flow). Refer to Figure 4.1c for location of these bends. Surveyed bathymetric data (2014) is shown in the background.

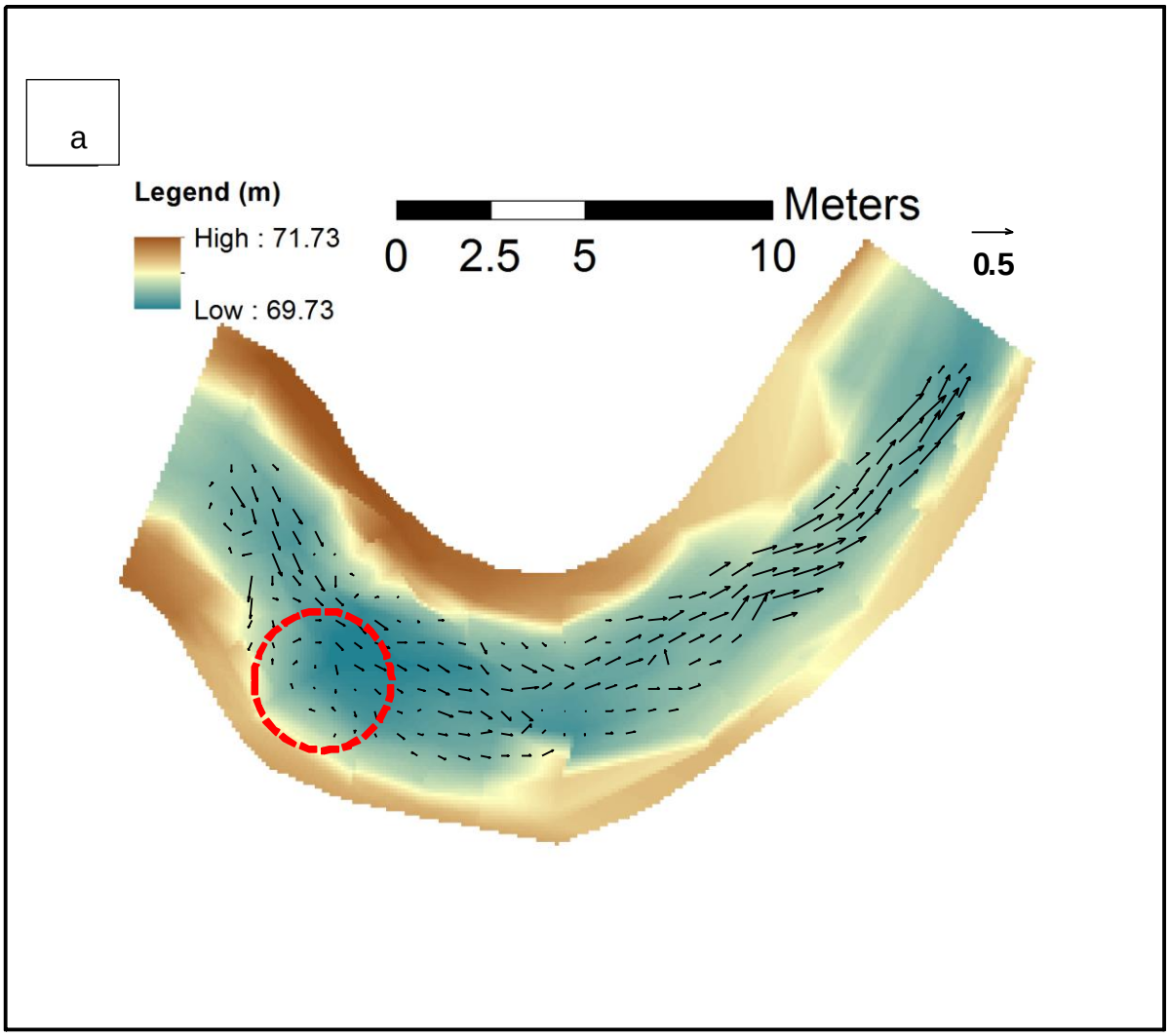
a
Legend (m)
High : 71.73
Low : 69.73
Meters
0
2.5
5
10
0.5

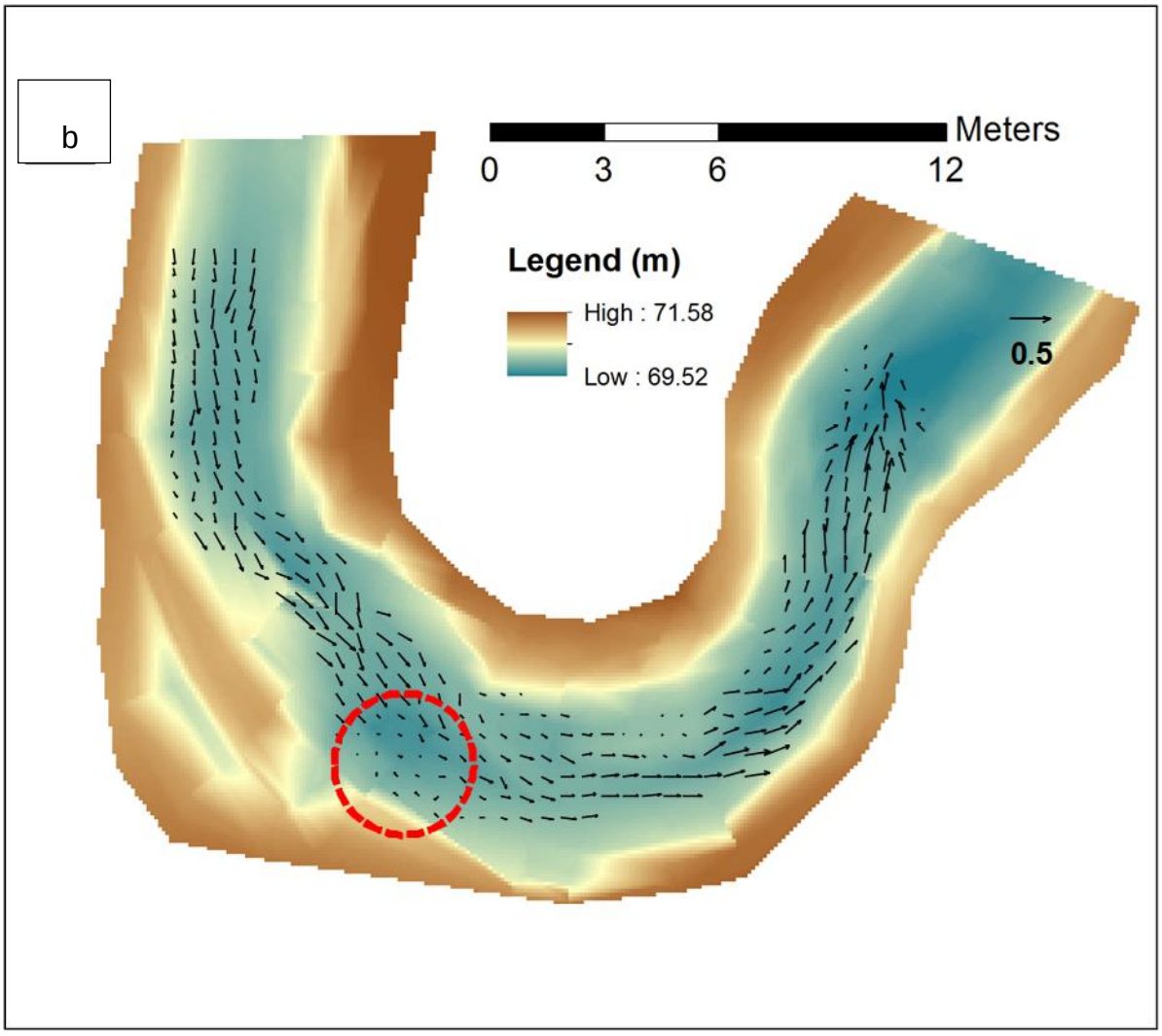
b
Meters
0
3
6
12
Legend (m)
High : 71.58
Low : 69.52
0.5

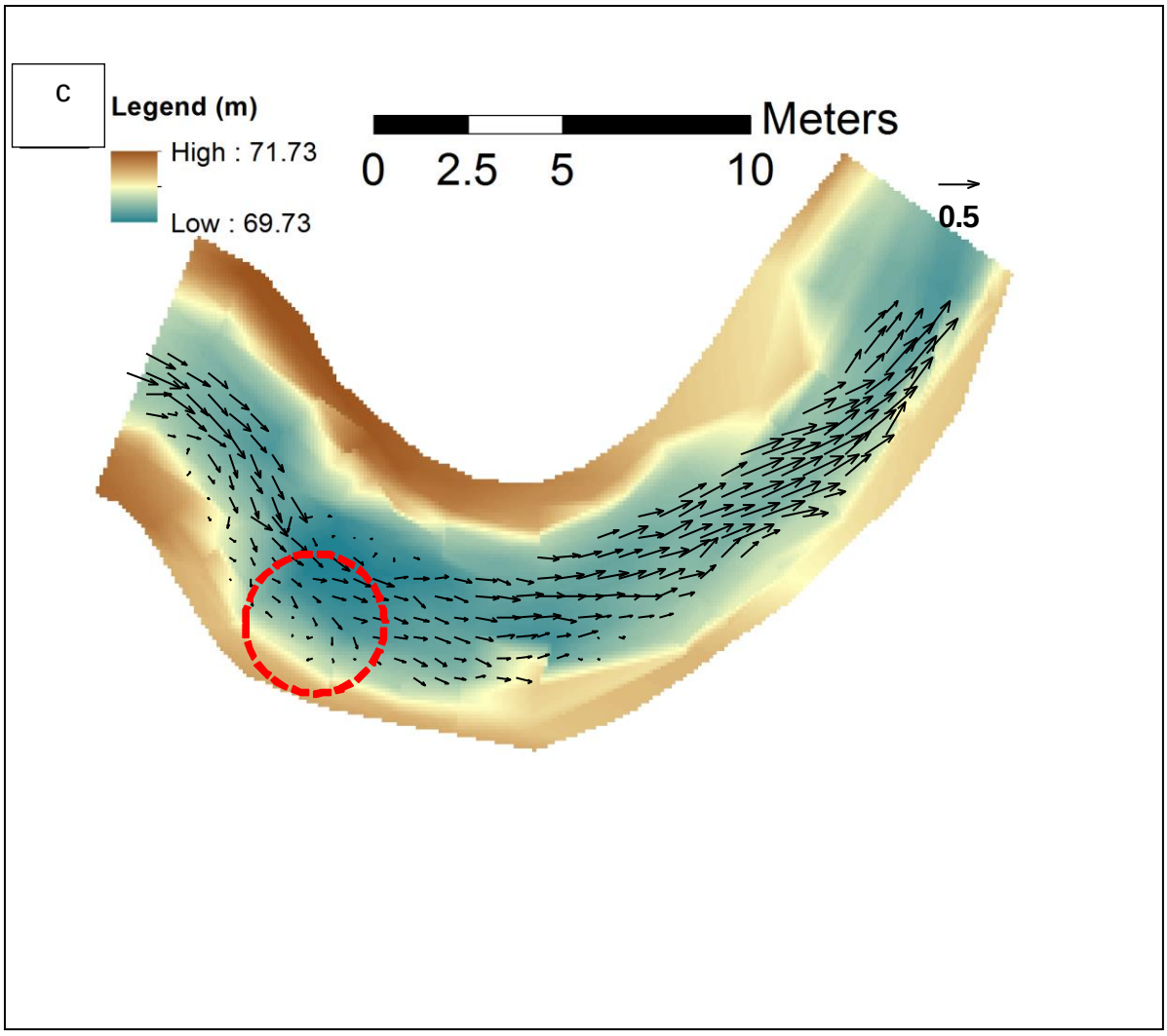
C
Legend (m)
High : 71.73
Low : 69.73
0 2.5 5 10
Meters
0.5

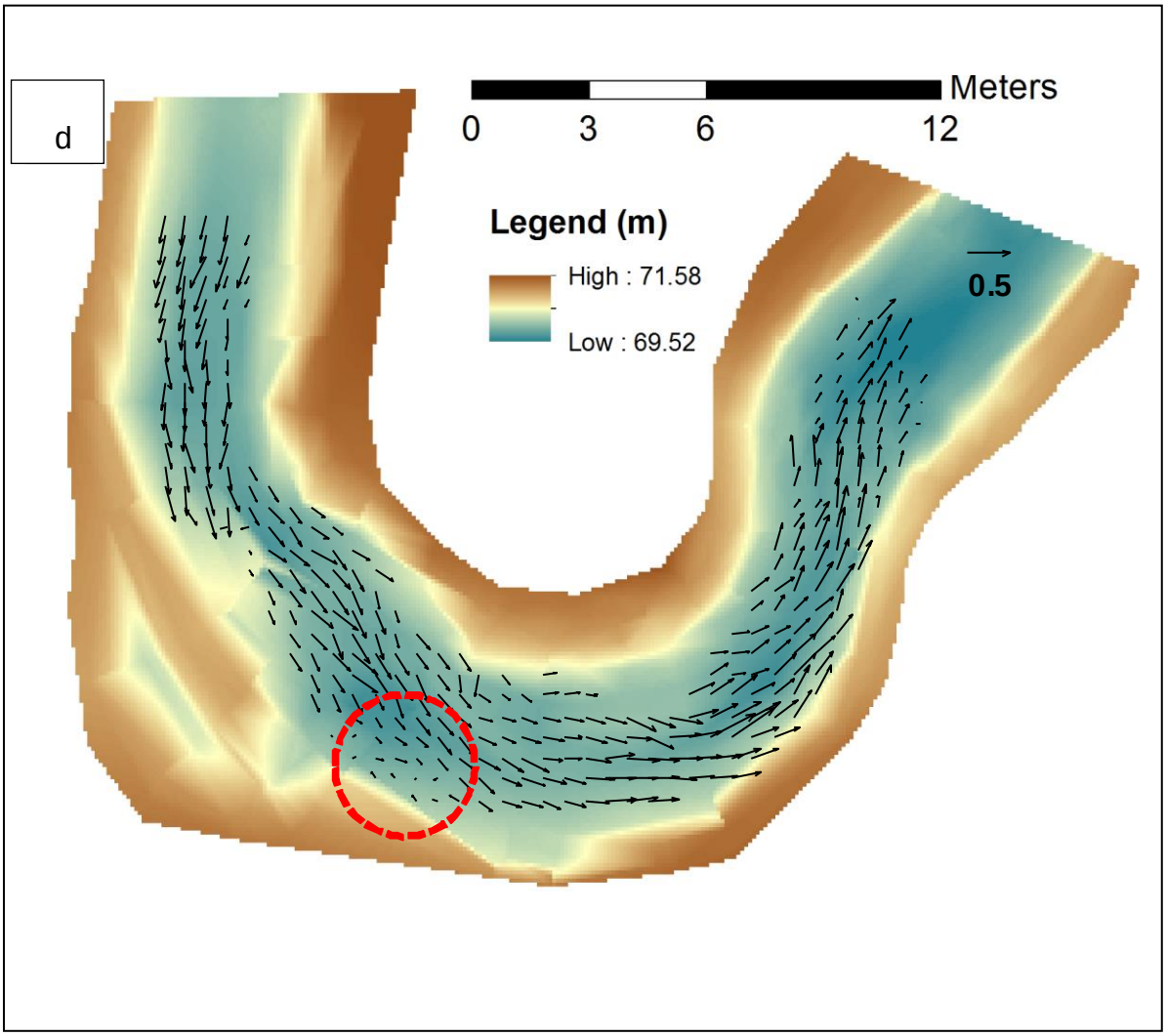

Figure 4.11. Measured depth-averaged ADCP velocities in the meander bends of the M4 sub-reach at: (a) first bend during August, 2014 (low flow), (b) second bend during August, 2014 (low flow) (c) fist bend during October, 2014 (high flow) (d) second bend during October, 2014 (high flow). Refer to Figure 4.1c for location of these bends. Surveyed bathymetric data (2014) is shown in the background.

4.4 Discussion

The morphology of meandering cohesive bed rivers is yet not fully understood, particularly when they are confined. The results of this study illustrated an irregular meandering pattern in the confined sub-reach of the study creek. This irregular meandering pattern included development of a concave-bank bench in the upstream portion of confined bends.

Page and Nanson (1982) developed a conceptual model for the formation of a concave-bank bench, which begins with cut-bank erosion that enlarges the channel. The possible growth of a point bar upstream of a sharp bend would deflect the flow and leave a region of flow expansion and separation downstream and beside the upstream limb of the concave bank which generates large eddies and induces reverse flow. The developed reverse flow causes the upstream margin of the inner bend to erode and thus widen the channel. Consequently, compensating sedimentation may occur in the downstream portion of the inner meander bend, which leads to downstream migration of the meander. The vacated zone at the upstream limb of the outer bend could be filled with eddy accretion consisting mostly of fine grains, leading to development of a concave-bank bench.

In coherence with the Page and Nanson conceptual model for development of a concave-bank bench, the encroachment of the railway embankment on the M4 sampling reach in the study area confined the lateral erosion and caused the meander to migrate downstream, which provided room for fine-grained accretion on the outer meander bends. On the other hand, lower ratio of the bedload to the suspended load in this semi-alluvial cohesive-bed river may have limited downstream development of the point bar (Makaske and Weerts, 2005; Jamieson et al., 2013). This may have created an open space for separation zone and flow expansion. The measured ADCP velocities in the confined meander (Figure 4.11) confirmed the creation of the reverse flows caused by the flow expansion which would favor the development of the concave-bank bench. The ADCP measurements employed in the present study provide the first corroborative proof for the theory developed by Page and Nanson (1982), which was not previously supported by detailed velocity field measurements.

Nanson and Page (1983) indicated that during the process of eddy accretion, a longitudinal-shaped bar could be developed, close to the concave bank and upstream of the meander apex, prior to the full formation of the bench. As a result, a secondary channel may occur since the generated longitudinal bar bench may fail to migrate completely to the concave bank. This longitudinal bar serves as a core for further deposition. Gradual deposition and aggradation of the bar leads to complete formation of the concave-bank bench. Figure 4.4a shows the creation of a longitudinal-shaped bar and an induced secondary channel in the confined M4 sampling reach. This can be caused by the sedimentation in the flow separation zone at the upstream of the outer bank.

Bank instability which was mostly observed in the confined section can be attributed to induced reverse eddy currents, which facilitate the undercut erosion and bank failure on the upstream of the outer banks. Another possible reason for the observed bank instability in the confined setting could be linked to elevated pore water pressure during flood drawdown, which cannot rapidly drain due to the cohesive nature of the bank. With decline of the spring freshet flow stage and removal of the confining river pressure, the elevated pore water pressure could reduce the frictional shear strength and increase the unit weight of the bank material, which may have contributed to the observed bank failures. Furthermore, construction of the railway embankment may have consolidated the river bank, further hindering dissipation and drainage of elevated pore water pressures in the river bank.

4.5 Conclusion

Despite previous research on meander migration patterns, both the impact of channel confinement and the detailed hydro-morphodynamics in a cohesive meandering clay bed river are not yet fully understood. The present study examined the meandering behavior of a cohesive clay bed river over a 10-year period. Two sub-reaches of the same meandering cohesive clay bed river were shown to have different morphodynamic characteristics and migration pattern. The unconfined sampling reach had a typical meandering pattern with erosion on the outer banks and deposition on the inner banks of meander bends. The sinuosity of the reach remained more-or-less constant over the

ten year period. On the other hand, analysis of aerial images along with LIDAR data, total station survey, and field examination revealed an irregular meandering pattern in the confined sub-reach. The sinuosity of this part of the creek decreased from 1.55 to 1.49. The results showed an evolution of the concave-bank bench on the upstream limb of the outer banks of the sharp menders in the confined reach, whereas bank instability was observed downstream of the bend apices. It was shown that different locations along a river, depending on degree of channel confinement, could have distinctly different morphological characteristics. To explore how the morphodynamics of each sub-reach could be linked to its hydrodynamics, we employed spatially intensive ADCP surveying. The results of ADCP depth-averaged velocities confirmed the occurrence of reverse flow on the upstream limb of the outer meander bends in the confined sub-reach, which could be linked to the irregular meandering pattern and generation of the concave-bank bench. The results of this study shed light on the potential impacts of channel confinement on the bank retreat and river migration in comparable case studies.

CHAPTER 5

Impact of channel morphodynamics on fish habitat utilization[4]

Abstract:

It is reasonable to expect that hydro-morphodynamic processes in rivers can affect fish habitat availability and quality, but the impacts of morphological changes in fluvial systems on fish habitat are not well studied. Herein we investigate the impact of morphological development of a cohesive meandering stream on the quality of fish habitat available for juvenile yellow perch (*Perca flavescens*) and white sucker (*Catostomus commersonii*). A three-dimensional (3D) morphodynamic model was first developed to simulate the hydro-morphodynamics of the study creek over a 1-year period (2014- 2015). The 3D hydro-morphodynamic model was successfully calibrated using an intensive acoustic Doppler current profiler (ADCP) spatial survey of the entire 3D velocity field and total station surveys of topographic changes in a meander bend in the study creek. The model predictions of morphodynamic changes (erosion and deposition) were incorporated into a fish habitat availability assessment at the end of the study period. Two fish sampling surveys were carried out at the beginning and the end of the study period to determine habitat utilization of each fish species in the study reach. ANOVA multiple comparison tests indicate that morphological development of the stream was a significant factor ($p < 0.05$) for the habitat utilization of juvenile yellow perch , whereas juvenile white sucker utilization of habitat was not significantly impacted by the changes in creek morphology. It is shown that juvenile yellow perch mostly utilized habitat where deposition occurred whereas they avoided areas of erosion. Flow depth, depth-averaged velocity, and suspended sediment transport also significantly influenced habitat utilization of the juvenile yellow perch. As

[4] This chapter has been submitted as: **Parsapour-Moghaddam, P**., Brennan, C. P., Rennie C. D., Elvidge, C. K., Cooke, S. J. (2018). Impact of channel morphodynamics on fish habitat utilization.

for the juvenile white sucker, the only significant habitat factor was the depth-averaged velocity. Results of the developed fish habitat model based on the standard habitat variables illustrated that the model could not reasonably predict the habitat quality of juvenile yellow perch. Accordingly, the results of the developed 3D hydro-morpohodynamic model were merged with the fish habitat model. Comparison of the predicted fish habitat map of the juvenile yellow perch with the results of fish sampling surveys revealed that the habitat quality was better predicted when the impact of morphological changes was taken into account in the fish habitat modelling. The results of this study and the proposed methodology could provide some insights into the potential impact of sediment transport processes on the fish community and has implications for effective river management.

Keyword: 3D morphodynamic modelling, River morphological changes, Fish habitat modelling, Fish sampling surveys, Fish habitat quality, Yellow perch, White sucker.

5.1 Introduction:

5.1.1 Morphodynamic modelling:

Studies of river morphological behavior are crucial for understanding river condition and the associated quality and availability of aquatic habitat. However, morphodynamic processes have been recognized as some of the least understood phenomena in natural rivers (Wu, 2007). Several morphodynamic models have been developed over the past decades in an attempt to improve understanding of the river morphodynamics. Appropriate choice of the morphodynamic model depends on the condition and complexity of the study area (Papanicolaou et al., 2008). Until recently, the state-of-the-art for morphodynamic modelling involved two-dimensional (2D) models (Pinto et al., 2012). However, direction and magnitude of the bed shear stress, which has a significance influence on the sediment transport, may not be accurately estimated from a 2D model (Lesser et al., 2001). This could be the case in particular for meandering rivers with dominant secondary flow structures, wherein secondary flow occurrence can increase the sidewall shear stress exerted on river banks (Papanicolaou et al., 2007). Furthermore, due to the complex nature of cohesive sediments, prediction of the

erosion and sedimentation of a cohesive bed river is even more challenging (Haralampides and Rodriguez, 2006; Peixoto et al., 2017). 3D models are more capable of reproducing complex 3D river hydro-morphodynamics processes compared to 1D and 2D models, and due to the advancement of computer technology, development of 3D hydro-morphodynamic models has been growing recently (e.g., Ruther and Olsen 2005; Khosronejad et al. 2007; Khosronejad et al. 2015).

Delft3D is a widely used hydro-morphodynamic open source code which is developed by Deltares and has a broad range of applications in river studies (e.g. Van Maren, 2007, Rinaldi et al., 2008; Sloff, 2010, Moerman, 2011; Spruyt et al., 2011; Williams et al., 2013; Schuurman et al., 2013; Schuurman and Kleinhans, 2015; Staines and Carrivick, 2015; Javernick et al., 2016; Kasvi et al., 2015a,b, Williams et al., 2016; Singh et al., 2017; Su et al., 2017; Mohammed, 2017). The morphological module of Delft3D has been validated by Lesser et al. (2004). 3D modelling with Delft3D 3D can be further divided to hydrostatic and non-hydrostatic modules. Parsapour-Moghaddam and Rennie (2017) showed that the hydrostatic module is able to predict the secondary flow in a tortuously meandering creek. Despite the growing need for 3D morphodynamic modelling, only a few studies have employed Delft3D for 3D morphodynamic modelling in meandering rivers. The Kleinhans group (Kleinhans et al., 2008; Schuurman et al., 2013; Schuurman and Kleinhans, 2015) have employed Delft3D to create 3D models to predict morphodynamics of meandering and braided rivers; however, their studies have focused on bifurcation dynamics with non-cohesive sediments. Kasvi et al., (2015a) studied the sensitivity and functionality of 2D and 3D hydro-morphodynamic Delft3D models. However, their results were limited to short-term (one flood event) morphodynamic processes. Moreover, their results focused on a sandy bed river bend. In the present study, we simulate 1-year of hydro-morphodynamics in a natural meandering cohesive bed river using a 3D Delft3D numerical model. The results of the hydro-morphodynamic module are then employed for a fish habitat quality assessment.

5.1.2 **River morphodynamics and fish habitat:**

Dynamic interaction of the hydro-morphodynamic processes and the aquatic environment define a river's ecological characteristics (Poff and Zimmerman, 2010). In

order to improve the conditions of an aquatic ecosystem, it is essential to know how the fish populations respond to the ecological changes and how different fish species are linked to their habitats (Portt et al., 2006). River hydro-morphodynamics influence the quality of habitat for fish and other aquatic species (Baranya et al., 2018; Tamminga and Eaton, 2018). Suspended sediment transport can influence the water temperature and dissolved oxygen levels, and can lead to biological impacts on aquatic organisms (Kjelland et al., 2015). It is important to study a river's morphological changes and the corresponding sediment loads to manage and preserve fish populations (Sullivan and Watzin, 2010).

Numerical simulation of fish habitat has been employed since the 1980s as a useful means for river management and environmental impact assessment (Mouton et al., 2007). Fish habitat models can quantify a river's ecological condition. They can also be used to investigate the impact of different restoration plans and river management measurements (De Kerckhove et al., 2008). Several fish habitat models have been developed to predict the impact of river ecological changes on fish abundance and diversity. Such models can be employed to preserve an aquatic habitat or declining species, since fish habitat models provide a better perception of the health and condition of the river ecosystem for effective river management (Tash and Litvaitis, 2007).

There have been few previous attempts to couple morphodynamic model predictions with fish habitat modelling. Kerle et al. (2002) and Baptist et al. (2002) indicated that long-term morphodynamic changes in the man-made secondary channels in the Rhine River could significantly affect the quality and availability of fish habitat. Baptist et al. (2002) used a 2D version of Delft3D to model the hydro-morphodynamics. The outputs of the model were then fed into a fuzzy habitat model, Casimir. However, no fish sampling survey was conducted during their study, and therefore, the fish habitat model could not be validated. Accordingly, the correlation between the morphodynamic changes and the availability of the fish habitat was not studied. Hauer et al. (2007) showed that riffles instability would negatively affect the reproduction of nase (*Chondrostoma nasus*), the main fish species in the Austrian lowland Sulm River. They suggested that morphological studies should be considered in river restoration projects.

Hauer et al. (2008) subsequently studied how juvenile nase could be impacted by morphodynamic processes in the river. They combined the results of 1D and 2D hydrodynamic models with a fish habitat model. They obtained the sedimentation and erosion of the study river by terrestrial surveys within three years. They also conducted an electrofishing survey to study how the juvenile nase respond to the morphological changes. The results of this study confirmed the reduction in the habitat suitability by the channel morphological changes; however, no morphodynamic simulation was employed. Moreover, the correlation of the sedimentation and erosion with the available fish habitat was not studied. Escobar-Arias and Pasternack (2010) evaluated in-stream ecological functionality based on the shear stress dynamics. However, calculated bed shear stress from the hydrodynamic numerical model may not be a good representative of the intricate dynamics of the sediment process and the impact of bed level changes on the hydraulics. Noack (2012) used the CASiMiR habitat model to simulate the suitability a river bed for reproduction of gravel-spawning fish. This study used a 3D morphodynamic model to account for the morphodynamic processes and considered the impact of bed level changes on the hydraulics. However, their habitat model was mainly based on the water depth, flow velocity, and dominant substrate, while the dynamic sedimentation and erosion processes were not correlated to the fish habitat.

In the present study, we will develop a 3D morphodynamic model to estimate the morphological changes of the study river. Two different fish sampling surveys were conducted within the study period. The results of the morphodynamic model were then used to discover if there is any correlation between erosion/ sedimentation processes and the availability and utilization of fish habitat in the study reach.

5.1.3 **Objectives and novelties:**

Ecological condition Ecological condition of a fluvial system, to a great extent, depends on its physical habitat (Maddock, 1999). Previous morphodynamic-fish habitat studies have mostly focused on the sediment grain size and distribution rather than the morphological changes. The long-term impacts of sediment transport on aquatic species are still not well understood and more study is needed to alleviate the potential

effects of sediment transport on fish communities (Kjelland et al., 2015). In the fluvial system's management, it is of practical importance to identify and protect fish that are sensitive to channel sedimentation and the associated sediment loads (Sullivan and Watzin, 2010).

The present study, for the first time, studies the correlation between morphological development and the fish community in the same river. We developed a 3D Delft3D model of a natural cohesive meandering stream using unsteady flow with the aim that this methodology and parameters employed therein could be useful in similar case studies. Total station topographic surveys were conducted in 2014 and 2016 to provide bathymetric change data for the morphodynamic module calibration. We also conducted spatially intensive ADCP survey in the study area to obtain data for the hydrodynamic module calibration. The calibrated 3D morphodynamic model was then run for a one-year period to assess how the fish habitat quality changed over this period. We performed two fish sampling surveys in the study area in 2014 and 2015 to find a relationship between the physical fish habitat and morphological changes of the study creek. The results of the 3D morphodynamic model were then employed to develop a fish habitat model for juvenile yellow perch. The next section (5.2) illustrates the area of the study. Section 5.3 explains the proposed methodology including the field studies (5.3.1), 3D morphodynamic modelling (5.3.2) and the fish habitat studies (5.3.3). Results are shown in Section 5.4 followed by the discussion (Section 5.5) and conclusions (Section 5.6).

5.2 Study Area:

The study site was a meandering reach of Watts Creek, which flows into the Ottawa River at Shirley's Bay in the Kanata region of the Municipality of Ottawa, Canada. Watts Creek flows east and north over National Capital Commission (NCC) greenbelt forest property (Fig. 5.1). The bed and bank materials are mostly cohesive (Salem and Rennie, 2017). Watts Creek provides crucial cool water fish habitat and has a high fish abundance (Maarschalk-Bliss, 2014). However, this creek has undergone erosion and degradation which can negatively impact the available aquatic habitat. The present

study attempts to understand the hydro-morphodynamics to gain a better understanding of the fish habitat quality in Watts Creek.

The study reach is adjacent to the City of Ottawa rail line. The meander confinement by the rail line has caused excessive erosion and irregular meandering pattern in the reach (Parsapour-Moghaddam and Rennie, 2018b). Core samples of bed sediment collected from the reach were identified as fine-grained, cohesive soils. Piston-flume critical bed shear stress analysis showed that the clay bed sediments in the study creek are not heavily consolidated (Salem and Rennie, 2017). Field reconnaissance of the creek revealed instabilities in the inner banks of meanders as well as the downstream limb of the outer bends. It was also observed that a concave-bank bench has been generated on the upstream portion of the outer bank at the last sharp bend (Parsapour-Moghaddam and Rennie, 2018b). These observations confirmed that the study reach is an active and unstable channel.

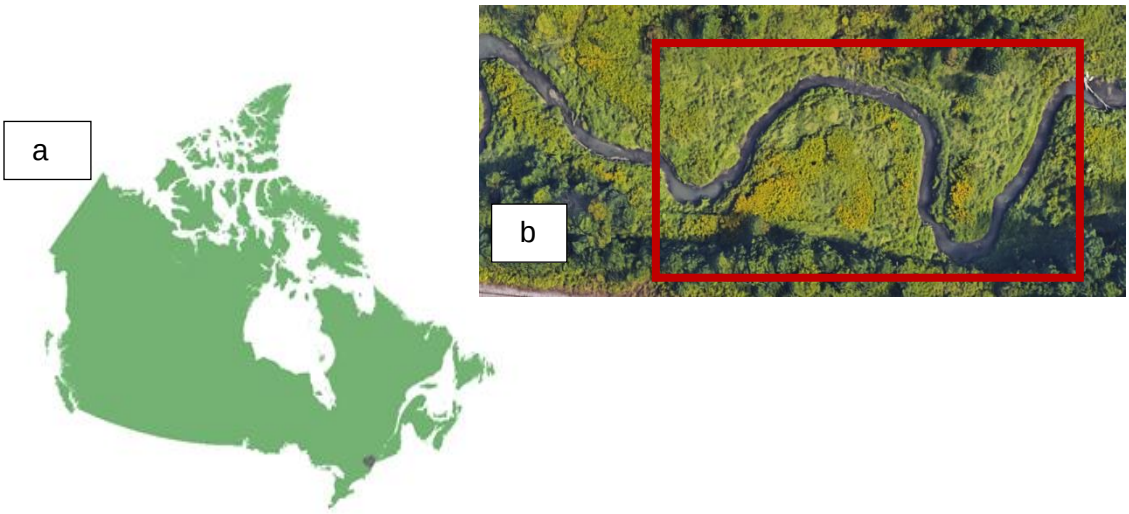

Figure 5.1. (a) **Location of the City of Ottawa in Canada (adapted from https://www12.statcan.gc.ca);** (b) **Study creek shown with the square (adopted from Google earth), flow from west (left) to east (right). The center point of the reach is situated at ~ 431086.6 m E 5021107.4 m N. Please note that the dimension of the red box is 90m*45m.**

5.3 Methodology:

5.3.1 Field studies

Initial bathymetric data needed for the morphodynamic modelling was first collected during summer 2014 using a total station survey with an average spacing of 1.2 m and 0.3 m in streamwise and transverse directions, respectively (Fig. 5.3b). We also conducted a Total station bathymetric survey in the second meander bend of the creek during summer 2016 to assess the morphological changes of the river within the two-year period (Fig. 5.2b). Bathymetric points were collected with an average spacing of 2.7 m and 0.6 m in streamwise and transverse directions, respectively. Triangular interpolation method (TIN) was then employed in ArcGIS10.2 to attain the digital elevation model (DEM) for both bathymetric surveyed data points.

Figure 5.2. Total station bathymetric points collected during summer: (a) 2014 (b) 2016. Flow from left to right. Background pictures taken from Google Earth.

We also employed a spatially intensive ADCP method to obtain the spatial distribution of 3D velocities all over the reach (Fig. 5.3a). An ADCP is a hydroacoustic tool which, based on the principles of Doppler shift, measures the 3D flow velocities. More detailed information on ADCP theory is available in Simpson (2001), Simpson and Oltman (1993), and Rennie and Church (2010). We mounted a Sontek M9 River Surveyor ADCP on an Ocean Sciences trimaran riverboat which was operated and moved, slower than the flow, in a zigzag pattern via ropes by two operators at each side

of the river. The sampling frequency of the moving boat was 1Hz. The compass was calibrated in situ through ADCP rotation with varying pitch and roll. The spatial distribution of 3D velocities, obtained from the ADCP survey, was then employed to calibrate the 3D hydrodynamic model. Calibration of the 3D hydrodynamic model with this method ensures better prediction of the 3D flow field (Parsapour-Moghaddam and Rennie, 2018a).

Figure 5.3. Field studies in Watts Creek: (a) ADCP mounted on an Ocean Sciences trimaran riverboat employed for spatially intensive ADCP survey (b) Total Station used for terrestrial survey.

5.3.2 **3D morphodynamic modelling:**

For 3D hydro-morphodynamic modelling of the study meandering creek, we employed the Delft3D modelling package (Delft-Flow version 4.01.01). Delft3D is a freely-available, open-source code developed by Deltares. This code includes different components interacting individually or in combination with other modules over a mutual interface (Deltares, 2014). It is capable of modelling 2D or 3D hydro-morphodynamics over a rectilinear or a curvilinear grid. The Delft3D hydrodynamic model solves 3D Navier–Stokes equations for incompressible flow under Boussinesq assumptions. The partial differential equations include the following flow and momentum continuity equations:

$$\frac{\partial \eta}{\partial t} + \frac{\partial (hU)}{\partial x} + \frac{\partial (hV)}{\partial y} = 0 \quad (5\text{-}1)$$

$$\frac{\partial u}{\partial t} + u\frac{\partial u}{\partial x} + v\frac{\partial u}{\partial y} + w\frac{\partial u}{\partial z} = -g\frac{\partial \eta}{\partial x} + \nu_h\left(\frac{\partial^2 u}{\partial x^2} + \frac{\partial^2 u}{\partial y^2}\right) + \frac{\partial}{\partial z}\left(\nu_v \frac{\partial u}{\partial z}\right) \quad (5\text{-}2)$$

$$\frac{\partial v}{\partial t} + u\frac{\partial v}{\partial x} + v\frac{\partial v}{\partial y} + w\frac{\partial v}{\partial z} = -g\frac{\partial \eta}{\partial y} + \nu_h\left(\frac{\partial^2 v}{\partial x^2} + \frac{\partial^2 v}{\partial y^2}\right) + \frac{\partial}{\partial z}\left(\nu_v \frac{\partial v}{\partial z}\right) \quad (5\text{-}3)$$

In shallow water applications, the vertical momentum equation is reduced to the hydrostatic pressure assumption:

$$\frac{\partial p}{\partial z} = -\rho g \quad (5\text{-}4)$$

where h is the water depth, η is the water surface elevation, U and V are the depth averaged velocities in x and y directions, respectively, and u, v and w denote velocity components; g is the gravitational acceleration; t is the time; υ_h and υ_v are, respectively, horizontal and vertical kinematic eddy viscosity coefficients.

After applying the approach of Reynold's averaging, turbulence closure models are employed to solve the RANS equations. Delft3D-Flow code is numerically solved based on the finite difference method. We employed σ coordinate system in which the vertical layers are bounded by the planes which follow the free surface and the bottom topography.

The horizontal grid was generated using orthogonal curvilinear grid cells covering the model domain (Fig. 5.1b). The initial bathymetry was obtained using the interpolated surveyed bathymetric data from the 2014 total station survey. To test the sensitivity of the model to the mesh, several grids were developed and examined. A proper grid cell resolution was attained considering the balance between the computational cost and grid cell resolution with a 6 s time step to meet the stability condition. Grid cell properties were examined to ensure the quality of the generated grid, i.e., aspect ratio <2 and orthogonality <0.05 (Fig. 5.4). The mesh was generated in a way to assure that the flow discharge was contained within the grid cell boundaries.

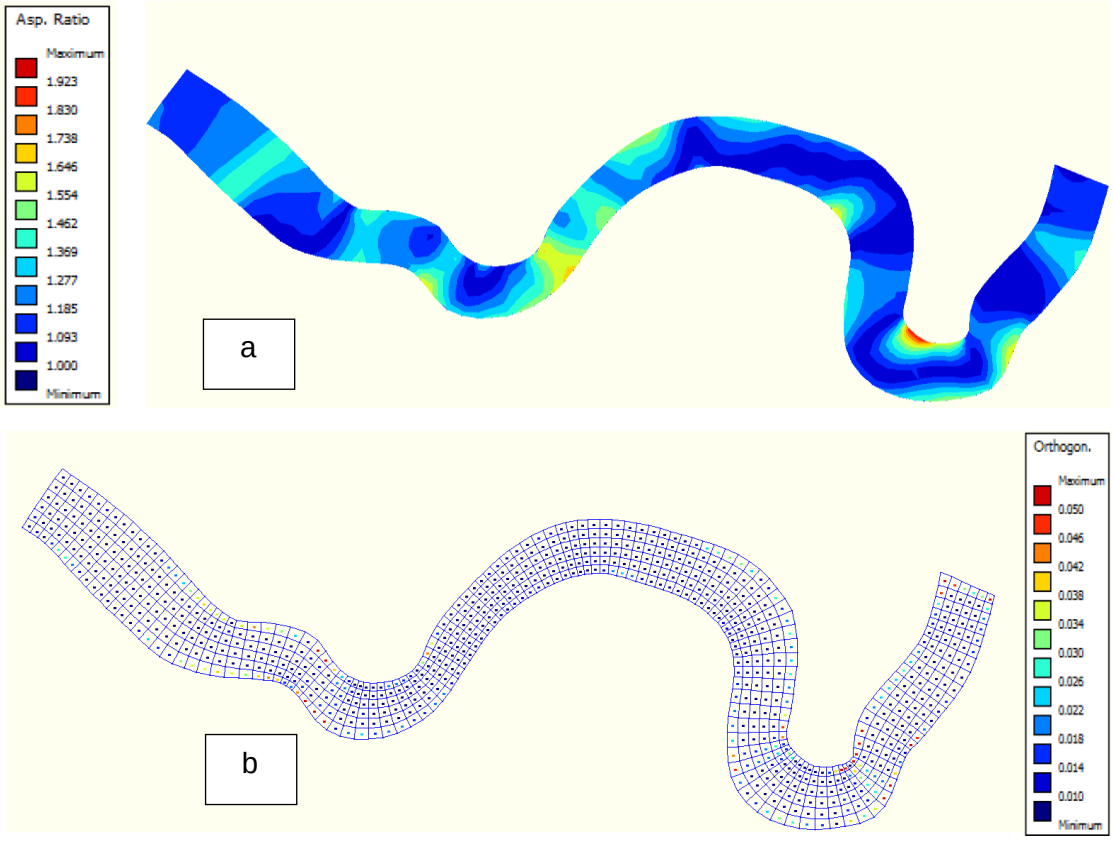

Figure 5.4. Generated mesh properties: (a) aspect ratio (b) grid orthogonality

Assuming that the gravity is much larger than the vertical acceleration, the hydrostatic version of Delft3D-Flow model was employed (Equations 1-4, i.e., the shallow water equations). Parsapour-Moghaddam and Rennie (2017) showed that the hydrostatic version of the Delft3D-Flow was capable of reasonably simulating the 3D flow structures in a tortuously meandering river. Ten vertical layers were defined in the σ coordinate system with the layer thickness ranging from 2% to 20% of the water depth with thinner layers close to the river bed.

Time series of discharge and water level were used for the upstream and downstream boundary conditions, respectively. SWMHYMO hydrologic modelling software was employed to simulate the continuous upstream boundary discharge and downstream water level (Brennan et al., 2018). Since Delft3D can accept a limited number of inputs for the time-varying boundary conditions, a Matlab code was developed to reconstruct and segmentize the hydrographs. To this end, a line was fitted

to k points of an initial hydrograph and its slope was calculated. If the relative error between the slopes of two consecutive lines was lower than ϵ, that slope was considered as a representative of two consecutive lines, and k was reduced by one. This process was continued until the entire hydrograph was covered. The selected lines were then evaluated against the initial hydrograph to ensure that all maximum and minimum points were captured. Using trial and error, ϵ and k were obtained as 0.1% and 20, respectively. In other words, the annual hydrograph was described by 20 piecewise line segments. To reduce the spinning time, hot start mode was applied. The model simulation was started from August 2014. Accordingly, the model was first run for a short period (60 minutes), based on the ADCP measured discharge in July 2014 (~ 0.08 m^3/s), until it converged. The results of this model were employed as the initial condition for the longer model run. The $\mathrm{k}-\varepsilon$ turbulence closure model, based on eddy viscosity theory of Kolmogorov and Prandtl (Deltares, 2014), was used to calculate the 3D turbulence. The hydrodynamic module was calibrated using the procedure described by Parsapour-Moghaddam and Rennie (2018a). Manning roughness and horizontal eddy viscosity were the calibration parameters, and the hydrodynamic module output was calibrated using spatially intensive surveyed ADCP data. That is, 3D simulated velocities were compared with the 3D measured ADCP throughout the entire reach obtained on October 2015 (~ 0.5 m^3/s).

The morphodynamic module of Delft3D is capable of simulating the sediment transport of suspended load and bedload for non-cohesive sediments and suspended load for cohesive sediments. As mentioned in Section 5.2, the study creek has cohesive bed and bank materials. For suspended sediments, Delft3D solves the 3D advection-diffusion equation:

$$\frac{\partial c}{\partial t}+\frac{\partial uc}{\partial x}+\frac{\partial vc}{\partial y}+\frac{\partial (w-w_s)c}{\partial z}=\frac{\partial}{\partial x}\left(D_x\frac{\partial c}{\partial x}\right)+\frac{\partial}{\partial y}\left(D_y\frac{\partial c}{\partial y}\right)+\frac{\partial}{\partial z}\left(D_z\frac{\partial c}{\partial z}\right) \quad (5\text{-}5)$$

where c is mass concentration of the sediment $(\mathrm{kg}/\mathrm{m}^3)$, $\mathrm{D_x}$, $\mathrm{D_y}$, and $\mathrm{D_z}$ are sediment eddy diffisivities $(\mathrm{m}^2/\mathrm{s})$, and $\mathrm{w_s}$ is sediment settling velocity (m/s). Eddy diffisivities and

local flow velocities are calculated according to hydrodynamic model results. Delft3D calculates the sedimentation and erosion of the cohesive sediment employing the Partheniades-Krone formulations (Partheniades, 1965):

$$E = MS(\tau_{cw}, \tau_{cr,e}) \tag{5-6}$$

$$D = w_s c_b S(\tau_{cw}, \tau_{cr,d}) \tag{5-7}$$

$$c_b = c\ (z = \frac{\Delta z_b}{2}, t) \tag{5-8}$$

where E is erosion flux, M is a user-defined erosion parameter, D is deposition flux, $\mathrm{c_b}$ is the average sediment concentration in the near bottom computational layer, $\mathrm{S}(\tau_{\mathrm{cw}}, \tau_{\mathrm{cr,e}})$ is an erosion step function:

$$S\left(\tau_{cw}, \tau_{cr,e}\right) = \begin{cases} \left(\frac{\tau_{cw}}{\tau_{cr,e}} - 1\right), & when\ \tau_{cw} > \tau_{cr,e} \\ 0, & when\ \tau_{cw} \leq \tau_{cr,e} \end{cases} \tag{5-9}$$

$S\left(\tau_{cw}, \tau_{cr,d}\right)$ is a deposition step function:

$$S\left(\tau_{cw}, \tau_{cr,d}\right) = \begin{cases} \left(1 - \frac{\tau_{cw}}{\tau_{cr,d}}\right), & when\ \tau_{cw} < \tau_{cr,d} \\ 0, & when\ \tau_{cw} \geq \tau_{cr,d} \end{cases} \tag{5-10}$$

τ_{cw} is maximum bed shear stress due to waves and current calculated through the wave-current interaction, $\tau_{\mathrm{cr,e}}$ is the user-defined critical shear stress for erosion, and $\tau_{\mathrm{cr,d}}$ is the user-defined critical shear stress for deposition.

The Delft3D morphodynamic module also includes bed level update as well as the bank erosion. Bank erosion is a function of erosion flux in the adjacent dry cell. In the developed model, 50% of the erosion in the wet cell was redistributed to the neighboring dry cells. Wet cells were defined to have at least 10cm of water depth.

For the upstream boundary condition of the morphodynamic model, we employed Neumann boundary conditions implying that the mud concentration gradient perpendicular to the inflow boundary is zero. To speed up the morphological adjustment, the morphological acceleration factor (MorFac) was implemented. A number of studies have implemented morphological factors in Delft3D morphodynamic

modelling and confirmed that MorFac can provide adequately realistic predictions of the long-term morphodynamic processes (eg., Lesser et al., 2004; Moerman, 2011; Schuurman et al., 2013; Williams et al., 2016; Yossef, 2016; Mool et al., 2017). That is, accurate long-term morphological changes would occur during a shorter flow duration simulation (Yossef, 2016). This helps to decrease the computational costs. For unsteady flow, input discharge time series should be compacted in accordance with the implemented scaling factor (Williams et al., 2016). Morphodynamic model calibration was achieved using the data from the two topographic surveys in one channel bend (Fig. 5.2). For calibration purpose, it was assumed that the input hydrograph in the second year (2015-2016) was the same as the first year (2014-2015) with a similar cycle. Accordingly, the morphological acceleration factor was set to 2. That is, the 2-year input flow hydrograph was condensed into a 1-year period. Several morphodynamic parameters, such as the erosion parameter, settling velocity, initial sediment layer thickness, critical bed shear stress for erosion and deposition, and horizontal eddy diffusivity were tested to find the sensitivity of the model to each. The model was most sensitive to the horizontal eddy diffusivity and the critical shear stresses for erosion and deposition, thus these parameters were used for morphodynamic model calibration.

5.3.3 **Fish habitat studies:**

In order to link the fish habitat quality with the erosion and sedimentation rate, fish sampling surveys were conducted in the creek using backpack electrofishing. Electrofishing is among the widely used methods for fish sampling surveys (e.g. Sharber and Sharber Black, 1999; Rosenberger and Dunham, 2005; Temple and Pearsons, 2007). To be able to assess how the fish community was changed by the morphological changes of the stream, two different fish sampling surveys were conducted during summer 2014 and summer 2015, which were respectively at the beginning and end of the study period. Based on ADCP measurements collected immediately following sampling in both 2014 and 2015, the flow discharge was ~0.08 m3/s and the temperature was ~18^{o}C during both surveys. Equivalent sampling procedure and effort were employed during both sampling events. The creek was

divided into 5m long subreaches covering all the study reach except for the very upstream end of the reach (Fig.5.5).

Fish sampling was started from downstream of the reach toward the upstream to ensure that the fish were not disturbed. All fish caught within discrete subreaches were measured to the nearest mm and identified separately to allow for a relationship with individual physical habitat spatially distributed throughout the creek. The two species found to be most abundant during sampling were yellow perch (N = 121, total length 80.38 mm ± 7.34 mm, mean ± SD) and white sucker (N = 39, 77.97 mm ± 35.49 mm). Yellow perch are a cool-water fish common throughout Eastern North America, and are usually found in shoals near vegetation and other submerged structures in lakes and pools in slow-moving streams (Suthers and Gee, 1986; Paukert et al., 2002; Froese and Pauly, 2018). They are more common in clear water and abundance generally decrease with increasing turbidity (Krieger et al., 1983). White sucker are an indiscriminate bottom-feeding species with broad environmental tolerances (Froese and Pauly, 2018) that is relatively abundant in the Midwest and Northeast regions of North America (Saint-Jacques et al., 2000), and are found near all types of substrates in lakes, streams and rivers (Minnesota DNR, 2018).

Figure 5.5. Fish sampling survey in the study reach: (a) Fish were hold in the bucket till they were measured and identified (b) Measurement and identification of the caught fish (c) Backpack electrofisher (d) Fish sampling in the study reach using backpack electrofishing (R-L: J. Foster, C.K. Elvidge, K. Birnie-Gauvin).

To study the linkage between the available fish community and the stream morphodynamics, we employed the results of the developed 3D hydro-morphodynamic model. The simulated results of cumulative erosion and sedimentation within a one-year monitoring plan (August 2014-August 2015) were spatially analyzed to calculate their statistics in each 5-m subreach. These results were compared to observed changes in the habitat utilization of both yellow perch and white sucker during the study period. Specifically, analysis of variance (ANOVA) tests (Tukey, 1953; Kramer, 1956) were used to test if the predicted morphological changes had a significant influence on fish community changes. We also analyzed the significance of other variables, such as predicted values of sediment concentration, flow depth, and depth-averaged velocity, on the observed yellow perch and white sucker community in 2015.

The results of the developed 3D hydro-morphodynamic model were also used to develop a fish habitat model of juvenile yellow perch. For fish habitat modelling, we used habitat suitability index (HSI) modelling, which is the most common way to study the fish response to their habitat (Noack, 2012). An HSI provides a measure of the quality of a given habitat variable to support particular fish at different life stages, with values ranging from 0 (the most unsuitable condition) to 1 (optimal condition) (Bovee, 1986). We used juvenile yellow perch habitat suitability curves for flow depth, velocity, and substrate based on Krieger et al., (1983). The creek bed substrate is mostly preferred particle size for the juvenile yellow perch, which according to Krieger et al. (1983) is less than 0.062 mm. We employed two different scenarios based on the: (I) hydraulic variables such as flow depth, velocity, and substrate (II) hydraulic variables in addition to the morphological changes (i.e. erosion/ sedimentation). For both scenarios, to combine the results of HSI modelling based on different parameters, we used the arithmetic mean to obtain a composite habitat suitability index (CSI):

$$CSI = \frac{\sum_{i=1}^{n} HSI_i}{n} \tag{5-11}$$

5.4 Results:

The hydrodynamic module of the developed 3D model was first calibrated for the Manning roughness and horizontal eddy viscosity using fully 3D ADCP velocities. The morphodynamic module was then calibrated for horizontal eddy diffusivity, critical bed shear stress for both erosion and sedimentation to which the 3D model was more sensitive. The calibrated parameter values are shown in Table 5.1. Fig. 5.6 shows the results of observed stream morphological changes and the calibrated 3D morphodynamic model from August 2014 to August 2016. The observed stream bend morphological development was calculated by differencing two total station surveys. As is shown, the calibrated model is in good agreement with the terrestrial measurements. Some discrepancies could still be seen close to the outer bank which can be attributed to the simple bank algorithm used in Delft3D. Nevertheless, considering all the uncertainties inherent to sediment transport modelling, these results are promising. The calculated mean absolute error of the bathymetric change is $0.11\,m$. It was confirmed

that the developed 3D model could be employed to predict the hydro-morphodynamics of the study creek.

Table 5.1. Calibration results of the developed 3D hydro-morphodynamic model

Calibration parameters	Values
Manning roughness	0.015
Background horizontal eddy viscosity	$1\ m^2/s$
Background horizontal eddy diffusivity	$4\ m^2\ /s$
Critical bed shear stress for erosion	$0.35\ N/m^2$
Critical bed shear stress for sedimentation	$0.35\ N/m^2$

The calibrated 3D model was then run from August 2014 to August 2015. Fig. 5.7 shows the results of the developed 3D model during the one-year study period. Fig. 5.7d shows morphological development of the study area. These results were also qualitatively consistent with the actual morphological changes based on the field reconnaissance in terms of the pattern and location of the sedimentation and erosion (Parsapour-Moghaddam and Rennie, 2018b).

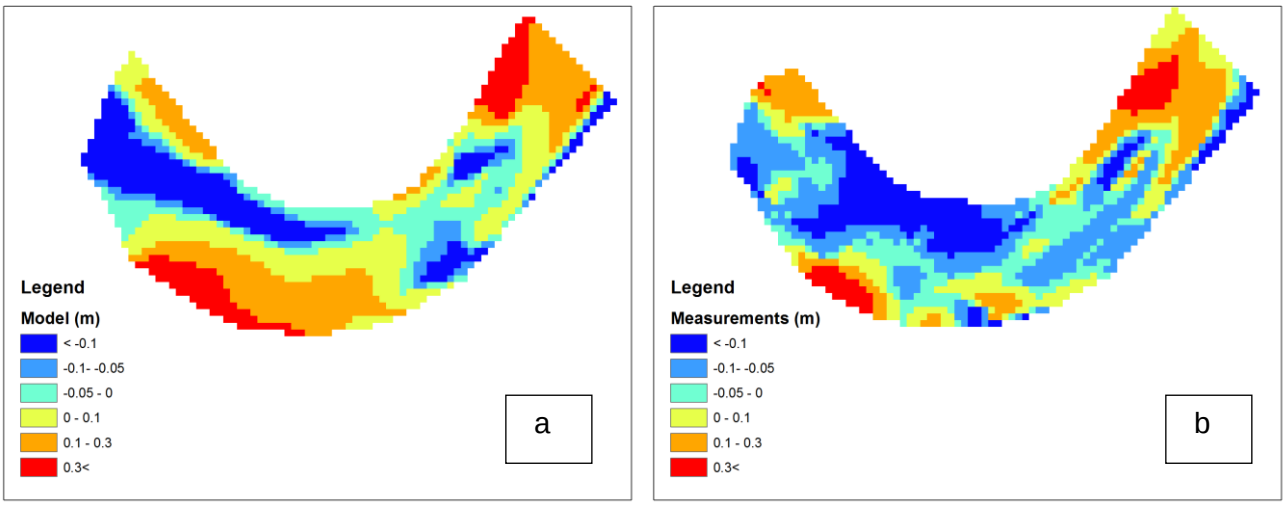

Figure 5.6. (a) Morphological changes over the study period (2014-2016) in one bend within the study reach (a) Results of the 3D morphodynamic model. (b) Observed changes based on total station surveys. Positive values indicate deposition and negative values indicate erosion. Flow from left to right.

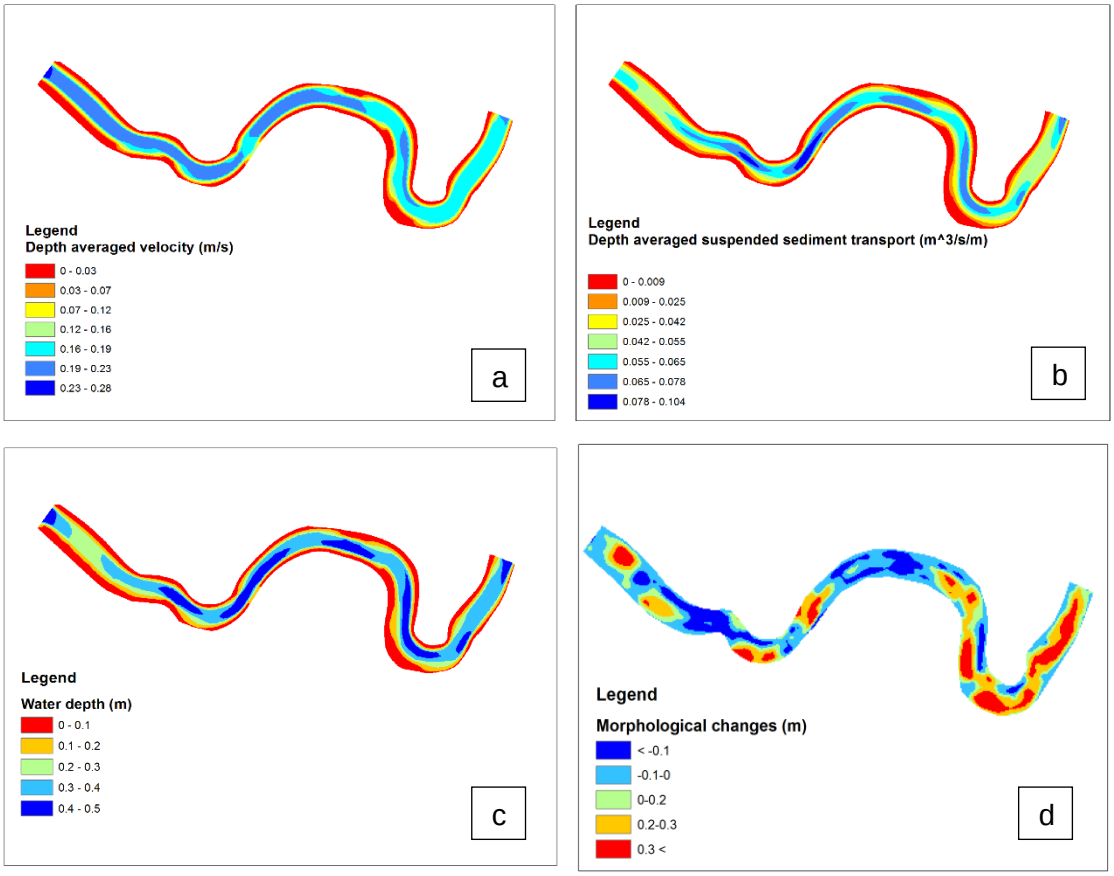

Figure 5.7. 3D morphodynamic model results at the end of the 1-year study period: (a) depth-averaged velocity (b) depth-averaged suspended sediment transport (c) flow depth (d) cumulative morphological development of the study creek. Flow from left to right.

Since both fish sampling surveys were conducted at the same time of year under very similar conditions of temperature and discharge, it may be reasonable to attribute these fish community changes to the stream morphological changes. Fig. 5.8 shows habitat utilization of white sucker and yellow perch during the two fish sampling surveys. Fig. 5.9 illustrates the changes in the habitat utilization of these two fish species with respect to the morphological changes during the study period.

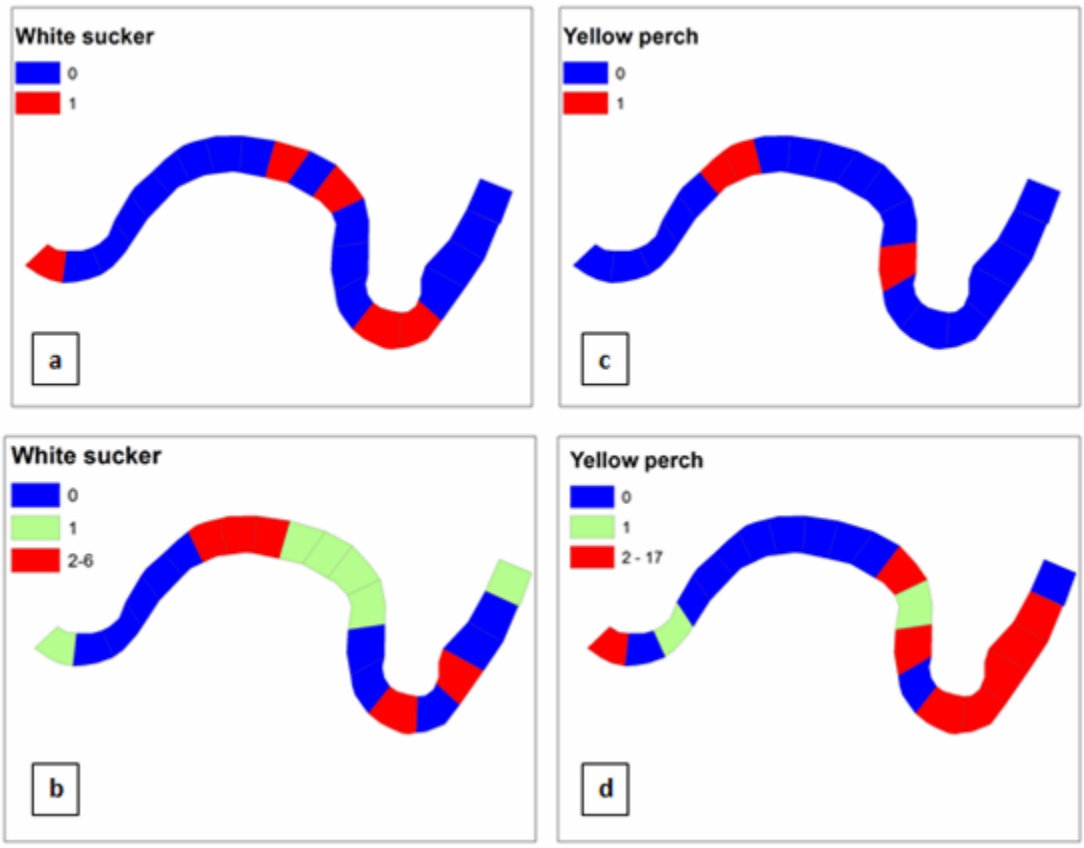

Figure 5.8. (a) Habitat utilization of: (a) white sucker in 2014, (b) white sucker in 2015, (c) yellow perch in 2014, (d) yellow perch in 2015. Note that the legend shows the number of the fish species caught in each subreach.

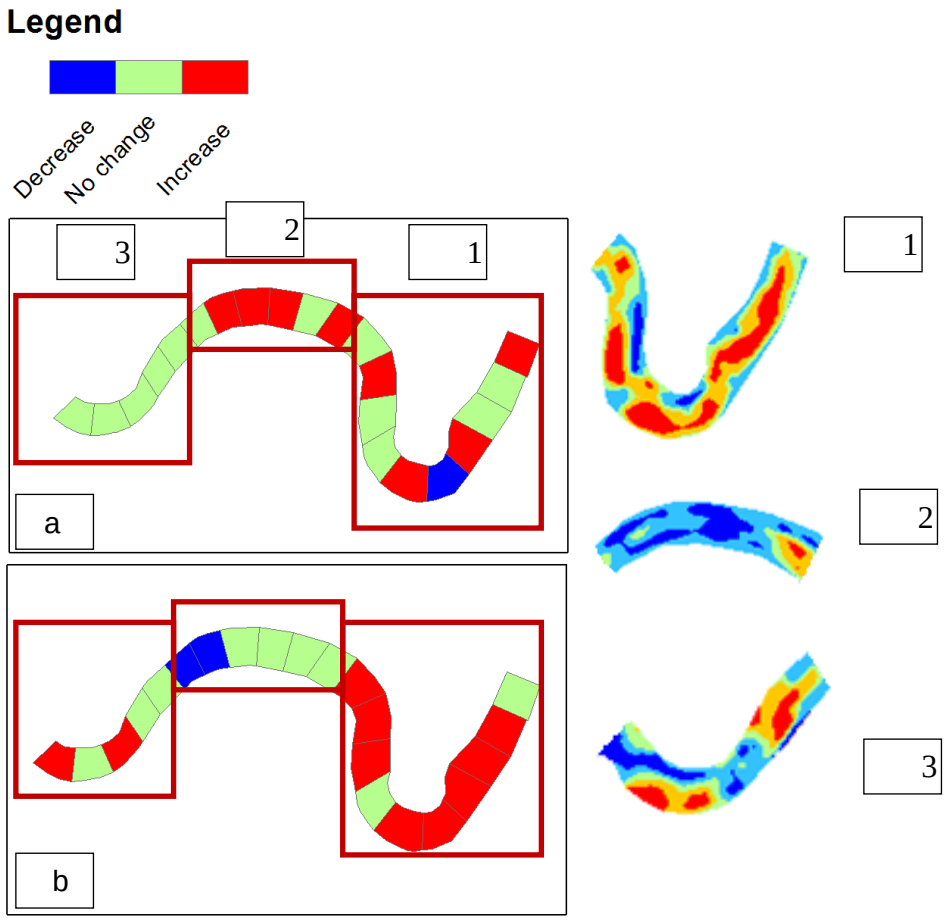

Figure 5.9. Changes in the habitat utilization during the 1-year study period: (a) white sucker (b) yellow perch. Morphological changes of each zone (1,2,3) in the study reach with blue and red indicating erosion and deposition, respectively. For the legend of the morphological development refer to Fig.5.7d

As shown in Fig. 5.9, between sampling surveys habitat utilization of yellow perch mainly increased in zone 1, where sediment deposition was mostly predicted. On the other hand, no consistent trend could be observed for white sucker in this zone since habitat utilization increased in four sampling subreaches, decreased in one subreach, and had no change in the other five sampling subreaches. In zone 2 where erosion was mostly dominant, the habitat utilization of yellow perch decreased or had no change. However, white sucker habitat utilization mostly increased in this zone. In zone 3, which had a mix of erosion and deposition, habitat utilization by yellow perch increased in two subreaches while in the other three subreaches no changes was observed. The white

sucker habitat utilization did not change in this zone during the study period. ANOVA tests were carried out to identify any significant relations between the model morphodynamic results and changes in the fish habitat utilization. Simulated changes in bed elevation during the 1-year study period were averaged in each 5-m sampling subreach, and then were compared to observed changes in relative abundance of fish within each sub-reach. ANOVA test results yielded P values of 0.035 and 0.239 for yellow perch and white sucker, respectively. The results of ANOVA test confirmed that the morphological changes during the study period were a significant factor for habitat utilization of yellow perch at the 5% significant level, whereas white sucker habitat utilization was not significantly affected by the erosion and sedimentation.

We also evaluated the influence of different habitat variables on fish utilization of habitat within the reach. This was achieved using multiple ANOVA tests (Table 5.2) to study if the flow depth, depth-averaged velocity, and suspended sediment transport had any impact on the habitat utilization of yellow perch and white sucker at the end of the 1-year study period.

Table 5.2. *P*-value obtained from the multiple comparison ANOVA analysis for juvenile yellow perch and white sucker.

	yellow perch	white sucker
Maximum suspended sediment transport	0.049	0.244
Maximum depth-average velocity	0.027	0.025
Spatially averaged flow depth	0.013	0.078

As is shown in Table 5.2, yellow perch utilization of habitat was significantly affected by all three of the maximum suspended sediment transport, maximum depth-averaged velocity, and the spatially averaged flow depth within each sampling subreach. However, white sucker showed significant influence of only spatial changes in the depth-averaged velocity; white sucker was not significantly impacted by the water depth and suspended sediment transport. Since the ANOVA test suggested juvenile yellow

perch utilization of habitat was significantly impacted by morphological changes, HSI models were subsequently developed for juvenile yellow perch, both with and without consideration of sediment erosion/deposition (Fig. 5.10). Results of the developed 3D morphodynamic model were employed as inputs for these fish habitat models. It should be noted that in order to incorporate the morphological changes in the HSI model in scenario II (Figure 5.10b), in the areas of erosion we applied HSI of 0 whereas in the deposition zones we applied HSI of 1

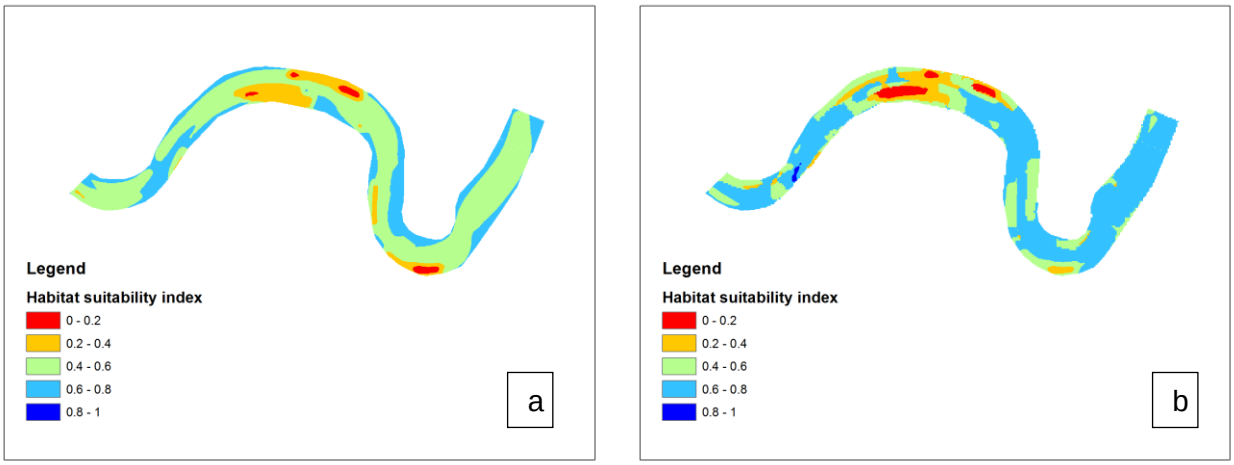

Figure 5.10. Predicted habitat suitability map for juvenile yellow perch based one: (a) scenario I (b) scenario II (with consideration of the morphological changes).

The suitability of each fish habitat model can be assessed by comparing Fig. 5.10 to the observed juvenile yellow perch utilization of habitat (Fig. 5.8d). It can be concluded that the habitat availability in zone 1 was better predicted in scenario II (refer to Fig. 5.9 for locations of each zone). In zone 2, both scenarios estimated relatively low habitat conditions, which is consistent with the results of the fish sampling surveys. As for zone 3, scenario I predicted very similar habitat quality all over the zone. However, based on the fish sampling surveys, habitat utilization of juvenile yellow perch was higher in two sampling subreaches. This higher quality of habitat of zone 3 was better predicted in scenario II. In general, it can be concluded that the habitat quality and variability was better predicted in scenario II in which the morphological changes were taken into account. Consideration of the morphological changes to the fish habitat model leads to

a habitat model specifically parameterized in accordance with the fluvial system's eco-morphological conditions.

5.5 Discussion:

It can be reasonably expected that the hydro-morphodynamic processes of a fluvial system can affect the quality and availability of fish habitat given the strong and inherent connections between the hydraulic and morphology of a river and its biota (Lapointe et al., 2014). Nevertheless, the impact of river's morphological changes on fish habitat is yet poorly studied. The study herein considered channel morphodynamics in fish habitat modelling. This could be of practical importance in river restoration strategies where fish habitat quality for a certain time period is understood, but change in the habitat quality over time is required. The morphological changes of a cohesive meandering creek, obtained from a 3D morphodynamic model, were correlated to changes in the habitat utilization of juvenile yellow perch and white sucker within a 1-year period. The results of the calibrated morphodynamic model reasonably agreed with observed morphological change obtained by terrestrial surveying. Deposition occurred on the outer bank which is consistent with what was reported by Parsapour-Moghaddam and Rennie (2018b). The results of their field study showed the generation of reverse flow eddies, which were interpreted to have caused the development of the concave bank bench in the study reach. Blanckaert et al. (2013) reported an occurrence of a dead water zone in the outer-bank widening of an open channel bend with an immobile gravel bed. It was shown that channel widening could promote a weak horizontal recirculation eddy. Similarly, the modelled outer bank deposition in the study creek can be attributed to the widening meander bend which reduces the flow velocities and consequently causes an outer bank deposition. The ability of the model to simulate this process confirms that the developed model could reasonably be employed to predict the morphological changes in this creek.

We carried out two fish sampling surveys, both of which occurred during the same season of summer low flow with very similar hydrodynamic characteristics and water temperature. Accordingly, it is reasonable to assume that hydrodynamic and other

habitat variables such as temperature and dissolved oxygen were not significant factors in the observed changes in fish utilization of habitat between surveys. Based on the modelling results of this study, it can be concluded that yellow perch was more susceptible to the suspended sediment concentration compared to white sucker. It was demonstrated that juvenile yellow perch utilization of habitat was significantly impacted by the morphological changes and the suspended sediment transport. In particular, yellow perch habitat utilization increased in areas of deposition, possibly suggesting that yellow perch were seeking habitat with lower suspended sediment concentration. Kjelland et al. (2015) reported that yellow perch death was increased with elevated sediment concentration. The results of the present study support this argument that yellow perch could be sensitive to the stream's morphological behavior. On the other hand, the present study illustrated that white sucker was not significantly impacted by the morphological changes and suspended sediment concentration. This is consistent with previous studies which reported that white sucker is tolerant to varying environmental circumstances (Saint-Jacques et al., 2000) and does not show health impairments when exposed to increased levels of fine sand (Merten et al., 2010). It should be noted that this study mainly focused on juvenile yellow perch and white sucker, while the results may be different for other life stages of these fish species.

There still may be some uncertainties in these results related to the field measurements, model predictions, estimation of the flow time series during the study period, fish sampling surveys, the uncertainties associated with the HSI modelling, and inter-annual differences in seasonal weather. In particular, only two fish surveys were conducted. Validation of the fish habitat-morphodynamic model with multi-year data could help to alleviate the uncertainties associated with the results. Regardless, to the best of our knowledge this study represents the first attempt to validate a stream morphodynamic-habitat model using fish sampling results. The results of this research suggest that much further study of the influence of channel morphodynamics on fish habitat is warranted. For example, habitat suitability curves could be developed based on the impact of morphological changes and suspended sediment concentrations on yellow perch.

5.6 Conclusion:

Morphological development of a cohesive meandering creek was studied to discover if morphodynamic processes could impact fish habitat quality for juvenile yellow perch and white sucker. Two fish sampling surveys were carried out at the beginning and end of the study period. Successful validation efforts indicated that the developed model could be reasonably employed to predict the hydro-morphodynamics of the study creek. ANOVA tests showed that morphological development was a significant factor in the habitat utilization of juvenile yellow perch, while juvenile white sucker utilization of habitat was not significantly impacted by the morphological changes in this creek. It was shown that habitat utilization of juvenile yellow perch mostly increased in the areas where sediment deposition occurred. Results of multiple ANOVA tests illustrated that flow depth, depth-averaged velocity, and the suspended sediment transport were all significant factors in habitat utilization of juvenile yellow perch. On the other hand, habitat utilization of juvenile white sucker was significantly impacted by the depth-averaged velocity, while the flow depth and suspended sediment transport did not have a significant effect on the habitat utilization of this fish species. The results of the developed hydro-morphodynamic model were fed into the fish habitat model of juvenile yellow perch. The results demonstrated that the fish habitat model for juvenile yellow perch yielded better predictions of fish habitat utilization when the effect of morphological changes was taken into account. The present study suggested that a stream's morphological changes may have an influence on fish habitat utilization. This could be a step toward better understanding and prediction of fish habitat quality with respect to stream morphological changes, providing some insights into the impact of sediment transport on fish communities. More study is needed to understand the effect of morphological changes on various fish species in a range of fluvial environments. Preferably, future studies will include more comprehensive fish population assessments that consider inter-annual and intra-annual variability in both target and control reaches.

CHAPTER 6

Conclusions and Future Research

6.1 Summary and concluding remarks

In the present thesis, 3D hydro-morphodynamic numerical models were developed for two meandering cohesive bed creeks. Total station terrestrial surveys were conducted for each creek to obtain the bathymetric data. For 3D hydro-morphodynamic modelling, Delft3D-Flow was used which is a widely used hydro-morphodynamic numerical model. Calibration and validation of the developed models were done based on field-based data to provide a more realistic approach to the natural rivers' simulation and subsequently, improve the understanding of morphological processes of meandering channels. New techniques were proposed for the calibration and validation of 3D morphodynamic-habitat models in an attempt to enhance understanding of the challenging hydro-morphodynamics. The results of the developed 3D hydro-morphodynamic model were employed to estimate how fish habitat availability can be impacted by a river's morphological changes.

In natural meandering rivers where 3D flow features are required, it would be of importance to develop a model specifically parameterized to predict the 3D flow field. This study proposed a novel methodology for an improved calibration of a 3D hydrodynamic model. Using field observations of fully distributed 3D velocities throughout a natural river provides opportunity for 3D model calibration that accounts for the variability and dynamics of the complex flow field in meandering rivers. Spatially intensive ADCP surveys were conducted in the studied creeks to attain fully 3D distributed velocities. For accurate and realistic comparison of the fully 3D predicted and measured velocities, an algorithm was developed to match the location of each ADCP bin with 3D model grid points. This study compared the results of the proposed calibration approach with the typical calibration methods to show how choosing different calibration methods could change the model predictive capability. The results suggested that different calibration approaches resulted in different calibration parameterizations whose simulated results could significantly differ from one another. It was shown that

the model which was calibrated based on the proposed 3D calibration approach had the best model performance. The results of the present study elucidated the importance of model calibration with comparable field data based on the nature and objectives of the numerical model. It was shown that fully 3D calibration is required to develop a model that best reproduces the fully 3D velocity distribution. Considering the fact that computational cost of the proposed calibration approach could be fairly similar to any other calibration methods, it could provide a better calibration potential for simulation of natural meandering rivers.

It is well known that secondary circulation plays an important role in sharp meandering rivers. Accordingly, the developed 3D hydrodynamic model was then validated based on the field-scale condition to discover if the developed Delft3D model could simulate the generated 3D flow structure. This study compared the performance of the hydrostatic versus non-hydrostatic pressure assumption in Delft3D 3D hydrodynamic modelling of a secondary flow. An ADV was employed to measure the 3D flow field in a sharp bend of the simulated meandering river during two different flow scenarios. The field-based ADV data were then employed to validate the simulated hydrodynamic models. To evaluate the performance of each model, different error statistics were calculated. In the hydrostatic model, the MAE were 8.4% and 4.5% in high flow and low flow, respectively, which were lower than those obtained in the non-hydrostatic model; i.e, 25.7% and 9.8%. Non-hydrostatic model errors were significantly greater ($\alpha = 0.05$) in both high flow and low flow scenarios compared to those based on the hydrostatic model. The results of the 3D hydrostatic model were in good agreement with the ADV measurements. The hydrostatic model was able to reproduce reasonably accurate predictions of streamwise and transverse velocity in terms of both magnitude and location of the primary secondary flow. Considering the uncertainties that may arise in both field measurements and modelling, the 3D hydrostatic Delft3D model was capable of producing the flow structures of the natural river bend with reasonable accuracy.

The results of the Delft3D model using non-hydrostatic approximation showed that the model was not mass conservative and could generate neither the secondary flow nor the streamwise velocity accurately. This study illustrated the superior performance

of the hydrostatic over non-hydrostatic Delft3D modelling of the secondary flow in the studied natural meandering creek. Several reasons could be responsible for the discrepancies between the non-hydrostatic results and the measurements, including the errors that might have arisen due to the pressure correction techniques, programming errors, and non-conservancy of the non-hydrostatic module.

To have a better understanding of a river's ecological condition and accordingly, the fish habitat quality, one needs to have information about the river's morphological behavior. The morphology of meandering cohesive bed rivers is yet not fully understood, particularly when they are confined. The present thesis examined the meandering behavior of a local cohesive clay bed river over a 10-year period. A paired sub-reach study approach was employed, wherein one sub-reach was freely meandering and the second adjacent sub-reach was confined by a railway embankment. Specifically, channel migration and morphological changes of the channel banks along each of these sub-reaches were analyzed by comparing historical aerial photography, LIDAR data and bathymetric data obtained from a total station survey. Furthermore, channel hydrodynamics were measured in both sub-reaches by spatially intensive ADCP surveying.

The unconfined sampling reach had a typical meandering pattern with erosion on the outer banks and deposition on the inner banks of meander bends. The sinuosity of the reach remained more-or-less constant over the ten year period. On the other hand, an irregular meandering pattern occurred in the confined sub-reach. The sinuosity of this part of the creek decreased from 1.55 to 1.49. The average rates of bank retreat were 0.2 m/year and 0.08 m/year in the confined and unconfined sub-reaches, respectively.

The results showed an evolution of the concave-bank bench on the upstream limb of the outer banks of the sharp menders in the confined reach, whereas bank instability was observed downstream of the bend apices. The results of spatially distributed ADCP depth-averaged velocities confirmed the occurrence of reverse flow on the upstream limb of the outer meander bends in the confined sub-reach, which could be linked to the irregular meandering pattern and generation of the concave-bank bench. The results of this study shed light on the potential impacts of channel confinement on the bank retreat and river migration in comparable case studies.

It can reasonably be expected that a river's hydro-morphodynamic processes can affect the quality and availability of fish habitat. Nevertheless, the impact of river morphological changes on fish habitat is yet poorly studied. The present thesis demonstrated that a stream's morphological changes may have an influence on fish habitat utilization. Morphological development of a cohesive meandering creek was studied to discover if it could impact the fish habitat quality of juvenile yellow perch and white sucker. A 3D morphodynamic model was first developed to simulate the hydro-morphodynamics of the study creek over a 1-year period. The 3D hydro-morphodynamic model was successfully calibrated using an intensive ADCP spatial survey of the entire 3D velocity field and total station surveys of topographic changes in a meander bend in the study creek. Two fish sampling surveys were carried out to determine the habitat utilization of each fish species in the study reach. Results of ANOVA tests confirmed that morphological development was a significant factor in habitat utilization of the juvenile yellow perch while juvenile white sucker habitat utilization was not significantly impacted by the creek's morphological changes. It was illustrated that juvenile yellow perch mostly utilized habitat where sediment deposition occurred. It was also shown that flow depth, depth-averaged velocity, and the suspended sediment transport were all significant factors in determining the habitat utilization of juvenile yellow perch. On the other hand, the juvenile white sucker utilization of habitat was significantly impacted only by the depth-averaged velocity, while the flow depth and suspended sediment transport did not have a significant effect on the presence of this fish species.

The results of the developed hydro-morphodynamic model were fed into the fish habitat model of juvenile yellow perch. The results demonstrated that the fish habitat model of the juvenile yellow perch produced better predictions when the effect of morphological changes was taken into account. The results of the morphodynamic-fish habitat model could provide some insights to the impact of the sediment transport on the fish community and therefore effective river management.

6.2 Recommendations for future research

There are some other aspects that may be further considered to improve the present study. This study proposed a novel methodology for an improved calibration of a 3D hydrodynamic model using spatially intensive ADCP survey. Further study is needed to investigate how many transects need to be surveyed to get the same results as the proposed calibration approach. This would be useful if the full spatial distribution of the fully 3D velocities is not available. This study illustrated the superior performance of the hydrostatic over non-hydrostatic Delft3D modelling of the secondary flow in the studied natural meandering creek. Further study is required to determine the exact reasons for the unfavorable performance of the non-hydrostatic Delft3D model. Delft3D code modifications may be developed to improve the non-hydrostatic version of the Delft3D model. The results can be compared with the results of the developed hydrostatic model. In addition, more sophisticated bank erosion routines may be developed considering both fluvial erosion and mass failure of the river banks, and the results can be compared with the proposed method to evaluate the current implemented bank routine within the Delft3D framework. Validation of the developed fish habitat-morphodynamic model with multi-year data could help to alleviate the uncertainties associated with the results. The present study mainly focused on habitat quality for juvenile yellow perch and white sucker. The effect of morphological changes on other fish species and other life stages of the studied fish species can be considered in future studies. Preferably, future studies will include more comprehensive fish population assessments that consider inter-annual and intra-annual variability in both target and control reaches.

References:

Abad, J. D., Musalem, R. A., García, C. M., Cantero, M. I., & García, M. H. (2004). Exploratory study of the influence of the wake produced by acoustic Doppler velocimeter probes on the water velocities within measurement volume. Proc., Critical Transitions in Water and Environmental Resource Management.

Afzalimehr, H., & Rennie, C. D. (2009). Determination of bed shear stress in gravel-bed rivers using boundary-layer parameters. *Hydrological sciences journal*, 54(1), 147-159.

Alvarez, L.V., Schmeekle, M.W., Grams, P.E. (2016). A detached eddy simulation model for the study of lateral separation zones along a large canyon-bound river. *Journal of Geophysical Research: Earth Surface*, 121, doi:10.1002/2016JF003895.

Baptist, M. J., Van Der Lee, G. E., Kerle, F., & Mosselman, E. (2002). Modelling of morphodynamics, vegetation development and fish habitat in man-made secondary channels in the river Rhine, the Netherlands. *4th International Ecohydraulics Symposium*, Cape Town.

Bathurst, J. C., Hey, R. D., & Thorne, C. R. (1979). Secondary flow and shear stress at river bends. *Journal of the Hydraulics Division*, 105(10), 1277-1295.

Bijvelds, M. D. J. P. (2001). Numerical modelling of estuarine flow over steep topography: Numerieke modellering van estuariene stroming over steile topografie (Doctoral dissertation, TU Delft, Delft University of Technology).

Biron, P. M., Choné, G., Buffin-Bélanger, T., Demers, S., & Olsen, T. (2013). Improvement of streams hydro-geomorphological assessment using LiDAR DEMs. *Earth Surface Processes and Landforms*, 38(15), 1808-1821.

Blanckaert, K. (2011). Hydrodynamic processes in sharp meander bends and their morphological implications. Journal of Geophysical Research: *Earth Surface*, 116(F1).

Blanckaert, K., & de Vriend, H. J. (2003). Nonlinear modeling of mean flow redistribution in curved open channels. *Water Resources Research*, 39(12).

Blanckaert, K., & De Vriend, H. J. (2004). Secondary flow in sharp open-channel bends. *Journal of Fluid Mechanic*s, 498, 353-380.

Blanckaert, K., & De Vriend, H. J. (2010). Meander dynamics: A nonlinear model without curvature restrictions for flow in open-channel bends. *Journal of Geophysical Research: Earth Surface* (2003–2012), 115(F4).

Blanckaert, K., & Graf, W. H. (2004). Momentum transport in sharp open-channel bends. *Journal of Hydraulic Engineering*, 130(3), 186-198.

Blanckaert, K., Kleinhans, M. G., McLelland, S. J., Uijttewaal, W. S., Murphy, B. J., Kruijs, A., Parsons D. R., & Chen, Q. (2013). Flow separation at the inner (convex) and outer (concave) banks of constant-width and widening open-channel bends. *Earth Surface Processes and Landforms*, 38(7), 696-716.

Bovee, K.D. (1986). Development and evaluation of habitat suitability criteria for use in the instream flow incremental methodology (No. FWS/OBS-86/7). USDI Fish and Wildlife Service.

Brennan, C. P., Parsapour-Moghaddam, P., Rennie, C. D., & Seidou, O. (2018). Continuous prediction of clay-bed stream erosion in response to climate model output for a small urban watershed. *Hydrological Processes.*

Bridge, J. S., & Jarvis, J. (1976). Flow and sedimentary processes in the meandering river South Esk, Glen Clova, Scotland. *Earth Surface Processes and Landforms*, 1(4), 303-336.

Burge, L. M., & Smith, D. G. (1999). Confined meandering river eddy accretions: sedimentology, channel geometry and depositional processes. *Fluvial Sedimentology VI (ed. ND Smith & J. Rogers), Special Publication of Internat, Association of Sedimentologists*, *28*, 113-130.

Busnelli, M. M. (2001). Numerical simulation of free surface flows with steep gradients. WL | Delft Hydraulics, Delft, The Netherlands. Ph.D. thesis.

Canestrelli, A., Nardin, W., Edmonds, D., Fagherazzi, S., & Slingerland, R. (2014). Importance of frictional effects and jet instability on the morphodynamics of river mouth bars and levees*. Journal of Geophysical Research: Oceans*, 119(1), 509-522.

Casagli, N., Curini, A., Gargini, A., Rinaldi, M., & Simon, A. (1997). Effects of pore pressure on the stability of streambanks: Preliminary results from the Sieve River, Italy. *Management of landscapes disturbed by channel incision*, 243-248.

Casulli, V. (1999). A semi-implicit finite difference method for non-hydrostatic, free-surface flows. *International journal for numerical methods in fluids*, 30(4), 425-440.

Casulli, V., & Stelling, G. S. (1998). Numerical simulation of 3D quasi-hydrostatic, free-surface flows. *Journal of Hydraulic Engineering*, 124(7), 678-686.

Choné, G., & Biron, P. M. (2016). Assessing the relationship between river mobility and habitat. *River Research and Applications*, *32*(4), 528-539.

Daniel, J. F. (1971). *Channel movement of meandering Indiana streams* (No. 732). United States Geological Survey Professional Paper 732-A (18 pp).

Darby, S. E., Rinaldi, M., & Dapporto, S. (2007). Coupled simulations of fluvial erosion and mass wasting for cohesive river banks. *Journal of Geophysical Research: Earth Surface*, 112(F3).

Dargahi, B. (2004). Three-dimensional flow modelling and sediment transport in the River Klarälven. *Earth Surface Processes and Landforms*, 29(7), 821-852.

De Kerckhove, D. T., Smokorowski, K. E., Randall, R. G., & Department of Fisheries and Oceans, Sault Ste. Marie, ON(Canada). Great Lakes Lab. for Fisheries and Aquatic Sciences. (2008). *A primer on fish habitat models*. Fisheries and Oceans Canada, Great Lakes Laboratory for Fisheries and Aquatic Sciences.

De Rose, R. C., & Basher, L. R. (2011). Measurement of river bank and cliff erosion from sequential LIDAR and historical aerial photography. *Geomorphology*, *126*(1), 132-147.

Deltares, Delft3D-FLOW Users manual. (2014). Simulation of multi-dimensional hydrodynamic flows and transport phe-nomena, including sediments.

Demers, S., Buffin-Bélanger, T., & Roy, A. G. (2011). Helical cell motions in a small ice-covered meander river reach. *River research and applications*, 27(9), 1118-1125.

Demuren, A. O. (1993). A numerical model for flow in meandering channels with natural bed topography. *Water resources research*, 29(4), 1269-1277.

Einstein, A. (1926). The Cause of the Formation of Meanders in the Courses of Rivers and of the So-Called Baer's Law. *Die Naturwissenschaften*, *14*(11), 223-224.

Escobar-Arias, M. I., & Pasternack, G. B. (2010). A hydrogeomorphic dynamics approach to assess in-stream ecological functionality using the functional flows model, part 1—model characteristics. *River research and applications*, *26*(9), 1103-1128.

Ferguson, R. I., Parsons, D. R., Lane, S. N., & Hardy, R. J. (2003). Flow in meander bends with recirculation at the inner bank. *Water Resources Research*, 39(11).

Froese, R. and Pauly, D. (2018). FishBase. World Wide Web electronic publication. www.fishbase.org, version (06/2018).

Gaarthuis, J. (1995). A non-hydrostatic pressure model for shallow water flow. Verslag ontwerpersafdeling TU Eindhoven also available at WL|| Delft Hydraulics.

Garcia, C. M., Oberg, K., & García, M. H. (2007). ADCP measurements of gravity currents in the Chicago River, Illinois. *Journal of Hydraulic Engineering*, 133(12), 1356-1366.

García, M. H. (Ed.). (2008). Sedimentation engineering: processes, measurements, modeling, and practice (No. 110). ASCE Publications.

Ghinassi, M., Ielpi, A., Aldinucci, M., & Fustic, M. (2016). Downstream-migrating fluvial point bars in the rock record. *Sedimentary Geology*, *334*, 66-96.

Güneralp, İ., Abad, J. D., Zolezzi, G., & Hooke, J. (2012). Advances and challenges in meandering channels research. *Geomorphology*, *163*, 1-9.

Haralampides, K., & Rodriguez, A. (2006). Erosional properties of the sediments in the Petitcodiac River estuary at Moncton, New Brunswick. *Canadian journal of civil engineering*, 33(9), 1209-1216.

Hauer, C., Unfer, G., Schmutz, S., & Habersack, H. (2007). The importance of morphodynamic processes at riffles used as spawning grounds during the incubation time of nase (Chondrostoma nasus). *Hydrobiologia*, 579(1), 15-27.

Hauer, C., Unfer, G., Schmutz, S., & Habersack, H. (2008). Morphodynamic effects on the habitat of juvenile cyprinids (Chondrostoma nasus) in a restored Austrian lowland river. *Environmental Management*, 42(2), 279.

Hooke, J. (2003). River meander behaviour and instability: a framework for analysis. *Transactions of the Institute of British geographers*, *28*(2), 238-253.

Hosseini, S. M., & Coonrod, J. (2011). Coupling Numerical and Physical Modeling for Analysis of Flow in a Diversion Structure with Coanda-effect Screens. *Water*, 3(3), 764-786.

Ikeda, S. & Parker, G. (eds.) River Meandering (1989), American Geophysical Union.

Jamieson, E. C., Rennie, C. D., Jacobson, R. B., & Townsend, R. D. (2011). 3-D flow and scour near a submerged wing dike: ADCP measurements on the Missouri River. *Water Resources Research*, 47(7).

Jamieson, E. C., Ruta, M. A., Rennie, C. D., & Townsend, R. D. (2013). Monitoring stream barb performance in a semi-alluvial meandering channel: flow field dynamics and morphology. *Ecohydrology*, 6(4), 611-626.

Jansen, P. H., van Bendegom, L., van den Berg, J., de Vries, M., and Zanen, A (1979). Principles of river engineering, Pitman, London.

Javernick, L., Hicks, D. M., Measures, R., Caruso, B., & Brasington, J. (2016). Numerical Modelling of Braided Rivers with Structure-from-Motion-Derived Terrain Models. *River Research and Applications*, *32*(5), 1071-1081.

Kail, J., Guse, B., Radinger, J., Schröder, M., Kiesel, J., Kleinhans, M., Schuurman, F., Fohrer, N., Hering, N. & Wolter, C. (2015). A modelling framework to assess the effect of pressures on river abiotic habitat conditions and biota. PloS one, 10(6), e0130228

Kamel, B., Ilhem, K., Ali, F., & Abdelbaki, D. (2014). 3D Simulation of Velocity Profile of Turbulent Flow in Open Channel with Complex Geometry. *Physics Procedia*, 55, 119-128.

Kasvi, E., Alho, P., Lotsari, E., Wang, Y., Kukko, A., Hyyppä, H., & Hyyppä, J. (2015a). Two-dimensional and three-dimensional computational models in hydrodynamic and morphodynamic reconstructions of a river bend: sensitivity and functionality. *Hydrological processes*, *29*(6), 1604-1629.

Kasvi, E., Alho, P., Vaaja M, Hyyppä H, & Hyyppä J. (2013a). Spatial and temporal distribution of fluvio-morphological processes on a meander point bar during a flood event. *Hydrology Research*, 44(6), 1022-1039.

Kasvi, E., Vaaja, M., Alho, P., Hyyppä, H., Hyyppä, J., Kaartinen, H., & Kukko, A. (2013b). Morphological changes on meander point bars associated with flow structure at different discharges. *Earth Surface Processes and Landforms*, 38(6), 577-590.

Kasvi, E., Vaaja, M., Kaartinen, H., Kukko, A., Jaakkola, A., Flener, C., Hyyppä, H., Hyyppä, J., & Alho, P. (2015b). Sub-bend scale flow–sediment interaction of meander bends—A combined approach of field observations, close-range remote sensing and computational modelling. *Geomorphology*, 238, 119-134.

Kerle, F., Zöllner, F., Schneiderb, M., Böhmer, J., & Kappusc, B. (2002). Modelling of long-term fish habitat changes in restored secondary floodplain channels of the river Rhine.

Khosronejad, A., Kozarek, J. L., Palmsten, M. L., & Sotiropoulos, F. (2015). Numerical simulation of large dunes in meandering streams and rivers with in-stream rock structures. *Advances in water resources*, 81, 45-61.

Khosronejad, A., Rennie, C. D., Salehi Neyshabouri, S. A. A., & Townsend, R. D. (2007). 3D numerical modeling of flow and sediment transport in laboratory channel bends. *Journal of Hydraulic Engineering*, 133(10), 1123-1134.

Kjelland, M. E., Woodley, C. M., Swannack, T. M., & Smith, D. L. (2015). A review of the potential effects of suspended sediment on fishes: potential dredging-related physiological, behavioral, and transgenerational implications. *Environment Systems and Decisions*, 35(3), 334-350.

Kleinhans, M. G., H. R. A. Jagers, E. Mosselman, and C. J. Sloff (2008), Bifurcation dynamics and avulsion duration in meandering rivers by one-dimensional and three-dimensional models, *Water Resour. Res*., 44, W08454, doi:10.1029/2007WR005912.

Koçyigit, M. B., Falconer, R. A., & Lin, B. (2002). Three-dimensional numerical modelling of free surface flows with non-hydrostatic pressure. *International Journal for Numerical Methods in Fluids*, 40(9), 1145-1162.

Kramer, C. Y. (1956). Extension of multiple range tests to group means with unequal numbers of replications. *Biometrics*, *12*(3), 307-310.

Krapesch, G., Tritthart, M., & Habersack, H. (2009). A model-based analysis of meander restoration. *River research and applications*, 25(5), 593-606.

Krieger, D. A., Terrell, J. W., & Nelson, P. C. (1983). Habitat suitability information: yellow perch. Western Energy and Land Use Team, Division of Biological Services, Research and Development, Fish and Wildlife Service, US Department of the Interior.

Lane, E. W. (1957). *A study of the shape of channels formed by natural streams flowing in erodible material*. US Army Engineer Division, Sediment Series, 9. Mississippi River Corps of Engineers, Ohama, Nebr.

Lane, S. N., Bradbrook, K. F., Richards, K. S., Biron, P. A., & Roy, A. G. (1999). The application of computational fluid dynamics to natural river channels: three-dimensional versus two-dimensional approaches. *Geomorphology*, 29(1), 1-20.

Lanzoni, S., & Seminara, G. (2006). On the nature of meander instability. *Journal of Geophysical Research: Earth Surface*, *111*(F4).

Lawler, D. M. (1995). The impact of scale on the processes of channel-side sediment supply: a conceptual model. *IAHS Publications-Series of Proceedings and Reports-Intern Assoc Hydrological Sciences*, *226*, 175-186.

Lesser, G. R., Roelvink, J. A., Van Kester, J. A. T. M., & Stelling, G. S. (2004). Development and validation of a three-dimensional morphological model. *Coastal engineering*, 51(8), 883-915.

Lesser, G. R., Van Kester, J., Roelvink, J. A., & Stelling, G. S. (2001). Three-dimensional morphological modelling in Delft3D-FLOW. *Paper in prep*.

Leupi, C., & Altinakar, M. S. (2005). 3D Finite Element Modeling of Free-Surface Flows with Efficient k–ε Turbulence Model and Non-hydrostatic Pressure. *Computational Science*–ICCS 2005 (pp. 33-40). Springer Berlin Heidelberg.

Lewin, J. (1978). Meander development and floodplain sedimentation: A case study from mid-Wales. *Geological Journal*, 13(1), 25-36.

Lewin, J., & Brindle, B. J. (1977). Confined meanders. In River Channel Changes. Edited by Gregory, K.J. John Wiley and Sons: Chichester, 221-233.

Leyland, J., Darby, S. E., Teruggi, L., Rinaldi, M., & Ostuni, D. (2015). A self- limiting bank erosion mechanism? inferring temporal variations in bank form and skin drag from high resolution topographic data. *Earth Surface Processes and Landforms*, 40(12), 1600-1615.

Li, C., & Zheng, Q. (2016). Breakdown of Hydrostatic Assumption in Tidal Channel with Scour Holes. Front. Mar. Sci, 3, 199.

Li, S. S., & Millar, R. G. (2011). A two-dimensional morphodynamic model of gravel- bed river with floodplain vegetation. *Earth Surface Processes and Landforms*, 36(2), 190-202.

Lohrmann, A., Cabrera, R., & Kraus, N. C. (1994). Acoustic-Doppler velocimeter (ADV) for laboratory use. In Fundamentals and Advancements in Hydraulic Measurements and Experimentation: (pp. 351-365). ASCE.

Maarschalk-Bliss, S. (2014). Seasonal Variation in Assemblage Structure and Movement of Small Stream Fish in an Urban Environment. M.S. Thesis, Biology, Carleton University.

Maddock, I. (1999): The importance of physical habitat assessment for evaluating river health. *Freshwater Biology*, 41: 373–391.

Makaske, B., & Weerts, H. J. (2005). Muddy lateral accretion and low stream power in a sub-recent confined channel belt, Rhine-Meuse delta, central Netherlands. *Sedimentology*, *52*(3), 651-668.

Mashriqui, H. S. (2003). Hydrodynamic and sediment transport modeling of deltaic sediment processes (Doctoral dissertation, Louisiana State University).

Merten, E. C., Loomis, J., Lightbody, A., & Dieterman, D. J. (2010). Effects of six-hour suspended sediment treatments on White Sucker (Catostomus commersoni) and Smallmouth Bass (Micropterus dolomieu) in an artificial stream. *Journal of Freshwater Ecology*, 25(4), 539-548.

Minnesota Department of Natural Resources, White Sucker. (2018). URL: https://www.dnr.state.mn.us/fish/whitesucker.html.

Moerman, E. (2011). *Long-term morphological modelling of the mouth of the Columbia River* (Doctoral dissertation, PhD Thesis, Delft University).

Mohammadi, B., & Pironneau, O. (1993). Analysis of the K-epsilon turbulence model. France: Editions MASSON.

Mohammed, Z. (2017). Morphodynamic Modelling of Sediment Control Groynes in a Meandering River Entering a Reservoir (Doctoral dissertation, Université d'Ottawa/University of Ottawa).

Mool, P., Popescu, I., Giri, S., Omer, A., Sloff, K., Kitamura, Y., & Solomatine, D. (2017). Delft3D morphological modelling of sediment management in daily peaking run-of-the-river hydropower (PROR) reservoirs in Nepal.

Moore, S. A., Jamieson, E. C., Rainville, F., Rennie, C. D., & Mueller, D. S. (2016). Monte Carlo Approach for Uncertainty Analysis of Acoustic Doppler Current Profiler Discharge Measurement by Moving Boat. Journal of Hydraulic Engineering, 143(3), 04016088.

Morlock, S. E. (1996). Evaluation of acoustic Doppler current profiler measurements of river discharge (pp. 95-4218). US Department of the Interior, US Geological Survey.

Mouton, A. M., Schneider, M., Depestele, J., Goethals, P. L., & De Pauw, N. (2007). Fish habitat modelling as a tool for river management. *Ecological engineering*, 29(3), 305-315.

Muste, M., Kim, D., & Merwade, V. (2012). Modern digital instruments and techniques for hydrodynamic and morphologic characterization of river channels. Gravel-Bed Rivers: Processes, Tools, Environments, 315-341.

Muste, M., Yu, K., & Spasojevic, M. (2004). Practical aspects of ADCP data use for quantification of mean river flow characteristics; Part I: moving-vessel measurements. *Flow measurement and instrumentation*, 15(1), 1-16.

Nanson, G. C., & Page, K. (1983). Lateral accretion of fine-grained concave benches on meandering rivers. In: Modern and Ancient Fluvial Systems (Eds J. Collinson and J. Lewin), Int. Assoc. Sedimentol. Spec. Publ., 6, 133–143.

Nardi, L., Campo, L., & Rinaldi, M. (2013). Quantification of riverbank erosion and application in risk analysis. *Natural hazards*, *69*(1), 869-887.

Nicholas, A.P., Sandbach, S.D., Ashworth, P.J., Amsler, M.L., Best, J.L., Hardy, R.J., Lane, S.N., Orfeo, O., Parsons, D.R., Reesink, A.J. and Smith, G.H.S (2012). Modelling hydrodynamics in the Rio Paraná, Argentina: An evaluation and inter-comparison of reduced-complexity and physics based models applied to a large sand-bed river. *Geomorphology*, 169, 192-211.

Nicoll, T. J. A. (2008). *Planform geometry and kinematics of confined meandering rivers on the Canadian prairies* (M.Sc. Thesis, Dept. of Geography, Simon Fraser University, Burnaby, BC, Canada.

Nicoll, T. J., & Hickin, E. J. (2010). Planform geometry and channel migration of confined meandering rivers on the Canadian prairies. *Geomorphology*, *116*(1), 37-47.

Noack, M. (2012). Modelling approach for interstitial sediment dynamics and reproduction of gravel-spawning fish. Ph.D thesis. Noack, M. ISBN 978-3-942036-18-4.

Olsen, N. R., & Stokseth, S. (1995). Three-dimensional numerical modelling of water flow in a river with large bed roughness. *Journal of Hydraulic Research*, 33(4), 571-581.

Page, K., & Nanson, G. (1982). Concave-bank benches and associated floodplain formation. *Earth Surface Processes and Landforms*, *7*(6), 529-543.

Papanicolaou, A. N., Elhakeem, M., & Hilldale, R. (2007). Secondary current effects on cohesive river bank erosion. *Water Resources Research*, *43*(12).

Papanicolaou, A. N., Elhakeem, M., & Wardman, B. (2010). Calibration and verification of a 2D hydrodynamic model for simulating flow around emergent bendway weir structures. *Journal of Hydraulic Engineering*, 137(1), 75-89.

Papanicolaou, A. T. N., Elhakeem, M., Krallis, G., Prakash, S., & Edinger, J. (2008). Sediment transport modeling review—current and future developments. *Journal of Hydraulic Engineering*, *134*(1), 1-14.

Parsapour-Moghaddam, P., & Rennie, C. D. (2015). ADCP Validation of 3D Morphodynamic Modelling in Clay-Bed Meandering Rivers. *Proceedings of the 36th IAHR World Congress*.

Parsapour-Moghaddam, P., & Rennie, C. D. (2017a). Hydrostatic versus nonhydrostatic hydrodynamic modelling of secondary flow in a tortuously meandering river: Application of Delft3D. *River Research and Applications*, 33(9), 1400-1410.

Parsapour-Moghaddam, P., & Rennie, C. D. (2017b). 3D versus 2D calibration of a 3D hydrodynamic model. *Proceedings of the 37th IAHR World Congress*.

Parsapour-Moghaddam, P., & Rennie, C. D. (2018a). Calibration of a 3D Hydrodynamic Meandering River Model Using Fully Spatially Distributed 3D ADCP Velocity Data. *Journal of Hydraulic Engineering*, 144(4), 04018010.

Parsapour-Moghaddam, P., & Rennie, C. D. (2018b). Influence of Meander Confinement on Hydro-Morphodynamics of a Cohesive Meandering Channel. *Water*, 10(4), 354.

Parsapour-Moghaddam, P., & Rennie, C.D. (2014). Morphodynamic modelling of a tortuous meandering clay bed river using Delft3D: Stillwater Creek, Ottawa. River flow, *International conference on fluvial hydraulics*: 1163-117.

Parsons, D. R., Jackson, P. R., Czuba, J. A., Engel, F. L., Rhoads, B. L., Oberg, K. A., ... & Riley, J. D. (2013). Velocity Mapping Toolbox (VMT): a processing and visualization suite for moving-vessel ADCP measurements. *Earth Surface Processes and Landforms*, 38(11), 1244-1260.

Partheniades, E. (1965). Erosion and deposition of cohesive soils. *Journal of the Hydraulics Division*, 91(1), 105-139.

Paukert, C. P., Willis, D. W., Klammer, Joel A. (2002). Effects of predation and environment on quality of yellow perch and Bluegill populations in Nebraska sandhill lakes. *North American Journal of Fisheries Management,* 22(1): 86–95.

Peixoto, R. D. S., Rosman, P. C. C., & Vinzon, S. B. (2017). A morphodynamic model for cohesive sediments transport. *RBRH*, *22*.

Piégay, H., Darby, S. E., Mosselman, E., & Surian, N. (2005). A review of techniques available for delimiting the erodible river corridor: a sustainable approach to managing bank erosion. *River Research and Applications,* 21(7), 773-789.

Pinto, L., Fortunato, A. B., Zhang, Y., Oliveira, A., & Sancho, F. E. P. (2012). Development and validation of a three-dimensional morphodynamic modelling system for non-cohesive sediments. *Ocean Modelling*, *57*, 1-14.

Pizzuto, J. (2009). An empirical model of event scale cohesive bank profile evolution. *Earth Surface Processes and Landforms*, *34*(9), 1234-1244.

Poff, N. L., & Zimmerman, J. K. (2010). Ecological responses to altered flow regimes: a literature review to inform the science and management of environmental flows. *Freshwater Biology*, *55*(1), 194-205.

Portt, C.B., Coker, G.A., Ming, D.L. and Randall, R.G. (2006). A review of fish sampling methods commonly used in Canadian freshwater habitats. Can. Tech. Rep. *Fish. Aquat. Sci*, 2604.

Rennie C.D. (2014). Linking sediment erodibility and channel stability to utilization of available habitats by fish populations in watts creek, Project Progress Report.

Rennie, C. D., & Church, M. (2010). Mapping spatial distributions and uncertainty of water and sediment flux in a large gravel bed river reach using an acoustic Doppler current profiler. *Journal of Geophysical Research: Earth Surface*, 115(F3).

Rennie, C. D., & Church, M. (2010). Mapping spatial distributions and uncertainty of water and sediment flux in a large gravel bed river reach using an acoustic Doppler current profiler. *Journal of Geophysical Research: Earth Surface*, 115, F03035, doi:10.1029/2009JF001556

Rennie, C. D., & Hay, A. (2010). Reynolds stress estimates in a tidal channel from phase-wrapped ADV data. *Journal of Coastal Research*, 26(1), 157-166.

Rennie, C. D., & Millar, R. G. (2004). Measurement of the spatial distribution of fluvial bedload transport velocity in both sand and gravel. *Earth Surface Processes and Landforms*, 29(10), 1173-1193.

Rennie, C. D., & Villard, P. V. (2004). Site specificity of bed load measurement using an acoustic Doppler current profiler. *Journal of Geophysical Research: Earth Surface*, 109(F3).

Rinaldi, M., & Casagli, N. (1999). Stability of streambanks formed in partially saturated soils and effects of negative pore water pressures: the Sieve River (Italy). *Geomorphology*, *26*(4), 253-277.

Rinaldi, M., & Darby, S. E. (2007). Modelling river-bank-erosion processes and mass failure mechanisms: progress towards fully coupled simulations. *Developments in Earth Surface Processes*, 11, 213-239.

Rinaldi, M., Casagli, N., Dapporto, S., & Gargini, A. (2004). Monitoring and modelling of pore water pressure changes and riverbank stability during flow events. *Earth Surface Processes and Landforms*, *29*(2), 237-254.

Rinaldi, M., Mengoni, B., Luppi, L., Darby, S. E., & Mosselman, E. (2008). Numerical simulation of hydrodynamics and bank erosion in a river bend. *Water Resources Research*, *44*(9).

Rodriguez, J. F., Bombardelli, F. A., García, M. H., Frothingham, K. M., Rhoads, B. L., & Abad, J. D. (2004). High-resolution numerical simulation of flow through a highly sinuous river reach. *Water Resources Management*,18(3), 177-199.

Rosenberger, A. E., & Dunham, J. B. (2005). Validation of abundance estimates from mark–recapture and removal techniques for rainbow trout captured by electrofishing in small streams. *North American Journal of Fisheries Management*, 25(4), 1395-1410.

Rousseau, Y. Y., Biron, P. M., & Van de Wiel, M. J. (2016). Sensitivity of simulated flow fields and bathymetries in meandering channels to the choice of a morphodynamic model. *Earth Surface Processes and Landforms*, 41(9), 1169-1184.

Rüther, N., & Olsen, N. R. (2005). Three-dimensional modeling of sediment transport in a narrow 90 channel bend. *Journal of Hydraulic Engineering*, 131(10), 917-920.

Rüther, N., & Olsen, N. R. B. (2007). Modelling free-forming meander evolution in a laboratory channel using three-dimensional computational fluid dynamics. *Geomorphology*, 89(3), 308-319.

Saint-Jacques, N., Harvey, H. H., & Jackson, D. A. (2000). Selective foraging in the white sucker (Catostomus commersoni). *Canadian Journal of Zoology*, 78(8), 1320-1331

Salem, H., & Rennie, C. D. (2017). Practical Determination of Critical Shear Stress in Cohesive Soils. *Journal of Hydraulic Engineering*, 143(10), 04017045.

Salem, H., Rennie, C. D., & Custodio, C. Z. (2014). Influence of Pore Pressure on Clay Erosion. *River Flow Proceedings*, Lausanne, Switzerland.

Schuurman, F., & Kleinhans, M. G. (2015). Bar dynamics and bifurcation evolution in a modelled braided sand-bed river. *Earth Surface Processes and Landforms*, 40(10), 1318-1333.

Schuurman, F., Marra, W. A., & Kleinhans, M. G. (2013). Physics-based modeling of large braided sand-bed rivers: Bar pattern formation, dynamics, and sensitivity. *Journal of geophysical research: Earth Surface*, 118(4), 2509-2527.

Schuurman, F., Shimizu, Y., Iwasaki, T., & Kleinhans, M. G. (2016). Dynamic meandering in response to upstream perturbations and floodplain formation. *Geomorphology*, 253, 94-109.

Sharber, N. G., & Sharber Black, J. (1999). Epilepsy as a unifying principle in electrofishing theory: a proposal. Transactions of the American Fisheries Society, 128(4), 666-671.

Shimizu, Y., Yamaguchi, H., & Itakura, T. (1990). Three-dimensional computation of flow and bed deformation. *Journal of Hydraulic Engineering*,116(9), 1090-1108.

Simon, A., & Collison, A. J. (2001). Pore- water pressure effects on the detachment of cohesive streambeds: seepage forces and matric suction. *Earth Surface Processes and Landforms*, 26(13), 1421-1442.

Simon, A., & Curini, A. (1998). Pore pressure and bank stability: The influence of matric suction. *Hydraulic engineering*, 98. ASCE, 358–363.

Simon, A., & Klimetz, L. (2008). Relative magnitudes and sources of sediment in benchmark watersheds of the Conservation Effects Assessment Project. *Journal of Soil and Water Conservation*, 63(6), 504-522.

Simon, A., Curini, A., Darby, S. E., & Langendoen, E. J. (2000). Bank and near-bank processes in an incised channel. *Geomorphology*, 35(3), 193-217.

Simpson, M. R. (2001). Discharge measurements using a broad-band acoustic Doppler current profiler (p. 123). US Department of the Interior, US Geological Survey.

Simpson, M. R., & Oltmann, R. N. (1993). Discharge-measurement system using an acoustic Doppler current profiler with applications to large rivers and estuaries (p. 32). US Government Printing Office.

Singh, U., Crosato, A., Giri, S., & Hicks, M. (2017). Sediment heterogeneity and mobility in the morphodynamic modelling of gravel-bed braided rivers. *Advances in water resources*, 104, 127-144.

Sinha, S. K., Sotiropoulos, F., & Odgaard, A. J. (1998). Three-dimensional numerical model for flow through natural rivers. *Journal of Hydraulic Engineering*, 124(1), 13-24.

Sinha, S., Liu, X., & Garcia, M. H. (2012). Three-dimensional hydrodynamic modeling of the Chicago River, Illinois. *Environmental fluid mechanics*, 12(5), 471-494.

Sloff, C. J. (2010). Mixed alluvial and non-alluvial bed topographies: observations modeling and implications. *River Flow Proceedings 2010*.

Smith, D. G., Hubbard, S. M., Leckie, D. A., & Fustic, M. (2009). Counter point bar deposits: lithofacies and reservoir significance in the meandering modern Peace River and ancient McMurray Formation, Alberta, Canada. *Sedimentology*, 56(6), 1655-1669.

SonTek, (1997). Acoustic Doppler Velocimeter (ADV) operation manual (Firmware Version 4.0). SonTek, San Diego, CA, 115 p.

Spruyt, A., Mosselman, E., & Jagers, B. (2011). A new approach to river bank retreat and advance in 2D numerical models of fluvial morphodynamics. In *RCEM 2011: Proceedings of the 7th IAHS Symposium of River, Coastal and Estuarine Morphodynamics, Tsinghua University Press, Beijng, China* (pp. 1863-1871).

Staines, K. E., & Carrivick, J. L. (2015). Geomorphological impact and morphodynamic effects on flow conveyance of the 1999 jökulhlaup at sólheimajökull, Iceland. *Earth Surface Processes and Landforms*, *40*(10), 1401-1416.

Stelling, G.S., (1984). On the construction of computational methods of shallow water flow problems, Rijkswaterstaat communications. No. 35, Government Printing Office, The Hague, The Netherlands.

Stone, M. C., & Hotchkiss, R. H. (2007). Evaluating velocity measurement techniques in shallow streams. *Journal of Hydraulic Research*, 45(6), 752-762.

Su, M., Yao, P., Wang, Z. B., Zhang, C. K., & Stive, M. J. (2017). Exploratory morphodynamic hindcast of the evolution of the abandoned Yellow River delta, 1578–1855 CE. *Marine Geology*, *383*, 99-119.

Sukhodolov, A. N. (2012). Structure of turbulent flow in a meander bend of a lowland river. *Water Resources Research*, 48(1).

Sullivan, S. M. P., & Watzin, M. C. (2010). Towards a functional understanding of the effects of sediment aggradation on stream fish condition. *River research and applications*, 26(10), 1298-1314.

Sutarto, T., Papanicolaou, A. N., Wilson, C. G., & Langendoen, E. J. (2014). Stability analysis of semicohesive streambanks with CONCEPTS: Coupling field and laboratory investigations to quantify the onset of fluvial erosion and mass failure. *Journal of Hydraulic Engineering*, *140*(9), 04014041.

Suthers, I. M., & Gee, J. H. (1986). Role of hypoxia in limiting diel spring and summer distribution of juvenile yellow perch (Perca flavescens) in a prairie marsh. *Canadian Journal of Fisheries and Aquatic Sciences*, 43(8), 1562-1570.

Tash, J.P. and Litvaitis J.A. (2007). Characteristics of occupied habitats and identification of sites for restoration and translocation of New England cottontail populations. *Biological Conservation*, *137*(4), 584-598.

Temple, G. M., & Pearsons, T. N. (2007). Electrofishing: backpack and drift boat. Salmonid field protocols handbook: techniques for assessing status and trends in salmon and trout populations. *American Fisheries Society*, Bethesda, Maryland, 95-132.

Thompson, A. (1986). Secondary flows and the pool- riffle unit: A case study of the processes of meander development. *Earth Surface Processes and Landforms*, 11(6), 631-641.

Thomson, J. (1876). On the origin of windings of rivers in alluvial plains, with remarks on the flow of water round bends in pipes. Proceedings of the Royal Society of London, 25(171-178), 5-8.

Trouw, K. J. M., Zimmermann, N., Mathys, M., Delgado, R., & Roelvink, D. (2012). Numerical modelling of hydrodynamics and sediment transport in the surf zone: a sensitivity study with different types of numerical models. *Coastal Engineering Proceedings*, 1(33), 23.

Tukey, J. W. (1953). The problem of multiple comparisons. Multiple Comparisons.

Ullmann, S. (2008). Three-dimensional computation of non-hydrostatic free-surface flows (Doctoral dissertation, Delft University of Technology).

Van De Wiel, M. J., Coulthard, T. J., Macklin, M. G., & Lewin, J. (2011). Modelling the response of river systems to environmental change: progress, problems and prospects for palaeo-environmental reconstructions. *Earth-Science Reviews*, 104(1), 167-185.

Van der Plas, P. (2009). A momentum conservative finite-volume scheme on a staggered z-layer grid for three-dimensional non-hydrostatic flow (Doctoral dissertation, TU Delft, Delft University of Technology).

Van Maren, D. S. (2007). Grain size and sediment concentration effects on channel patterns of silt-laden rivers. *Sedimentary Geology*, 202(1-2), 297-316.

Van Rijn, L. C. (1989). The state of the art in sediment transport modelling. In Sediment Transport Modeling: (pp. 13-32). ASCE.

Van Sabben, A. J. (2010). Sharp bend flow: Comparison of Delft3D-FLOW with LES and measurements for sharp bends (Master dissertation, TU Delft, Delft University of Technology).

Venditti, J. G., Rennie, C. D., Bomhof, J., Bradley, R. W., Little, M., & Church, M. (2014). Flow in bedrock canyons. *Nature*, 513(7519), 534-537.

Vermeulen, B., Hoitink, A. J. F., & Labeur, R. J. (2015). Flow structure caused by a local cross-sectional area increase and curvature in a sharp river bend. *Journal of Geophysical Research: Earth Surface*, 120(9), 1771-1783.

Vermeulen, B., Hoitink, A. J. F., & Sassi, M. G. (2011). Coupled ADCPs can yield complete Reynolds stress tensor profiles in geophysical surface flows. *Geophysical Research Letters*, 38(6).

Vermeulen, B., Sassi, M. G., & Hoitink, A. J. F. (2014). Improved flow velocity estimates from moving-boat ADCP measurements. *Water Resources Research*, 50(5), 4186-4196.

Viscardi, J. M., Pujol, A., Weibrecht, V., Jirka, G. H., & Olsen, N. R. (2006). Numerical simulations on the Paraná de las Palmas River. *River Flow* (pp. 367-377).

Wagner, C. R., & Mueller, D. S. (2002). Use of velocity data to calibrate and validate two-dimensional hydrodynamic models. *Proceedings of the Second Federal Interagency Hydrologic Modeling Conference*.

Williams, R. D., Brasington, J., Hicks, M., Measures, R., Rennie, C. D., & Vericat, D. (2013). Hydraulic validation of two- dimensional simulations of braided river flow with spatially continuous aDcp data. *Water Resources Research*, 49(9), 5183-5205.

Williams, R. D., Measures, R., Hicks, D. M., & Brasington, J. (2016). Assessment of a numerical model to reproduce event- scale erosion and deposition distributions in a braided river. *Water resources research*, 52(8), 6621-6642.

Williams, R. D., Rennie, C. D., Brasington, J., Hicks, D. M., & Vericat, D. (2015). Linking the spatial distribution of bed load transport to morphological change during high- flow events in a shallow braided river. *Journal of Geophysical Research: Earth Surface*, 120(3), 604-622.

Wilson, C. A. M. E., Boxall, J. B., Guymer, I., & Olsen, N. R. B. (2003). Validation of a three-dimensional numerical code in the simulation of pseudo-natural meandering flows. *Journal of Hydraulic Engineering,* 129(10), 758-768.

Wu, W. (2007). Computational river dynamics. CRC Press.

Wu, W., Rodi, W., & Wenka, T. (2000). 3D numerical modeling of flow and sediment transport in open channels. *Journal of Hydraulic Engineering*, 126(1), 4-15.

Yalin, M. S., and da Silva, A. M. F. (2001). “Fluvial processes.” IAHR Monograph, A. A. Balkema, Delft, Netherlands.

Yossef, M. F. (2016). Morphological model of the River Rhine branches in The Netherlands.

Zeng, J., Constantinescu, G. E. O. R. G. E., & Weber, L. A. R. R. Y. (2005). A fully 3d non-hydrostatic model for prediction of flow, sediment transport and bed morphology in open channels. *Proceedings of the 31st IAHR Congress* (pp. 1327-1338).

Zeng, J., Constantinescu, G., Blanckaert, K., & Weber, L. (2008). Flow and bathymetry in sharp open-channel bends: Experiments and predictions. *Water Resources Research*, 44(9).

Zhang, J. X., Sukhodolov, A. N., & Hua, L. I. U. (2014). Non-hydrostatic versus hydrostatic modelings of free surface flows. *Journal of Hydrodynamics*, Ser. B, 26(4), 512-522.